University of Nottingham
UK | CHINA | MALAYSIA

The Role of Glial Fibrillary Acidic Protein (GFAP) in Astrocyte and Central Nervous System (CNS) Dysfunction

Thesis submitted to the University of Nottingham for the degree of Master of Research

February 2026

Renée Lewis, B.Sc.

20382632

Dr Prof. Claire Friel

Dr Kim Chisholm

Dr Paul Millns

Word count – 31,094

School of Life Sciences

University of Nottingham

i. Acknowledgements

First and foremost, I would like to sincerely thank my supervisors – Claire, Kim, and Paul – a team I truly struck gold with, each of whom brought their own unique strengths and insights to the project. Claire, for her methodical and experienced guidance that consistently helped me regain focus whenever I felt stuck; Kim, for her unwavering resilience and infectious enthusiasm in exploring new ideas and opportunities, even when the science seemed against us; and Paul, for teaching me almost everything I have learned in the lab this year with the patience of a saint. I'd also like to thank everyone in D119 for endless laughs and crosswords which made every day that little bit brighter.

This project would not have been half of what it is without the generous support and expertise shared by Dr Charles Bensidonne, Dr Katherine White, Sophie McCann, Dr Alex Tarr, Paul Radford, Dr Mattea Finelli, and many others.

Having started this year somewhat burnt out after completing my BSc degree, I can honestly say my MRes has reminded me exactly why I chose to pursue a career in neuroscience and has grown my passion for the science (and astrocytes) exponentially. I am heartbroken to close this chapter of my education but extremely grateful to be able to carry forward all the skills, knowledge, and experiences I have gained throughout this year.

ii. Abstract

Astrocytes are a subtype of glial cells in the central nervous system (CNS), acting as key regulators of homeostasis, neuronal support, and signalling regulation, and maintaining blood–brain barrier (BBB) integrity. Astrocytes undergo astrogliosis in response to inflammatory stimuli, which involves undertaking a 'reactive' phenotype responsible for neurotoxic and neuroprotective functions that influence neuronal microenvironments.

Reactive astrocytes can be categorised into two forms; A1 (neurotoxic) or A2 (neuroprotective), where A1 astrocytes promote synaptic loss as well as neuronal and oligodendrocyte death, while A2 astrocytes provide neurotrophic support, synaptogenesis, and tissue repair. However, this binary classification is increasingly recognised as an oversimplification, as more recent research has indicated that astrocyte reactivity represents a spectrum of states, rather than two fixed phenotypes.

Notably, glial fibrillary acidic protein (GFAP), the hallmark cytoskeletal protein in astrocytes, is upregulated in reactive astrocytes, with increased expression observed in a variety of neurodegenerative diseases. One of these is Alexander Disease (AxD), a rare leukodystrophy caused by single-point mutations in the GFAP gene in astrocytes, leading to the accumulation of GFAP aggregates, known as Rosenthal fibres. These aggregates result in the dysregulation of astrocytic activity, causing neurodegeneration in patients; currently, no effective treatments exist. Notably, AxD is the only known genetic disorder affecting only astrocyte cells, providing a unique opportunity to investigate astrocyte-driven mechanisms of CNS dysfunction.

This project aimed to explore the effects of altered GFAP expression on astrocyte function and the broader impact this has on the CNS. In vitro models of human primary astrocytes were produced using lentiviral transduction to overexpress either wild-type (WT) GFAP (OVER-GFAP) or the AxD-associated R79H mutant variant (MUT-GFAP), alongside a GFP-control, where qualitative analysis demonstrated high levels of GFAP expression in both mutant and WT conditions; however, protein expression was not quantitatively measured and therefore could not be directly compared with in vivo levels. Using these models, astrocyte-conditioned media (ACM) were profiled via cytokine arrays and applied to endothelial cells, cortical neurons, and naïve astrocytes to assess how GFAP alterations influence astrocytic interactions and communication with the surrounding CNS, with cortical neurons used to evaluate astrocyte-derived trophic support, endothelial cells to assess astrocyte signalling at the Blood-brain barrier, and naïve astrocytes to examine astrocytic network signalling. This involved the optimisation of a calcium imaging assay to evaluate astrocytic responsivity to various neurotransmitters after ACM treatment, providing a functional readout of astrocyte signalling behaviour.

Significant differences were observed between ACM conditions effect on cortical neuronal viability and neurite outgrowth. MUT-ACM produced the greatest reduction in

neuronal survival and axonal length, whereas OVER-ACM increased neuronal cell counts and partially restored neurite length relative to GFP-ACM, indicating that AxD-associated GFAP mutations disrupt astrocyte-derived neurotrophic support, while GFAP overexpression displayed restorative effects, indicating that GFAP overexpression can enhance the release of neurotrophic factors relative to GFP-control and MUT-GFAP astrocytes. While ACM did not significantly alter E-selectin expression in CRISPR-edited Human Umbilical Vein Endothelial Cells (HUVECs), indicating no significant endothelial inflammatory activation, cytokine profiling identified distinct differences in secretome profiles between control, OVER, and MUT conditions. Most notably, eight cytokines (ANGPT2, CD26, IFNG, IL-5, IL-17, KLK3, CSF1 and CCL19) were significantly altered, with all eight downregulated in MUT-ACM relative to OVER-ACM, and IL-5 and CSF1 additionally reduced compared to GFP-ACM. This pattern suggests a loss of neurotrophic and immune-modulatory support in MUT-GFAP astrocytes, whereas OVER-ACM showed a trend toward increased expression of the same mediators.

Calcium imaging further demonstrated reduced astrocyte responsivity following exposure to MUT-ACM, specifically showing a reduction in histamine-evoked Ca^{2+} response intensity, while ATP-evoked responses remained unaffected. The efficacy of this optimised calcium imaging assay was reinforced by the detection of clear differences in calcium signalling between reactive-like and quiescent-like astrocytes, including increased proportions of responding cells and enhanced glutamate-evoked Ca^{2+} responses in reactive-like astrocytes, highlighting the heterogeneity of calcium signalling dynamics depending on astrocyte phenotype changes.

Overall, these findings indicate that AxD pathology extends beyond a toxic gain-of-function and instead involves a loss of essential astrocyte support throughout the CNS, underscored by a breakdown of astrocytic communication. Notably, GFAP mutations and WT-GFAP upregulation produced markedly different functional outcomes, highlighting the need to distinguish between these mechanisms when investigating AxD pathology. More broadly, by integrating molecular, cellular, and functional analyses this project reinforces the central role of astrocytes in maintaining neuronal microenvironments and identifies how astrocyte dysfunction and impaired astrocyte signalling are key contributors to CNS dysfunction, highlighting restoration of astrocyte homeostatic support as a promising therapeutic strategy for neurodegenerative disease.

Table of Contents

Table of Figures

Table of Tables

Abbreviations

Abbreviation	Full Name
ACM	Astrocyte-Conditioned Media
AD	Alzheimer's Disease
AGS	Astrocyte Growth Supplement
AM	Astrocyte Basal Medium
ANGPT2	Angiopoietin-2
ATP	Adenosine Triphosphate
AxD	Alexander Disease
BBB	Blood–Brain Barrier
BSA	Bovine Serum Albumin
Ca^{2+}	Calcium ion
CCL19	C-C Motif Chemokine Ligand 19
CCL2	C-C Motif Chemokine Ligand 2
CD26 (DPP4)	Cluster of Differentiation 26 / Dipeptidyl Peptidase-4
CNS	Central Nervous System
CRISPR	Clustered Regularly Interspaced Short Palindromic Repeats
CSF	Cerebrospinal Fluid
CSF1	Colony Stimulating Factor 1
CXCL10	C-X-C Motif Chemokine Ligand 10
DAPI	4',6-diamidino-2-phenylindole
DMEM	Dulbecco's Modified Eagle Medium
DMSO	Dimethyl Sulfoxide
DPBS	Dulbecco's Phosphate-Buffered Saline
EAAT1/2	Excitatory Amino Acid Transporter 1/2
ER	Endoplasmic Reticulum
ELISA	Enzyme-Linked Immunosorbent Assay
FACS	Fluorescence-Activated Cell Sorting
FBS	Fetal Bovine Serum
GFP	Green Fluorescent Protein
GFAP	Glial Fibrillary Acidic Protein
GS	Glutamine Synthetase
HBSS	Hanks' Balanced Salt Solution
HBMEC	Human Brain Microvascular Endothelial Cell
HEK293T	Human Embryonic Kidney 293T Cells
HUVEC	Human Umbilical Vein Endothelial Cells
ICC	Immunocytochemistry
IFNG	Interferon Gamma
iNOS	Inducible Nitric Oxide Synthase
IP3R2	Inositol 1,4,5-Trisphosphate Receptor Type 2
Kir	Inward-Rectifier Potassium Channel
K^{+}	Potassium ion
KLK3	Kallikrein-Related Peptidase 3

mGlu1	Metabotropic Glutamate Receptor 1
MUT	Mutant (R79H)
NVU	Neurovascular Unit
NO	Nitric Oxide
OMM	Outer Mitochondrial Membrane
Overexpressed	OVER
P2X	Purinergic Receptor P2X
P2Y	Purinergic Receptor P2Y
PBS	Phosphate-Buffered Saline
PDLO	Poly-DL-Ornithine Hydrobromide
PEI	Polyethylenimine
PFA	Paraformaldehyde
P/S	Penicillin/Streptomycin
RNS	Reactive Nitrogen Species
ROS	Reactive Oxygen Species
TERT2	Telomerase Reverse Transcriptase 2
TSPO	Translocator Protein
TU	Transduction Units
WT	Wild Type
YKL-40	Chitinase-3-like Protein 1

Chapter 1: Introduction

1.1 The Active Role of Astrocytes in the Central Nervous System (CNS)

Astrocytes are a subtype of Glial cell in the central nervous system (CNS), functioning alongside microglia and oligodendrocytes to support neuronal activity and maintain overall brain health. Despite their inability to generate electrical impulses, astrocytes are the most abundant cell type in the CNS, comprising approximately 40% of all cells, and they play a crucial role in the protection, regulation, and homeostasis of neural networks.

First named in 1895 by Michael von Lenhossék (Lenhossék, 1895), astrocytes are characterised by their distinct star shaped morphology. Initially it was believed these cells were passive, and simply provided structural support for neurons, however in recent decades, research has uncovered the complexity of astrocyte function, revealing their highly heterogenous cell population which underpins their ability to perform a wide range of critical processes within the CNS as reviewed by Giovannoni and Quintana (2020).

1.1.1 Homeostatic Function of Astrocytes

Astrocytes are central to maintaining CNS homeostasis, ensuring the delivery of oxygen and nutrients, the clearance of waste products, and the regulation of both neuronal and glial microenvironments. Their widespread distribution and close proximity to neurons, endothelial cells, and other glia allow them to perform a diverse range of homeostatic functions.

1.1.1.1 Astrocytes Role at Blood Brain Barrier, Oxygenation and Blood Flow Regulation

Astrocytes' unique positioning beside blood vessels, makes them a critical component of the blood–brain barrier (BBB; *see figure 1-1*) - a selective semi-permeable membrane between the blood and the brain, allowing for the movement of ion and molecules from cerebral blood vessels into brain tissue (Gawdi and Emmady, 2020). The BBB is composed of endothelial cells, pericytes, capillary basement membrane, and astrocyte end-feet which filter neurotoxic substances out of the brain whilst also supplying the brain with nutrients from the bloodstream (Correale and Villa, 2009).

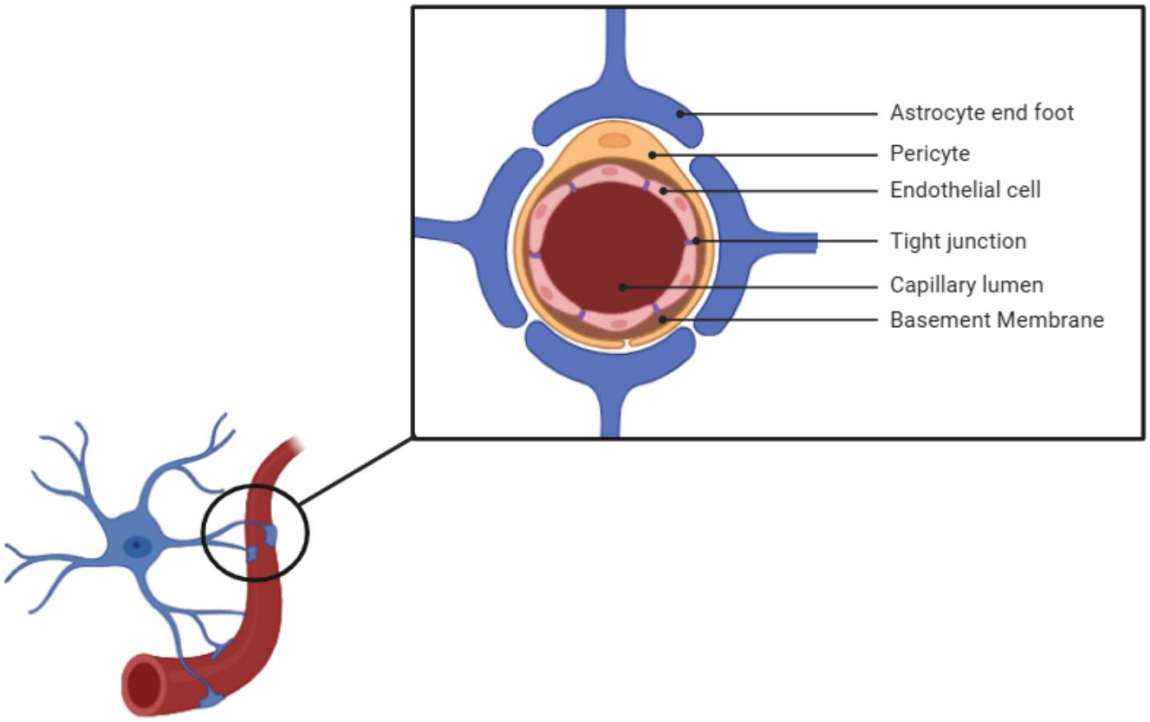

Figure 1-1: Cross section of the Blood-Brain Barrier (BBB). *Astrocytes project their endfeet to enwrap the cerebral capillaries, to allow for transportation of molecules between the blood and CNS. The capillary is composed of endothelial cells connected by tight junctions, surrounded by the basement membrane and pericyte cells. Images created by the author using BioRender.com.*

Astrocytes perivascular endfeet ensheath capillaries, allowing for the transfer of essential substrates such as oxygen and glucose from the blood to the neurons they support (Liu et al., 2020). Astrocytes are also unique in their ability to convert glucose into glycogen for storage, which can subsequently be metabolized into lactate to serve as an immediate energy substrate for surrounding brain cells (Brown and Ransom, 2007).

Their strategic location also enables astrocytes to actively regulate cerebral blood flow by releasing vasodilators such as nitric oxide (NO) and arachidonic acid, ensuring an increased supply of nutrients during periods of heightened neuronal activity, and establishing them as a key element of the neurovascular unit (NVU) (Lawrence et al., 2023).

Beyond their role in BBB formation, astrocytes help maintain the integrity of the BBB through secretion factors such as Angiopoietin-1, which reinforces endothelial tight junctions, and by providing structural support via their endfeet (Williamson et al., 2021). This is particularly important following CNS injury or BBB compromission, where astrocytes respond by forming a glial scar to restore barrier integrity (Bush et al., 1999). Compromised BBB integrity can result in pathogenic and immune cell infiltration, the release of pro-inflammatory cytokines, and the accumulation of reactive oxygen species (ROS), leading to neuroinflammation and potential neurodegeneration. Therefore, astrocytic regulation of the BBB is essential not only for neuronal metabolism but also for protection of the CNS against neurotoxicity.

1.1.1.2 Role in Neuronal Functioning and Synaptic Homeostasis

Astrocytes also ensheathe neuronal synaptic terminals to form tripartite synapses (see figure 1-2) allowing them to modulate individual synapses and provide homeostatic support through the precise control of neuronal microenvironments (Araque et al., 1999).

After neurotransmitter release by neurons, astrocytes assist in the reuptake and recycling of glutamate to prevent excitotoxicity. Astrocytes express high-affinity excitatory amino acid transporters (EAAT1 and EAAT2) that rapidly uptake glutamate from synaptic clefts following neurotransmission. Within astrocytes, glutamate is converted into glutamine by glutamine synthetase, via the glutamate-glutamine cycle. Glutamine is then shuttled back to neuronal presynaptic terminals as a precursor for neurotransmitter resynthesis (Andersen, 2025). Not only does this process prevent excitotoxicity but also ensures effective signal termination.

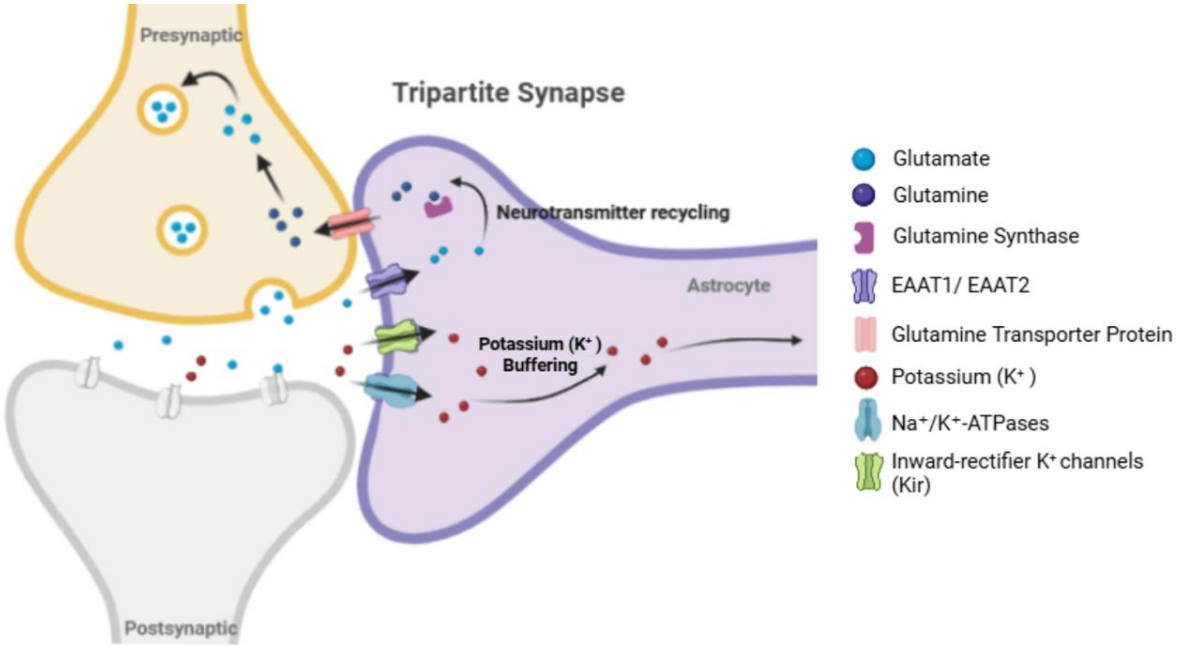

Figure 1-2: Neurotransmitter recycling and Potassium (K+) uptake at the tripartite synapse. *Astrocytes clear the synaptic cleft of excess neurotransmitters (in this example, glutamate) and recycle them for future use and ensure effective signal termination. Excess glutamate can cause excitotoxicity, to prevent this astrocytes uptake Glutamate through EAAT1/2 receptors and convert it back into its precursor, glutamine through the enzyme glutamine synthetase (GS). Glutamine can then be shuttled back to neurons where it is converted back to glutamate ad can be packaged into vesicles by neurons for release. Astrocytes take up K+ via inward-rectifier potassium channels (Kir) and Na^+/K^+-ATPases activity, once K+ enters the cell it can then be redistributed to other astrocytes in syncytium and released. Images created by the author using BioRender.com.*

In addition to the reuptake of glutamate, astrocytes are also responsible for the clearance and recycling of other neurotransmitters, such as γ-aminobutyric acid (GABA) however, additional enzymatic steps are required to first convert GABA into glutamate before it can be transformed into glutamine in astrocytes. Likewise, neurons must reconvert glutamine into glutamate and then into GABA for release (Doengi et al., 2009).

Additionally, during periods of elevated neuronal activity, extracellular potassium (K^+) levels rise as a result of repetitive action potential firing and neurotransmitter release.

Sustained exposure of neurons to elevated K^+ causes hyperexcitability and eventually neuronal death (Balestrino, Aitken and Somjen, 1986). To prevent this, astrocytes clear excessive K^+ from the extracellular space via spatial K^+ buffering, a process where K^+ is redistributed from sites of high concentration to those of low concentration. Astrocytes take up K^+ via inward-rectifier potassium channels (Kir) and Na^+/K^+-ATPases activity (*see figure 1-2*), K^+ is then redistributed through the astrocytic syncytium via gap junctions to low-K^+ regions such as endfeet, where it can safely be released back into the extracellular space or cleared into the vasculature via kir channels (Murakami and Yoshihisa Kurachi, 2015).

The tripartite synapse is a critical modulatory hub in the central nervous system for both excitatory and inhibitory neurotransmission and highlights astrocytes as a promising therapeutic target for neurological disorders associated with signalling pathways dysregulation.

1.1.2 Signalling in Astrocytes

Astrocytes express a variety of neurotransmitter receptors, allowing them to detect and respond to neuronal signals despite being electrically passive. Their ability to detect synaptic activity enables them to engage in communication with neurons at the tripartite synapse (Araque et al., 1999). Astrocytes' primary signalling mechanism relies on fluctuations of calcium (Ca^{2+}) transients, resulting in the release of gliotransmitters, which interact with surrounding synapses and modulate their strength (Araque et al., 2014; figure 1-3).

1.1.2.1 Calcium Signalling

Ca^{2+} transients are a key form of astrocyte signalling. Astrocytic receptors can be categorised into ionotropic and metabotropic classes, both of which trigger calcium responses. Ionotropic receptors are Ligand-gated ion channels - allowing for direct opening of the channel upon ion binding, whereas neurotransmitter binding to metabotropic channels activates G-proteins, triggering a secondary messenger pathway as described in *figure 1-3*.

Increased synaptic activity can elevate astrocytic Ca^{2+} levels through the activation of metabotropic G-protein–coupled receptors (GPCRs), such as glutamate-sensitive mGlu1 receptors and P2Y receptors responsive to extracellular nucleotides including ATP. Astrocytes detect and uptake synaptic spillover of neurotransmitters such as glutamate (Lalo et al., 2011), GABA (Perea et al., 2016), ATP (Darabid, St-Pierre-See and Robitaille, 2018) and Histamine (Perdan-Pirkmajer et al., 2012), triggering intracellular signalling cascades that lead to rises in Ca^{2+} concentrations from internal stores.

These intracellular Ca^{2+} events are mediated by the inositol 1,4,5-trisphosphate receptor type 2 (IP_3R2) signalling pathway that mobilizes Ca^{2+} from the endoplasmic reticulum (ER) to the cytosol. In turn, astrocyte Ca^{2+} elevation promotes Gliotransmission, which is the release of signalling molecules, such as glutamate, GABA and ATP, that can influence the activity of other astrocytes and neurons, causing large-scale synaptic modulation (Araque et al., 2014) whilst also facilitating sustained and spatially distributed Ca^{2+} responses as a result of neuronal activity.

In contrast, ionotropic receptors including Ca^{2+}permeable AMPA receptors and ATP-activated P2X receptors, can rapidly increase astrocyte Ca^{2+} levels through the direct entry of calcium into the cell (Lalo et al., 2011). Ionotropic receptor activation commonly alters single synaptic plasticity through the release of gliotransmitters to a single synapse (Grosche et al., 2002; Hoogland & Kuhn, 2009). This highlights the complexity of Ca^{2+} signalling within astrocytes, ranging from slow, widespread, global Ca^{2+} events to rapid, local Ca2+ transients. It also establishes astrocytes as integral players in both local and network-level communication in the brain, while contributing to synaptogenesis and neuronal circuit dynamics.

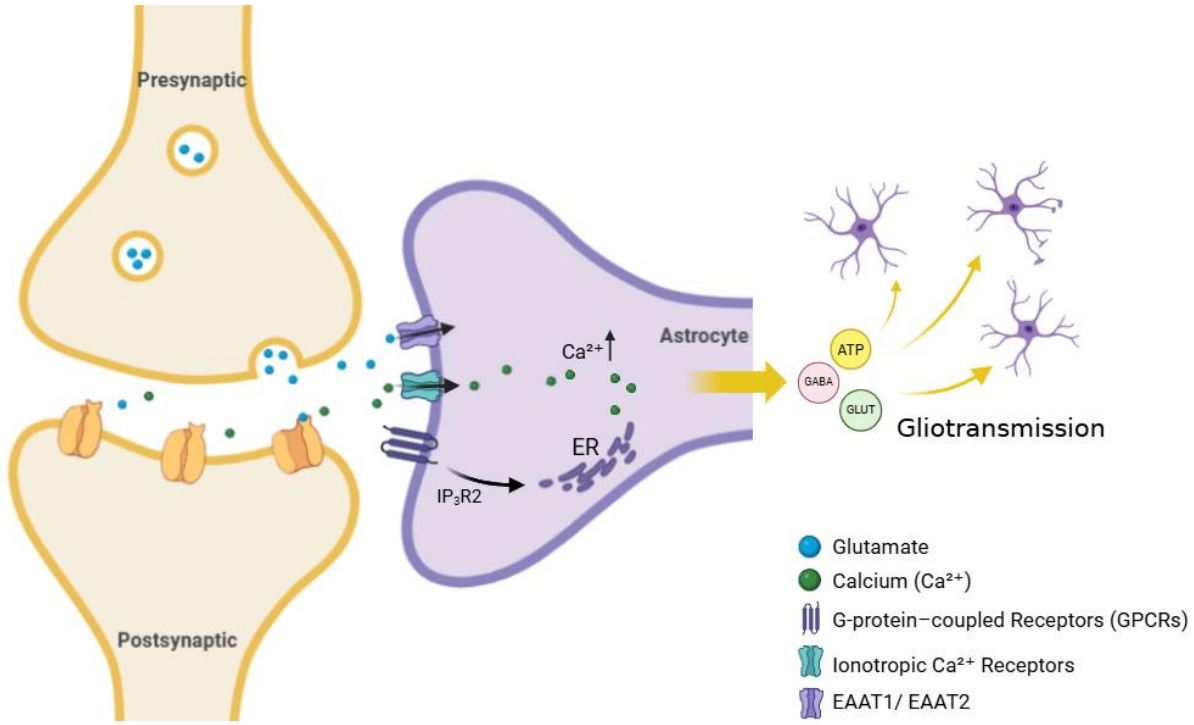

Figure 1-3: Calcium signalling at the tripartite synapse. *Astrocytes regulate neurotransmission through the uptake of excess neurotransmitters (in this example glutamate) from the synaptic cleft via EAAT1/2 receptors. Metabotropic GPCR receptors also respond to neurotransmitter release. GPCR receptor activation triggers an increase in intracellular calcium (Ca^{2+}). Ca^{2+} is mobilised indirectly via IP_3 receptor type 2 (IP_3R2)–mediated release from the endoplasmic reticulum (ER), creating large increases in intracellular Ca^{2+}. Elevated intracellular Ca^{2+} drives signal propagation to surrounding astrocytes through gliotransmitter release (such as ATP, glutamate (GLUT), and GABA) to activate neighbouring astrocyte calcium responses – creating a widespread response. Ca2+ ions can directly enter astrocytes via Ionotropic Ca^{2+} receptors enabling rapid, single cell responses and synapse modulation. Image was created by the author using BioRender.com.*

1.1.3 Astrocytes Reactivity States

Many astrocyte functions described above occur in quiescent astrocytes, however astrocytes undergo a vast set of functional, morphological and genetic changes in response to both disease and injury that impact the functional outcome of CNS recovery. This shift in phenotype to a reactive state is known as astrogliosis and often compromises the quiescent astrocyte function and instead prioritises the immune response (Liddelow et al., 2017).

Although reactive astrocytes are key for an effective neuroimmune response, this phenotype also has harmful consequences if their activity is prolonged. Reactive astrocytes can be divided into two polarised states: A1 astrocytes, which exhibit neurotoxic properties, and A2 astrocytes, which are associated with neuroprotective and reparative functions (Liddelow et al., 2017; *Figure 1–4*).

A1 astrocytes are induced by microglia-derived neuroinflammatory cytokines such as IL-1α and TNF-α and are characterised by their neurotoxic effects in the CNS, promoting synaptic loss as well as oligodendrocyte and neuronal death (Guttenplan et al., 2021). Despite their destructive nature, A1 astrocytes are essential for protecting the CNS from pathogens and inflammation is a vital step in the immune response. However, when their activation is prolonged, they begin to harm the system they once protected. In contrast, A2 astrocytes exhibit a neuroprotective phenotype, upregulating genes involved in neurotrophic support, synaptogenesis, and tissue repair (Liddelow et al., 2017). Additionally, Zou et al. (2019) observed that A1 astrocytes have longer dendrites in comparison to A2 astrocytes which exhibited fewer dendrites and a more hypertrophic morphology, further reinforcing the distinct difference between the two phenotypes.

However, it is to be noted that this binary classification is widely considered an oversimplification, and astrocyte reactivity exists along a spectrum. As reviewed by Escartin et al. (2021), astrocyte reactivity encompasses a diverse and dynamic range of phenotypes that are highly context dependent, where astrocytes can express both neurotoxic and neuroprotective genetic markers simultaneously. Brain region, prolonged inflammation, and disease type are all factors believed to be capable of influencing astrocyte reactivity (Escartin et al., 2021).

While the A1/A2 classification remains a useful conceptual tool for describing maladaptive versus trophic astrocyte behaviours, reliance on this simplified model alone risks obscuring the complexity of astrocyte behaviour observed in vivo. Furthermore, the diversity and complexity observed in astrocyte phenotypes highlights the importance of comprehensive profiling approaches and underscores the need to study astrocyte communication in a holistic manner, rather than focusing on a single altered molecule or factor.

Notably, a hallmark of this morphological change is increased expression of glial fibrillary acidic protein (GFAP), the main cytoskeletal protein in astrocytes, which is upregulated to support the mechanical changes astrocytes undergo during astrogliosis (Yu et al., 2011).

Additional, markers of astrocyte reactivity include a downregulation of EAAT1/2 receptors, which are crucial for astrocytic uptake of glutamate to prevent excitotoxicity at the synapse, as discussed in section *1.1.1.2 Role in Neuronal Functioning and Synaptic Homeostasis*. A downregulation in EAAT expression coincides with the neurotoxic environment associated with prolonged A1 astrocyte activity, ultimately causing neuronal death. Studies such as (Simpson et al., 2010) report a downregulation of EEAT2 expression in Alzheimer's Disease patients, where a significant inverse association between GFAP and EAAT2 expression was identified.

Chitinase-3-like protein 1 (YKL-40) is another known biomarker for Alzheimer's disease diagnosis however it is also a key indicator of general astrocytes inflammation (Lomiguen et al., 2018). Elevated YKL40 levels in the Cerebral spinal fluid (CSF) is frequently seen in chronic neuroinflammatory conditions such as multiple sclerosis, and is induced in reactive astrocytes, specifically those in close proximity to injury sites (Bonneh-Barkay et al., 2010).

Other biomarkers of astrocyte reactivity such as the translocator protein (TSPO), provide an insight into potential mitochondrial mediated homeostatic changes during astrogliosis, due to its location on the outer mitochondria membrane (OMM) of astrocytes. Although little is known about the specific function of TSPO in astrocytes recent studies, such as Tournier et al. (2023), have shown astrocytic regulation of TSPO expression in response to inflammatory stimuli. When considered alongside other established inflammatory biomarkers, TSPO provides an additional layer of insight into the complexity of reactive astrocyte behaviour, with many biomarkers expression varying according to the pathological context of inflammation.

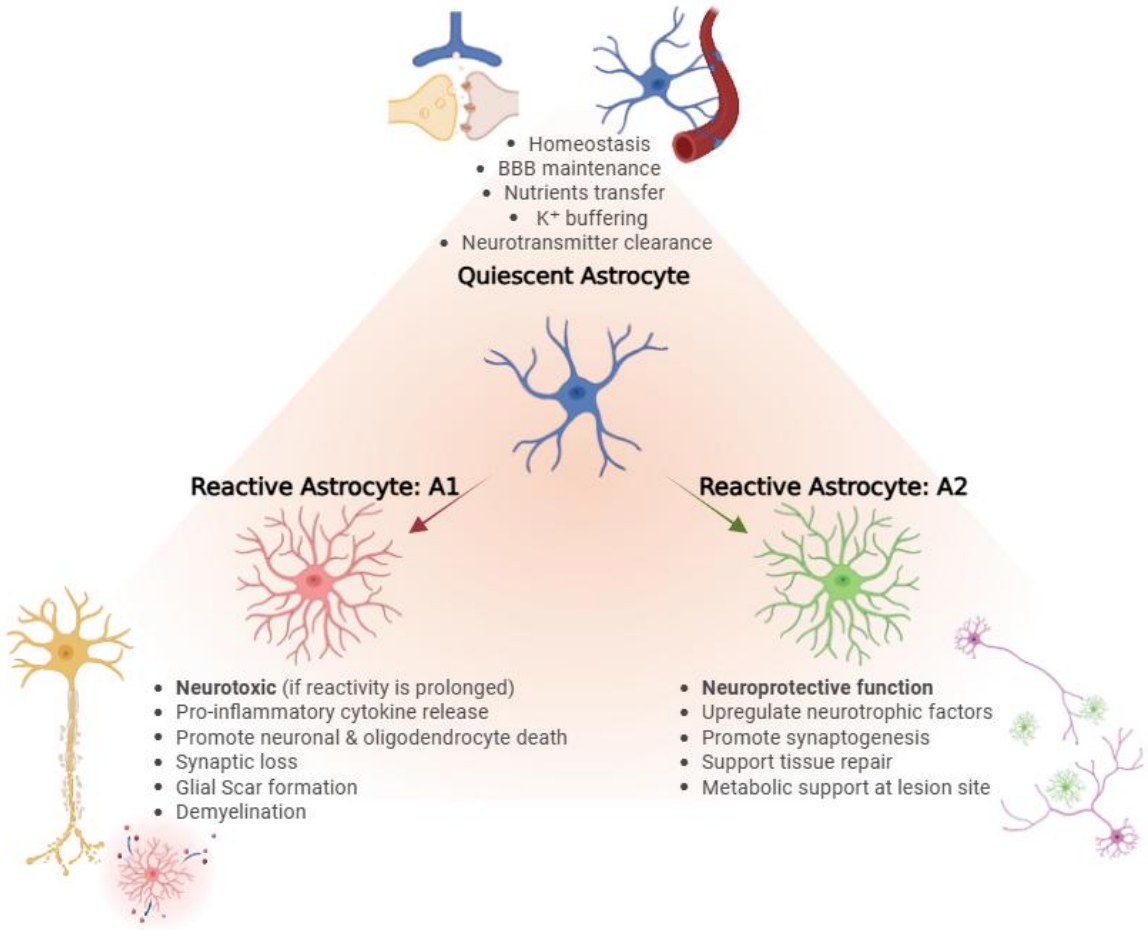

Figure 1-4: Astrocyte phenotypes and functions. *Astrocytes typically exist in a quiescent state of reactivity, where they assist in metabolic, neurovascular and maintenance functions. However, Astrocytes are known to change phenotype in response to harmful stimuli, including disease of injury. These phenotypical changes can have both neurotoxic and neuroprotective effects on the CNS. A1 phenotype is associated with inflammation and prolonged reactivity is a key factor in neurodegeneration and neurotoxicity, they're release of inflammatory mediators further exacerbates the neuroinflammatory response. The A2 phenotype is associated more beneficial functions during the neuroinflammatory response, providing metabolic support and encouraging remyelination and repair through the release of neurotrophic factors. Image was created by the author using BioRender.com.*

After CNS injury A combination of both A1 and A2 astrocytes are responsible for the formation of the glial scar, an injury response heavily dependent on astrocyte reactivity. Reactive astrocytes become highly proliferative in response to injury and migrate towards the lesion site. they promote inflammatory signalling, exacerbate neuronal and oligodendrocyte loss, and reinforce the inhibitory properties of the scar by upregulating molecules that restrict axonal regrowth at the site of injury. Their presence at the lesion border strengthens the scar's rigidity due to an upregulation in GFAP expression and elongation and overlap of processes, which help to isolate the lesion site, however this also contributes to its role as a barrier to regeneration.

In contrast, the neuroprotective phenotype of A2 astrocytes upregulate growth factor secretion, synaptogenesis, and metabolic support at the site of injury, ultimately helping to stabilize the microenvironment and promote tissue survival. Their presence is

essential for counteracting the degenerative effects of A1 astrocytes, reflecting the complexity of the coexistence of the two phenotypes and the potential for CNS degeneration as a consequence of astrocyte dysfunction.

1.2 Astrocyte-Mediated Neurodegeneration and CNS Dysfunction

Whilst astrocytes are not the sole drivers of neurodegeneration, their prolonged inflammatory response promotes a cascade of deleterious mediators, including reactive oxygen and nitrogen species (ROS and RNS), cytokines —that collectively contribute to axonal injury, demyelination, and neuronal cell death (Chitnis and Weiner, 2017).

One crucial mechanism behind neurodegeneration involves the increase of reactive oxygen species (ROS) by astrocytes. In astrocytes low ROS levels assist in vascular regulation, however excessive production induces oxidative stress, impairing mitochondrial, ultimately leading to neuronal apoptosis (Sheng et al., 2013).

Inducible nitric oxide synthase (iNOS), is also upregulated in astrocytes under inflammatory conditions, generating high concentrations of Nitric NO that can inhibit mitochondrial respiration. This promotes the release of glutamate, creating excitotoxic conditions which results in neuronal death. Furthermore, the interaction of NO with superoxide can generate peroxynitrite anion, a highly toxic oxidant that directly damages myelin by peroxidation causing demyelination making axons vulnerable to degeneration (van and Roberts, 1999).

Cytokine release by reactive astrocytes further amplifies neurodegenerative cascades, astrocytic TNF-α is particularly relevant to demyelination as it induces apoptosis of oligodendrocytes, the myelin-forming cells of the CNS, and thereby directly drives demyelination (Katerina Akassoglou et al., 1998). Notably, TNF-α has been observed to play either neuroprotective or neurotoxic roles, depending on expression of other factors including NO (Hemmer et al., 2001).

It is evident through the sustained production of inflammatory mediators, reactive astrocytes progressively damage neurons and impair oligodendrocyte survival - further impacting synaptic transmission and myelin integrity, causing cell death. This positions astrocyte-driven inflammation as a key mechanism in demyelination and neuronal loss observed in neurodegenerative disorders.

1.3 The Significance of Glial Fibrillary Acidic Protein (GFAP)

Glial Fibrillary Acidic Protein (GFAP) is the hallmark intermediate filament protein found in astrocytes. Since its discovery and characterization in 1969 by Lawrence Eng, GFAP

has become one ofthe most reliable and widely used molecular marker for identifying astrocytes and astrocyte mediated inflammation.

GFAP exhibits structural similarities to other non-epithelial class III intermediate filament members, such as vimentin and peripherin, and is composed of three major domains: head, rod, and tail (Yang and Wang, 2015). Although GFAP is encoded by a single gene, alternative splicing of the GFAP gene, means several different GFAP isoforms exists. Despite, their common backbone these isoforms differ slightly in their ends, which influences not only how they function but where they are expressed.

GFAP-α is the most abundant isoform in the CNS, which forms the main structural framework of the astrocytic cytoskeleton. A second major isoform, GFAP-δ, is prominent in astrocyte in the subventricular zone of the brain and has been linked to neurogenic processes (Roelofs et al., 2005). Other, less common isoforms — collectively known as GFAP+1 variants — are expressed selectively in astrocyte subpopulations, with noted increase in expression in certain pathological conditions, including Alzheimer's Disease (AD) (Kamphuis et al., 2014).

Aside from GFAP's significant cytoskeletal and mechanical strength functions (Lawrence et al., 2023), GFAP supports a range of astrocytic functions, these include astrocytic motility, proliferation and BBB integrity (Brenner, 2014). The existence of multiple GFAP isoforms within the CNS likely underpins its functional versatility in astrocytes depending on different physiological and pathological contexts.

Consequently, GFAP has become a key biomarker of astrogliosis, with increased GFAP expression being observed in injured brain tissue (Absinta et al., 2021). Specifically, elevated GFAP has become a hallmark characteristic of neurodegeneration for both disease and traumatic brain injury, including stroke, Alzheimer's, and multiple sclerosis. Wunderlich, Wallesch and Goertler (2006) observed elevated GFAP levels after ischemic stroke, with a strong correlation between GFAP expression, infarct volume and neurological deficit severity. Elevated GFAP is also frequently observed in the blood of Alzheimer's Disease (AD) patients (Frost and Li, 2017) and Multiple Sclerosis patients, where GFAP levels correlated with indicators of myelin and axonal loss in normal appearing white matter (Saraste et al., 2021).

Whilst it is evident that GFAP expression is deeply intertwined with astrocyte reactivity and neuroinflammation it is unclear whether GFAP expression is a cause or consequence of CNS dysfunction in the majority of neurodegenerative disorders.

1.4 Alexander Disease

Leukodystrophies are a group of rare, genetic demyelinating diseases leading to progressive neurodegeneration including oligodendrocytes, and astrocytes

abnormalities. Typically, dysfunction in myelin production and maintenance is observed in Leukodystrophies, resulting in impaired neuronal signalling and neurodegeneration (Vanderver et al., 2015). It is common for Leukodystrophies to be inherited; however, this is not always the case, additionally whilst some forms are present at birth, onset can also occur in juveniles and during adulthood - often presenting symptoms of both motor and cognitive impairment (Muthusamy et al., 2023).

One of these disorders is Alexander Disease (AxD), a very rare neurodegenerative disease caused by missense point mutations in the GFAP gene and currently the only known genetic disorder affecting only astrocyte cells. It is, thus, an example of a primary disease of astrocytes. Currently no effective treatments exist, and juvenile-onset cases are typically fatal (Kuhn and Cascella, 2020).

1.4.1 Clinical Features of Alexander Disease

It is estimated AxD has a prevalence of approximately 1 in 2.7 million (Yoshida et al., 2011), however an exact prevalence is unknown due to a lack of clinical awareness that leads to frequent misdiagnosis (Gagliardi et al., 2024). Typically, AxD presents in infants, however other variants are occasionally seen, with multiple clinical forms spanning from neonatal, infantile, juvenile, and adult. It is widely believed that early onset of the disease correlates with an increase in the severity of symptoms as outlined by Srivastava and Naidu (2015):

- **Neonatal form** (first 30 days after birth): Severe developmental delays/ regression, Hydrocephalus, Megalencephaly, seizures, hypotonia, gastroesophageal reflux. Death typically occurs within two years of onset.
  I**nfantile form** (< 2 years): most common form of the disease, developmental and language delays, loss of gross and fine motor skills, seizures, difficulty swallowing (Dysphagia) and speaking (Dysarthria), frequent vomiting.
- **Juvenile form** (during childhood/ adolescence): Similar manifestations but milder than those in the infantile form.
- **Adult form** (late teens onwards): Speech and swallowing problems, impaired motor skills, overactive reflexes (hyperreflexia), poor coordination (ataxia), sleep apnea, involuntary eye movements (nystagmus) and double vision, weakness on one side of the body (hemiparesis) or all four limbs (quadriparesis) or quadriplegia.

Additionality, AxD can be divided into two types with type I patients having frontal predominance of lesions, and a more aggressive form of the disease, typically seen in early onset cases. Whereas, type II patients have hindbrain predominance, with later onset and typically milder symptoms and slower disease progression (Perng et al., 2006).

Although Brenner et al. (2001) Identified a genetic basis for Alexander disease, familial cases are rare due to the high morbidity rate of the disease. Additionally, GFAP mutations identified to date are heterozygous, resulting in a toxic gain of function in GFAP (Messing and Brenner, 2020), interrupting the typical GFAP network and forming abnormal protein bundles, known as Rosenthal fibers (Tang et al., 2010).

1.4.2 Rosenthal Fibers

First characterised in 1949 by W. Stewart Alexander (Alexander, 1949), AxD is marked by the presence of Rosenthal fibers (*see figure1-5*), these are intracellular inclusions found in astrocytes and represent an accumulation of GFAP as a result of the gene mutation inducing GFAP upregulation (II, Perry and J Lennerz, 2006). The over production and reduction in clearance of GFAP combined with other proteins such as heat shock proteins and ubiquitin ultimately form these aggregates which have a deleteriously affects astrocyte function (II, Perry and J Lennerz, 2006).

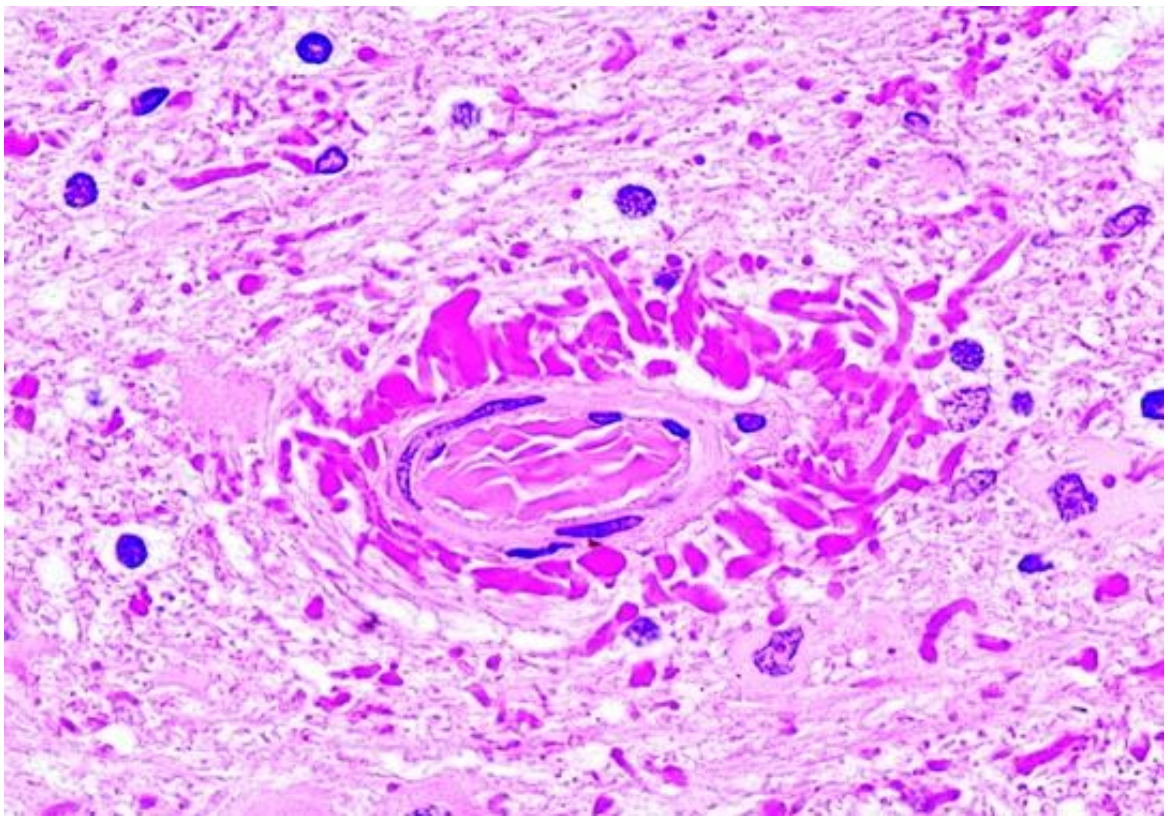

Figure 1-5: Rosenthal Fibers *Taken from Wippold, Perry and Lennerz (2025), Staining of Rosenthal Fibers which have accumulated in astrocyte end feet. Hematoxylin-eosin (H&E) stain shows bright pink staining of Rosenthal fibers surrounding a blood vessel within the perivascular zone from a AxD patient (Photomicrograph; original magnification, 1000x).*

One mechanism by which Rosenthal fibres disrupt astrocyte function is through impairment of cytoskeletal integrity. GFAP aggregation destabilises the intermediate filament scaffold required for proper localisation and function of membrane

transporters, including astrocytic glutamate transporters (Hughes et al., 2004). Increasing evidence indicates that GFAP aggregates exert maladaptive effects on glutamate clearance and neuronal signalling. For example, Lin et al. (2021) demonstrated that transgenic mice expressing elevated GFAP and Rosenthal fibres in astrocytes had significantly impaired glutamate uptake compared with controls. The reduced capacity for glutamate buffering also resulted in neurotoxic effects on neighbouring neurons, further indicating a loss of this essential homeostatic function. As glutamate transporters are essential for maintaining extracellular glutamate homeostasis in astrocytes (Bjørnsen et al., 2013), reduced expression or mislocalisation may critically compromise glutamate clearance, thereby promoting excitotoxic stress and neuronal dysfunction.

Furthermore, studies have indicated Rosenthal fibres have a maladaptive effect on Calcium signalling, specifically on the propagation of intracellular calcium waves. Jones et al. (2018) demonstrated that GFAP aggregates impact the structural integrity of the endoplasmic reticulum (ER), the primary intracellular Ca^{2+} store and a critical organelle for IP_3-mediated calcium release. Specifically, in AxD patient-derived astrocytes with GFAP aggregation, ER exhibited enlarged, heterogeneous morphology and perinuclear localisation, which was accompanied by reduced propagation of calcium waves to adjacent astrocytes due to impaired IP_3-dependent ATP release, despite ATP production remaining intact (Jones et al., 2018). This study concludes that GFAP aggregation prevents the stimulus-evoked ATP secretion required to activate purinergic receptors on adjacent astrocytes, therefore inhibiting purinergic calcium wave spread and compromising astrocyte–astrocyte communication in AxD

In addition to impaired structural integrity, proteotoxic stress caused by mutant GFAP aggregation can induce proteostasis, a dysregulation in protein homeostasis, this only facilitates the accumulation of Rosenthal fibers further and reinforces the dysfunctional condition of astrocytes in patients with AxD (Wen et al., 2023).

Although GFAP accumulation occurs in astrocytes, many other cells in the CNS are markedly affected as a result, notable by the extensive white matter degeneration seen in AxD patients. Significant microglial activation and neuronal loss highlight the implications of pathological astrocytes in the function and survival of other cells throughout the CNS, making AxD a crucial disease for investigating the cellular and molecular changes brought about by pathological astrocytes (Hagemann et al., 2005).

Notably, Álvaro Viedma-Poyatos et al. (2022) observed mutant variants of GFAP are more severely disrupted by exposure to oxidants such as diamide and hydrogen peroxide (H_2O_2) than WT, which exacerbates GFAP aggregation. Furthermore, H_2O_2 caused reversible filament alterations in GFAP wild type, but irreversible damage in mutant GFAP expressing cells, and induced a more oxidative state in pathogenic astrocytes, resulting in increased mitochondrial superoxide generation (Álvaro Viedma-Poyatos et al., 2022). This study highlights the upregulation of A1 astrocyte functions in AxD patients, and the

release of inflammatory mediators which may have maladaptive effects on other glial cells and neurons.

1.4.3 Astrocyte-Driven Neuronal and Neurovascular Dysfunction in Alexander Disease (AxD)

Although AxD is derived from single point mutations in an astrocyte specific protein, many other cell types in the CNS are markedly affected as a result, notable by the extensive white matter degeneration seen in AxD patients (as previously discussed in *section 1.4 Alexander Disease*). Significant neuronal loss highlights the implications of pathological astrocytes in the function and survival of other cells throughout the CNS, making AxD a valuable model for investigating how astrocyte dysfunction propagates cellular and molecular changes beyond just astrocytes themselves (Hagemann et al., 2005).

Demyelination and axonal death in AxD suggest a failure of astrocyte-mediated metabolic and trophic support to neurons. For example, Berman et al. (2025) demonstrated AxD model rats exhibit a neurodegenerative profile, including reduced expression of synaptic and mitochondrial proteins essential for neuronal function. Alongside this, these rat models showed impaired performance in Barnes maze and novel object recognition tests, demonstrating cognitive impairment (Berman et al., 2025). Together, these findings support the hypothesis that AxD derived mutations in astrocytes have maladaptive effects on neuronal function and communication and suggest that cortical neuron networks are particularly vulnerable to dysfunction arising from GFAP mutations, which may contribute to the cognitive deficits observed in AxD patients.

Additionally, research has indicated that astrocyte-derived signalling can directly induce neuronal death in Drosophila models of AxD. Wang et al. (2015) demonstrated that expression of mutant human GFAP in astrocyte-like glial cells caused a marked increase in NO production, triggering neuronal apoptosis. Interestingly, transgenic drosophila that express WT GFAP at levels equivalent to R79H GFAP did not exhibit GFAP aggregation nor neurotoxicity, suggesting that the neurotoxic effect of GFAP are linked to the single point mutation and or protein aggregation in the form of Rosenthal fibres. Reducing NO production rescued neuronal survival, while inhibition of the neuronal NO receptor attenuated cell death, confirming that the toxic signal originating in astrocyte-like cells acts directly on neurons. These findings provide strong evidence that pathological astrocytes in AxD actively drive neuronal dysfunction and degeneration in a manner distinct from WT GFAP overexpression, further reinforcing the critical role of astrocyte-mediated signalling observed in AxD pathology on neurons.

Beyond Alexander disease, there is a plethora of research linking reactive astrocyte signalling and cytokine release to neurodegeneration. As reviewed by Lawrence et al. (2023), astrocytes that adopt a neurotoxic phenotype downregulate neurotrophic support and upregulate pro-inflammatory cytokines and chemokines which impair

neuronal function, thereby promoting neurodegeneration. The correlation between maladaptive cytokine profiles in astrocytes and neuronal loss is particularly relevant for AxD, given that maladaptive astrocytic cytokine release has already been implicated in its pathology (Markel Olabarria et al., 2015; Kondo et al., 2016).

The above evidence therefore shows that profiling astrocyte-derived secretomes provides a powerful strategy to isolate how astrocyte signalling alone alters neuronal viability and synaptic integrity.

In addition to neuronal dysfunction, astrocytes major structural and functional role at the BBB (see *section 1.1.1.1 Astrocytes Role at Blood Brain Barrier, Oxygenation and Blood Flow Regulation*) renders neurovascular functions vulnerable to impairment following astrocyte pathology. Whilst direct research of BBB dysfunction in AxD remains limited, disruption of astrocyte signalling is known to disrupt endothelial cell behaviour and increase BBB permeability through the release of pro-inflammatory cytokines and Matrix metalloproteinase (MMPs) that degrade BBB components and promote leukocyte infiltration (Che et al., 2024). For example, Feng et al. (2022) showed that increased astrocyte-derived MMP-9 following stroke plays a deleterious role in BBB permeability, while inhibition of astrocytic MMP-9 improved BBB damage (Feng et al., 2022). These findings suggest that compromised astrocyte–endothelial interactions may contribute to altered vascular permeability, inflammatory infiltration, and impaired cerebral homeostasis in AxD, extending disease pathology beyond astrocytes alone.

Overall, current literature demonstrates that astrocytes influence neuronal and endothelial cell behaviour through their signalling and secretory functions. Therefore, investigating changes in astrocyte communication and signalling provides a mechanistically relevant approach to isolate astrocyte-driven effects on the wider CNS. This approach can be applied to AxD research to interrogate how pathogenic GFAP expression alters astrocyte–neuron and astrocyte–endothelial interactions.

1.4.4 GFAP Mutation Variants

Since GFAP mutations were identified as the cause of AxD in 2001 (Brenner et al., 2001), upwards of 100 mutations have been reported to be associated with AxD. These are typically categorised by protein domain and common mutation regions of the gene, with the most notable being R79, R88, R239, and R416 (Yasuda et al., 2019). Furthermore, clear genotype – phenotype trends has been identified amongst variants, the most prevalent variants (>70%) R79 and R239 are associated with infantile and juvenile onset of the disease, typically exhibiting the most severe symptoms (Yoshida et al., 2011). Meanwhile other variants such as R416W are more prominent in adult onset, and familial cases.

Additionally, as previously mentioned in *section 1.4.2 Rosenthal Fibers, the* reorganisation of astrocyte structure caused by GFAP aggregation also disrupts key signalling organelles and membrane receptors necessary for astrocyte communication with neighbouring cells (Jones et al., 2018). Therefore, we can predict cytoskeletal disruption induced by these GFAP mutations may impair astrocyte–astrocyte and astrocyte–CNS communication, shifting astrocytes from a homeostatic state toward a maladaptive phenotype with reduced trophic support.

To investigate this mechanistic link between GFAP mutation, astrocyte dysfunction, and impaired astrocyte communication, this thesis focuses specifically on the highly prevalent R79H GFAP variant, given its strong association with severe cognitive impairment and CNS dysfunction (Perng et al., 2006) This offers a biologically justified method to explore how pathogenic GFAP mutations alter astrocyte signalling networks and how the resulting downstream effects drive CNS dysfunction and neurodegeneration.

1.5 Aims

It is evident that astrocytes play a central role in maintaining neuronal homeostasis, regulating synaptic activity, and BBB integrity. Given this, understanding astrocyte dysfunction is critical to uncovering mechanisms of astrocyte-mediated neurodegeneration. This highlights GFAP mutations associated with AxD as particularly valuable models, as they specifically impair astrocytic processes and drive maladaptive behaviours such as astrogliosis, oxidation and protein aggregation.

Thus, this thesis aims to investigate the implications of GFAP mutations for astrocyte-derived CNS dysfunction, with a particular focus on pathogenic astrocyte secretome characterisation and their influence on other cells within the CNS, including healthy astrocytes, cortical neurons, and endothelial cells. Since astrocyte communication is largely mediated by calcium signalling and inflammatory cytokine release, functional and molecular analyses will be used to assess how pathogenic GFAP expression disrupts both local astrocytic responses and wider neural network integrity.

Specifically, this project focuses on comparing the effects of WT GFAP overexpression with the AxD-associated R79H variant, to distinguish between dysfunction caused by general GFAP upregulation, commonly observed during prolonged astrogliosis, and dysfunction specifically attributable to AxD astrocytes. The work seeks to identify potential therapeutic targets for AxD as well as other maladaptive inflammatory conditions which are hallmarked by increased GFAP expression.

1.5.1. Key Objectives

1. ***Establish an in vitro model of Alexander Disease (AxD):***

Produce primary human astrocytes overexpressing either WT GFAP or the R79H mutant variant. This model can then be used to distinguish how GFAP expression alters astrocytic structure, cytokine release, inflammatory marker expression, and calcium signalling.

2. ***Examine astrocyte–endothelial cell interactions:***
   Assess how the secretome from R79H GFAP expressing astrocytes as well as astrocytes over expressing WT GFAP affect E-selectin expression in CRISPR Edited TERT2HUVEC endothelial cells. This assay not only gives indirect measurements of pro inflammatory cytokine levels in astrocyte secretomes but also gives insight into the impact of astrocytic dysfunction on neurovascular cells, reflecting astrocytes' key position between neuronal circuits and blood vessels.
3. ***Profile inflammatory markers in reactive astrocytes***
   Using a cytokine array to identify and compare inflammatory mediators, including common cytokine and chemokines secreted by astrocytes depending on GFAP expression. Immunocytochemistry was also used to quantify changes in protein expression in relation to changes in GFAP expression.
4. ***Develop and optimise a calcium imaging assay for astrocytes:***
   Create a robust calcium imaging assay to characterise astrocyte–astrocyte communication to various neurotransmitters, providing a quantitative readout of astrocytic signalling. This assay can then be used to assess differences is astrocyte responsivity after treatment with healthy, GFAP overexpressing and Mutant GFAP expressing astrocytes whilst avoiding the complexities of co-culture. Optimise the assay to detect changes in calcium signalling following both neurotransmitter stimulation and pathogenic secretome treatment.
   The effectiveness of this assay could then be confirmed by investigating other aspects of astrocyte heterogeneity on calcium signalling, particularly by comparing calcium signalling in reactive and resting astrocytes.
5. ***Investigate astrocyte–neuron interactions:***
   Measure the impact of secretomes from R79H GFAP expressing astrocytes as well as astrocytes over expressing WT GFAP on cortical neuron viability, axonal growth, and excitotoxic vulnerability. This will allow for insight into potential mechanisms by which astrocytic dysfunction contributes to synaptic instability, axonal degeneration, and neuronal loss in AxD.

Through these objectives, this thesis aims to present a detailed analysis of how changes GFAP expression drives maladaptive astrocyte behaviour and the wider impact of this astrocyte dysfunction on the surrounding CNS. By integrating cellular, molecular, and functional data, it aims to explore a wide range of readouts to generate a full picture on how R79H GFAP contributes to demyelination, neuroinflammation, neuronal dysfunction in AxD patients, and identify potential therapeutic targets for not only AxD but broader

neurodegenerative disorders characterised by GFAP overexpression and chronic astrocyte reactivity.

This project tests the hypothesis that human primary astrocytes overexpressing the AxD-associated R79H-GFAP mutation exhibit a maladaptive secretomes profile that disrupts astrocyte communication and wider CNS interactions, independent of and mechanistically distinct from the effects of non-pathological WT-GFAP upregulation. Specifically, I hypothesise that R79H-GFAP expression:

1) changes the secretome of mutant astrocytes and reduces neuroprotective while upregulating neurotoxic cytokines
2) has a significant impact on essential astrocyte-derived trophic and homeostatic support to cortical neurons and endothelial cells
3) disrupts calcium dependant signalling within astrocyte subpopulations

Furthermore, I hypothesised that alterations in astrocyte–astrocyte communication will differ between quiescent and reactive astrocyte phenotypes, reinforcing the influence of astrocyte heterogeneity and reactivity on signalling dynamics within astrocyte subpopulations.

Chapter 2: Materials and Methods

All reagents were purchased from Merck Sigma-Aldrich, UK, unless stated otherwise.

Table 2-1: Composition of frequently used buffers.

Buffer	pH	Components	Solvent
Calcium Imaging Buffer	7.4	▪ 136.9 mM Sodium Chloride ▪ 2.7 mM Potassium Chloride ▪ 10 mM HEPES - 15 mM Glucose ▪ 1 mM Magnesium Sulfate ▪ 2 mM Sodium Formate	Deionised Water
Phosphate-Buffered Saline (PBS)	7.4	▪ 136.9 mM Sodium Chloride ▪ 2.7 mM Potassium Chloride ▪ 1.4 mM Sodium Dihydrogen Phosphate (anhydrous) ▪ 1.5 mM Potassium Dihydrogen Phosphate (anhydrous)	Deionised Water
Hanks' Balanced Salt Solution (HBSS)	7.4	▪ 2 mM Sodium Pyruvate ▪ 145 mM Sodium Chloride ▪ 10 mM D-Glucose - 5 mM Potassium Chloride ▪ 1 mM Magnesium Sulfate Heptahydrate ▪ 10 mM HEPES - 1.3 mM Calcium Chloride Dihydrate ▪ 1.5 mM Sodium Bicarbonate	Deionised Water

2.1 General Cell culture Protocol

All cell culture work was conducted in aseptic conditions, within class II Laminar flow cell culture hoods. All cell lines were maintained in a humidified tissue culture incubator (37 °C, 5 % CO_2) unless required for use. All reagents were warmed to 37 °C to minimise thermal shock to the cells.

2.1.1 General Thawing and Maintenance of Cell Lines Protocol

All cell lines were stored in cryogenic vials within vapour phase liquid nitrogen. For thawing, vials were retrieved from storage and allowed to defrost at room temperature. 1ml of cells was then transferred into T75 culture flasks containing 10 mL of the appropriate growth medium.

After 24 h, the medium was replaced with fresh medium to aid removal of cell debris from the thawing process. Subsequently, cultures were maintained by replacing the medium every three days, except when passaging was performed. When flask confluency reached ≥70%, cells were either passaged for continued maintenance or allocated for experimental use.

2.1.2 General Passaging of Cell Lines Protocol

Once confluency exceeded 70%, medium was aspirated from the flask and cells detached using Trypsin solution from porcine pancreas (Cat. No. T4549) diluted 1:20 in PBS, unless otherwise specified.

10ml of the trypsin solution was added and left to incubate for ≤5 minutes. After, trypsin was immediately neutralised by adding 10ml of Astrocyte basal Medium (AM) (Cat. No.1801), supplemented with 2% fetal bovine serum (FBS) (Cat. No. 0010), 1% astrocyte growth supplement (AGS) (Cat. No. 1852) and 1% penicillin/streptomycin solution (P/S) (Cat. No. 0503) (all ScienCell Research Laboratories, USA), unless otherwise stated.

Cells were then centrifuged at 200 xg for 5 minutes RT and the supernatant aspirated. Following centrifugation, the resulting pellet was resuspended 2ml of the appropriate growth medium, and cells were either reseeded at the desired split ratio back into T75 flasks (with 10 mL growth medium) or prepared for experimental seeding.

2.1.3 Human Primary Astrocyte Cell Lines

Human primary cortical astrocytes (SC1800s) were purchased from ScienCell Research Laboratories (USA) (cat# 1800) and kept frozen in liquid nitrogen upon arrival. SC1800s were isolated by ScienCell from human cerebral cortex and cryopreserved before delivery.

Cells were maintained in Astrocyte basal Medium (AM) (cat#1801), supplemented with 2% fetal bovine serum (FBS, Cat. No. 0010), 1% astrocyte growth supplement (AGS, Cat. No. 1852) and 1% penicillin/streptomycin solution (P/S, Cat. No. 0503) (all ScienCell Research Laboratories, USA).

Apon arrival, the original ScienCell vial of astrocytes was seeded into 2x T75 flasks. Once flasks exceeded 70% confluency, cells were passaged once at a split ratio of 1:6 into 12x T75 flasks (*as described in the above section*).

2.1.3.1 Cryopreservation

Cells were passaged a final time before being cryopreserved at passage level 2. Each T75 flask was split into 2 cryovials (1ml/vial) in 90% FBS and 10% dimethyl sulphoxide (DMSO), resulting in a total of 24 vials at passage 3 from the original ScienCell vial. These were cryopreserved in liquid nitrogen, where they remained until future use.

2.2 Immunocytochemistry (ICC) General Protocol

2.2.1 Coverslip Preparation and Fixing

Immunocytochemistry (ICC) was performed on cell seeded on 19mm coverslips. Cells were fixed using 4% paraformaldehyde (PFA) diluted in PBS for 20 minutes RT, followed by three washes with PBS containing 0.02% sodium azide.

2.2.2 Coverslip Staining

Immunocytochemistry was performed according to a standard protocol. However, buffer compositions varied depending on the cell type being labelled (e.g., cortical neurons or primary astrocytes). The specific buffers used throughout the ICC protocol are detailed in ***table 2-2.***

Table 2-2: Composition of Buffers used during Immunocytochemistry. *All Buffers were prepared using PBS as the solvent.*

Buffer	Cortical Neurons	Primary Astrocytes
Wash Buffer	- 0.1% (v/v) Triton X-100	- 0.05% (w/v) sodium azide
Permeabilisation Buffer	- 0.075% (w/v) glycine - 0.2% (v/v) Triton X-100	- 0.05% (w/v) sodium azide - 0.1% (v/v) Triton X-100 - 0.1% (w/v) Glycine
Blocking Buffer	- 3% (w/v) Bovine Serum Albumin (BSA)	- 0.05% (w/v) sodium azide - 0.1% (v/v) Triton X-100 - 3% (w/v) Donkey Serum

Coverslips were washed three times for 3 minutes in the appropriate Wash Buffer, followed by a 30-minute incubation in Permeabilisation Buffer at RT. After aspirating the permeabilisation solution, cells were incubated for 30 minutes in Blocking Buffer to prevent non-specific antibody binding. Primary antibodies (see ***table 2-3***) were diluted in Blocking Buffer and applied to the coverslips, which were then incubated overnight at 4 °C.

Table 2-3: Antibodies used during Immunocytochemistry and their dilutions. *All antibodies were diluted in the appropriate Blocking Buffer (see table 2-2).*

Antibody	Dilution	Primary/ Secondary	Host Species	Supplier/ Identifier
Anti – ALDH1L1	1:250	Primary	Rabbit	ABCAM (ab177463)
Anti - Acetylated Tubulin antibody	1:200	Primary	Mouse	Sigma-Aldrich (T7451)
Anti – GFAP	1:1000	Primary	Mouse	Thermofisher

				(MA5-12023)
Anti – TSPO	1:100	Primary	Goat	Thermofisher (PA5-18565)
Anti – mouse Alexa Fluor 488	1:300	Secondary	Goat	Invitrogen (A11001)
Anti – rabbit Alexa Fluor 568	1:500	Secondary	Donkey	Invitrogen (A10042)
Anti – mouse Alexa Fluor 647	1:500	Secondary	Donkey	Invitrogen (A31571)
Anti – goat Alexa Fluor 750	1:500	Secondary	Donkey	ABCAM (ab175745)

The next day, coverslips were washed 3x for 3 min in Wash Buffer to remove any unbound primary antibody. Secondary antibodies were diluted in Blocking Buffer and added to coverslips, before being incubated for 2 hours at RT in the dark. Coverslips remained protected from light for the remainder of the staining protocol. After incubation, secondary antibody solution was aspirated, and coverslips were washed again 3 × 3 min in Wash Buffer.

2.2.3 Nuclear staining with 4',6-diamidino-2-phenylindole (DAPI)

Nuclear staining was performed using 4',6-diamidino-2-phenylindole (DAPI). DAPI was either co-incubated with the secondary antibody solution (1 µg/mL) or applied afterward as a 3-minute wash step diluted in Wash Buffer (0.01 mg/mL).

2.2.4 Coverslip Mounting

A final 3 min wash of distilled water was added to coverslips before being left to dry for 10 minutes.

Following staining, coverslips were rinsed with distilled water and allowed to dry for 10 minutes. They were then mounted onto glass microscope slides using either VectorShield mounting media (Vector laboratories, UK) or Fluoromount™ Mounting Medium and sealed with nail varnish. Slides were left to dry and subsequently stored at 4 °C until imaged.

2.3 Production of Astrocyte-Conditioned media (ACM)

To investigate the effects of GFAP expression on astrocyte–astrocyte communication and interactions with other CNS cells, astrocytes were transduced to overexpress GFP tagged wild-type GFAP, overexpress a GFP-tagged GFAP variant (R79H) associated with

Alexander disease or receive a control transduction (GFP only). This method was used to generated astrocyte cultures expressing mutant GFAP (MUT-GFAP), overexpressed wild-type GFAP (OVER-GFAP), or a control vector containing only GFP (GFP-control). The spent media from these cultures, which contains the secretome of these transduced astrocytes, was collected for future use.

Two different methods of lentiviral transduction were used **(transduction 1 or transduction 2)**, however the viral plasmids used to produce lentiviral particles were the same. Three plasmids were produced by OriGene Technologies GmbH:

- **pLenti-C-mGFP-P2A-Puro (GFP-control)** – Lentiviral control vector containing a monomeric GFP sequence (mGFP)
- **pLenti-P2A-tGFP (PS100108) (OVER-GFAP)** – Encodes wild-type human GFAP. The P2A sequence allows bicistronic expression of GFAP and tGFP from a single transcript.
- **pLenti-P2A-tGFP-GFAP(R79H) (MUT-GFAP)** – This construct was generated from the OVER-GFAP plasmid (PS100108) by site-directed mutagenesis, introducing a single point mutation in the GFAP gene associated with AxD. The R79H mutation, is associated a with particularly aggressive form of AxD, seen in neonatal/ juvenile onset of the disease.

These plasmids were designed to enable identification of transduced cells through expression of GFP followed by a P2A self-cleaving peptide, allowing for GFP to be cleaved from the GFAP protein, so that GFP signal reports on GFAP expression but are not connected in a single polypeptide. Ampicillin resistance was also used for bacterial selection during plasmid amplification.

2.3.1 Lentiviral Transduction 1

2.3.1.1 Human Primary Astrocyte Cell Culture

Human primary astrocytes were cultured and passaged to passage 3 (P3) as previously outlined in *section 2.1 General Cell Culture Protocol*. Upon reaching 70% confluency, cells were split a final time. Viable cells were counted using 0.4% Trypan Blue (T8154, Sigma-Aldrich, UK) on a dual-chambered cell count slide (1450011, Bio-Rad Laboratories, UK) with a TC20 Automated Cell Counter (Sigma-Aldrich, UK). Cells were seeded at 70,000 cells per well in 2 mL astrocyte medium in 6-well plates.

2.3.1.2 Lentiviral Transduction (Transduction 1)

Ready-to-use lentiviral particles (GFP-control, OVER-GFAP or MUT-GFAP) were purchased from OriGene Technologies GmbH (Germany) at a concentration of $>1 \times 10^7$ transduction units (TU)/mL and stored at −80 °C until use. On the day of transduction, virus stocks were thawed on ice and briefly centrifuged (Sprout mini-bench top

centrifuge) to collect contents. The plasmids used to generate these particles are described section *2.3 Production of Astrocyte-Conditioned media (ACM)*.

Spent astrocyte medium was removed and replaced with a mixture containing 426 µL astrocyte medium, 4 µL polybrene and 70 µL of the appropriate lentiviral particles, yielding a total volume of 500 µL per well. Cells were put back in the incubated for 20h.

After 20h, viral particle containing medium was replaced with 2 mL fresh astrocyte medium, and cultures were monitored daily for morphology and GFP expression.

2.3.1.3 FACS Sorting of Transduced Astrocytes

When transduced cultures reached confluence, GFP-positive cells and GFP- negative cells were separated via fluorescence-activated cell sorting (FACS).

Astrocyte medium was aspirated, and cells were washed once with Dulbecco's phosphate-buffered saline (DPBS), before incubation with 200 µL Trypsin–EDTA for 5 minutes. Trypsin was immediately neutralised with 2ml astrocyte medium. Cells were pelleted by centrifugation (350 × g, 5 min) and resuspended in 500 µL PBS + 1% bovine serum albumin (BSA) on ice.

FACS sorting was performed using a BD Biosciences flow cytometer. Sorted cells were replated at 100,000 cells/well in 1 mL astrocyte growth medium. The medium was replaced the following day to remove residual sorting buffer, and cultures were maintained until passage 8.

2.3.1.4 Astrocyte-Conditioned Media (ACM) collection

After 72h plates were removed from the incubator and spent media collected under aseptic conditions within a Class II laminar flow cell culture hood. Media from all wells corresponding to the same experimental condition (OVER-GFAP, MUT-GFAP, or GFP-Control) was pooled, mixed thoroughly, split into 1ml aliquots, and stored at −80 °C. Spent media was collected at passages 6 and 8.

2.3.2 Lentiviral Transduction 2

Lentiviral transduction of human primary astrocytes was performed by the group of Alex Tarr, molecular virology lab at the University of Nottingham, following a protocol adapted from previously published work (Jalal et al., 2019).

2.3.2.1 Lentiviral Particle Production

HEK293-T cells were seeded at a density of 1.5 x10^6 cells per 10cm high-binding tissue culture dish in 8 ml of high-glucose Dulbecco's Modified Eagle Medium (DMEM) (41965, Gibco, UK). After 24 hours cells were examined to confirm even distribution and healthy morphology.

For transfection, 2,000 ng of pCMVR8.74 capsid-coding plasmid and 2,000 ng of pDM2 VSV-G glycoprotein-coding plasmid were incubated together with 2,000 ng of the respective transgene plasmid (OVER-GFAP, MUT-GFAP, or GFP-control) in 600 µL of OptiMEM I (Thermo Fisher Scientific). To this, 24 µL of polyethylenimine (PEI; Polysciences) was added. The mixture was gently mixed by pipetting and incubated for 40 minutes at room temperature to allow for the formation of PEI–DNA complexes.

During the incubation period, DMEM in each HEK293T dish was replaced with 7 mL of OptiMEM I. The entire 600 µL volume of PEI–DNA complexes were then added to the corresponding dish, and plates were gently agitated to promote uniform distribution. Cultures were incubated for 5 h at 37 °C in a humidified atmosphere containing 5% CO_2, after which the medium was replaced with 10 mL of high-glucose DMEM.

Cells were maintained for 4 days in a humidified tissue culture incubator (37 °C, 5 % CO_2) to allow viral particle production. Supernatants were harvested and clarified by filtration through a 0.45 µm polyethersulfone (PES) membrane. Viral particles were concentrated by ultracentrifugation at 100,000 × *g* for 2.5 h at 4 °C through a 1 mL 20% (w/v) sucrose cushion. Supernatants were discarded, and psueudoparticles were resuspended in 500 µL of sterile PBS overnight at 4 °C.

2.3.2.2 Human Primary Astrocyte Cell Culture

Astrocytes were cultured using standard cell culture procedure as described in *section 2.1 General Cell Culture Protocol*. Cells were either seeded in 12 well plates directly or into 12 well plates containing 19mm coverslips pre-coated with poly-DL-ornithine hydrobromide (PDLO). PDLO coating was prepared by diluting a 2 % stock solution to 0.1 % in filter-sterilised (0.22 µm) deionised water, adding 1 mL to each coverslip, and incubating at 37 °C for 1h. Coverslips were then washed three times with filter-sterilised deionised water to remove excess PDLO and air-dried within class II Laminar flow cell culture hoods for at least 2 h before use. Astrocytes were counted using trypan blue and an TC20 Automated Cell Counter before being seeded at a density of 1.5 x10^6 cells per well. Cells were left to adhere for 24h in a tissue culture incubator.

2.3.2.3 Lentiviral Transduction (Transduction 2)

After 24h Astrocyte medium was removed and replaced with 500µl OptiMEM I per well. one of the three spueudoparticles conditions (OVER-GFAP, MUT-GFAP, or GFP-control) were added to each relevant well at either a neat concentration (50µl) or 1 in 5 concentration (10µl) and put back in the incubator for 4h. After 4h the 500µl OptiMEM I per well was replaced with 2mL of astrocyte medium.

After the media change astrocytes were either returned to incubators or immediately placed within the Livecyte Imaging Chamber (PhaseFocus; see section below). After 24 hours, plates that were returned to incubators underwent another 2ml astrocyte media

change before being returned to the incubator for a maximum of 24h for neat lentiviral particle concentration or 48h for 1:5 diluted lentiviral particles.

2.3.2.4 Transduced Astrocytes PhaseFocus LiveCyte Acquisition

After the media change, Astrocytes that had been seeded into a 12-well clear flat-bottomed plate (3513, Corning®) were placed within the humidified PhaseFocus Livecyte Imaging chamber within 1h post-transduction where they were maintained at 37°C, 5% CO2 in air.

Four regions per well were imaged: Two 1 mm2 regions with a 10× objective and two 0.5 mm2 regions with a 20× objective. Phase contrast and fluorescence images were acquired for each region every hour over a 72h period, each condition had a repeat of 2 wells with 4 FOVs per well imaged. Image datasets were analysed using PhaseFocus Cell Analysis Toolbox across the full duration of the assay. Data from every FOV per condition were averaged together and normalised to their baseline value. Due to the low number of repeats per condition, statistical analysis was not performed for this experiment. Data is represented as mean ± SDEV.

2.3.2.5 Astrocyte-Conditioned Media (ACM) Collection

At the completion of the LiveCyte acquisition, plates were removed from the incubator and spent media collected under aseptic conditions within a Class II laminar flow cell culture hood. Media from all wells corresponding to the same experimental condition (OVER-GFAP, MUT-GFAP, or GFP-Control) was pooled, mixed thoroughly, aliquoted, and stored at −80 °C.

Spent media from the other 12-well plates was collected in an identical manner after a designated incubation time (see section *2.3.2.3 Lentiviral Transduction (Transduction 2)*).

2.3.2.6 Plate Fixing and Immunocytochemistry of Transduced Astrocytes

Following media aspiration, coverslips were immediately fixed in 4% paraformaldehyde (PFA) as described in *Section 2.2.1 Coverslip Preparation and Fixing* and stained according to the ICC protocol described in *Section* 2.2 *Immunocytochemistry (ICC) General Protocol*. Following permeabilisation and blocking GFAP, ALDH1L1 and TSPO primary antibodies were diluted to the appropriate concentration in blocking buffer and incubated with coverslips overnight. The secondary antibodies, Anti – rabbit Alexa Fluor 568, Anti – mouse Alexa Fluor 647 and Anti – goat Alexa Fluor 750 were applied at a 1:500 dilution in blocking buffer together for 2h, followed by DAPI staining (0.01 mg/mL). Coverslips were mounted onto microscope slides using Fluoromount™ Mounting Medium and sealed with nail varnish.

2.3.2.7 Transduced Astrocyte Immunocytochemistry (ICC) Image Analysis

Slides were imaged using a fluoroviewMP4000 confocal multiphoton lasers scanning microscope. Image analysis was conducted using Fiji ImageJ software, regions of interest (ROI) were drawn around astrocytes in the field of view. A mean grey value of each ROI was calculated for each channel. An average background signal was also measured for each channel and subtracted from ROI values. Due to the low number of repeats per condition statistical analysis was not conducted for this experiment. Data is represented as mean ± SDEV.

2.4 CRISPR-Edited TERT2-HUVECs E-selectin Expression Assay

2.5.1 Cell Culture of CRISPR Edited TERT2 Huvecs (Clone C8)

To assess the effect of astrocyte conditioned medium on endothelial cells, we made use of CRISPR edited Tert2HUVECs which report on e-selectin upregulation in endothelial cells. E-selectin is upregulated in endothelial cells which enhances adhesion and recruitment of immune cells – thereby reflecting a form of inflammatory response in endothelial cells. The Human umbilical vein endothelial cells (HUVECs) were previously edited by collaborators. In brief, human umbilical vein endothelial cells (HUVECs), immortalised through the expression of human telomerase reverse transcriptase (hTERT2), were obtained from a single newborn human female donor (American Type Culture Collection [ATCC], CRL-4053, Lot# 70023166).

These cells were edited using CRISPR-Cas9 to insert a NanoLuc Binary Technology (NanoBiT) system HiBiT tag at the endogenous E-selectin gene locus, allowing for the monitoring of E-selectin expression, as described by Ogrodzinski et al. (2023). The validated clone (Clone 8) was expanded, cryopreserved, and stored in liquid nitrogen for future use.

2.5.1.1 Thawing and Passaging of CRISPR Edited TERT2 Huvecs (Clone C8)

Subsequent culturing of these cells was performed by the COMPARE Laboratory, University of Nottingham, in accordance with their standard endothelial cell culture protocol. This procedure is consistent with the method described in section *2.1 Cell Culture Protocol,* except for the passaging step. In this instance, cells were detached using Trypsin/Ethylenediaminetetraacetic (T4049, Sigma-Aldrich, UK) diluted 1:4 in PBS. Enzymatic activity was neutralised using 10ml of Dulbecco's Modified Eagle Medium (DMEM) supplemented with 10 % foetal calf serum (FCS).

Cells were maintained in Medium 200 (M200500, ThermoFisher Scientific, USA) supplemented with 2.2% large vessel endothelial supplement (LVES) (50X, A1460801, ThermoFisher Scientific (Gibco), USA).

2.5.1.2 Seeding of CRISPR Edited TERT2 HUVECs (clone C8)

After reaching 70% confluency, cells were detached (as described in the above section) and centrifuged at 200 xg for 5 minutes RT and the supernatant aspirated. Following centrifugation, the resulting pellet was resuspended in 2 mL of Medium 200. 10µl of cell suspension was loaded onto a haemocytometer. Cells were counted 3 times within the central 1mm^2 square and the average taken from each count was multiplied by 10,000; representing the average amount of cells present in 1ml of media. From this the volume required to obtain a seeding density 32,000 per well was calculated, and the cell suspension was diluted appropriately using Medium 200.

100µL of hTERT2 HUVECs cell suspension per well was seeded onto flat bottomed white Greiner-96 well plates (655089, Greiner Bio-one, UK) and left in the incubator for 24h before experimentation, to allow for cell adherence.

2.5.2 Establishing TERT2 HUVEC Cell Viability in Conditioned Media

GFP-control astrocyte-conditioned media (GFP-ACM) which was collected from lentiviral transduction 1 astrocytes (see section *2.3 Production of Astrocyte-Conditioned media*) was thawed from −80 °Cat RT and used immediately. The GFP-ACM was diluted with Medium 200 to generate six concentrations: 100%, 80%, 60%, 40%, 20%, and 0% (100% medium 200, positive control) and applied to hTERT2 HUVECs cells seeded on a white Greiner-96 well plate (as described in above sections), with each well receiving a final volume of 50 µL. For each concentration, an additional well containing the corresponding dilution without hTERT2 HUVECs was added to serve as a background control. After GFP-ACM was applied to the cells they were placed back into the incubator for 24 hours.

2.5.2.1 Fluorescence Detection

Following the incubation, 5 µl of 10X PrestoBlue (A13261, ThermoFisher Scientific, USA) was added to each well and incubated for an additional hour. After incubation, the plate was removed from the incubator, and an opaque plate back was placed on the bottom of the wells to improve the florescence signal detection. Florescence intensity was measured using a PHERAstar FS plate reader (BMG LabTech) with filters set to detect emissions at a 570–590 nm range.

2.5.2.2 Data Analysis

The background control was subtracted from each corresponding well, and all readings were normalised to the average positive control value. All numerical data was analysed using Prism version 10.0 (GraphPad Software), and appropriate statistical analysis (one-way ANOVA test) was conducted (ns ≥ 0.05, * ≤ 0.05, ** ≤0.01, *** ≤ 0.001, **** ≤ 0.0001). Data is represented as mean ± SDEV.

2.5.3 CRISPR-Edited TERT2-HUVECs E-selectin Assay

2.5.3.1 Media Preparation and 96 Well Plate Layout

hTERT2 HUVECs were seeded into duplicate sets of white Greiner 96well plates for two time points (6 h and 24 h): **Plate A** for assessment of cell viability and **Plate B** for quantification of luminescence signalling (as described in Section *2.5.2 Establishing TERT2 HUVEC cell viability in conditioned media*). Each well received 50 µL of astrocyte-conditioned media (ACM) from one of three astrocyte conditions:

- GFP control ACM (GFP-ACM)
- GFAP-overexpressing ACM (OVER-ACM)
- GFAP ACM (MUT-ACM)

ACM was collected from **lentiviral transduction 1** (see section 2.3.1 *Lentiviral Transduction 1*).

ACM was thawed from −80 °C at RT and used immediately. Wells containing 50 µL of fresh astrocyte medium served as the negative control, while positive control wells were treated with 50 µL of 1 nM TNF-α prepared in fresh astrocyte medium. Plates were incubated at 37 °C, 5 % CO_2 until the designated end point (6 h or 24 h).

2.5.3.2 Luminescence Detection

Following incubation, luminescence was measured to assess the amount of e-selectin expression. Purified LgBiT protein (N3030, Promega, USA) was diluted 1:400 in HEPES buffer (10mM) containing 0.1% BSA and added to plate B wells. Cells were incubated for 20 min at 37°C.

Subsequently, Furimazine substrate (N1110, Promega, USA) for the purified LgBiT protein was diluted 1:400 in Hanks' Balanced Salt Solution (HBSS) supplemented with 0.1% BSA and added to each well. Plates were incubated for 5 minutes in the dark at RT.

After incubation, the plates were removed from the incubator, and an opaque plate back was placed on the bottom of the plate to improve signal detection. Luminescence was then measured using a PHERAstar FS plate reader with filters configured to detect emission at 400 nm.

2.5.3.3 Fluorescence Detection

Cell viability was measured for Plate A following the same protocol previously described in Section *2.5.2 Establishing TERT2 HUVEC cell viability in conditioned media*.

2.5.3.4 Data Analysis

All numerical data was analysed using Prism version 10.0 (GraphPad Software), and appropriate statistical analysis (two-way ANOVA) was conducted to assess the effects of ACM treatment and incubation time on E-selectin expression. Post hoc comparisons were performed using Tukey's multiple comparisons test. Statistical significance was

defined as (ns ≥ 0.05, * ≤ 0.05, ** ≤0.01, *** ≤ 0.001, **** ≤ 0.0001). Data is represented as mean ± SDEV.

2.5 Cytokine Array

To identify and compare cytokines present in astrocyte conditioned media (ACM) harvested from astrocytes either over expressing GFAP, expressing mutant GFAP (as seen in AxD) or a GFP control, a cytokine array was performed using the Proteome Profiler Human XL Cytokine Array Kit (ARY022B; R&D Systems, UK) to identify cytokines present in astrocyte-conditioned media. All procedures were conducted according to the manufacturer's instructions.

Array buffer 6 was applied as a blocking solution for the nitrocellulose membranes containing 105 different capture antibodies, cells were incubated in the solution at room temperature for 1h. Following blocking, 500 µL of either CON-ACM, OVER-ACM or MUT-ACM collected from lentiviral transduction 1 (*see section 2.3.1 Lentiviral Transduction 1*) was diluted in 1 mL of Array Buffer 6 and incubated with the membranes overnight at 4 °C.

After incubation, membranes were washed three times for 10 minutes each in 1× Wash Buffer, then incubated with the Detection Antibody Cocktail for 1 hour at room temperature. The membranes were subsequently washed three additional times, as previously described. Streptavidin-HRP was then applied to the membranes and incubated for 30 minutes at room temperature, followed by a further three washes.

Enhanced chemiluminescence (ECL) reagents (Perkin Elmer, UK) were then added to the membranes, which were immediately exposed to Amersham Hyperfilm® ECL (Scientific Laboratory Supplies, UK). Multiple exposure times (ranging from 2 to 10 minutes) were performed to avoid overexposure. Films were developed in Ilford PQ Universal developer (Ilford Photos, UK) until signal detection, rinsed briefly in water, and then fixed using Ilford Hypam Fixer (Ilford Photos, UK).

2.5.1 Cytokine Array Analysis

The mean pixel intensity of each cytokine spot was measured using FIJI software. Each cytokine was represented by two duplicate spots per membrane, which were averaged to generate a single value. Positive and negative control spots, located at the four corners of each array, were also measured. A background correction was applied to each spot by subtracting the mean background pixel intensity, and values were subsequently normalised (divided by to the average intensity of the positive control spots) to account for membrane-membrane variation. Following normalisation, each spot was mapped back to the original cytokine array template to identify the corresponding cytokine of interest.

Numerical data was analysed using Prism version 10.0 (GraphPad Software), and appropriate statistical analysis (Two-way ANOVA) was conducted. Post hoc comparisons were performed using Tukey's multiple comparisons test to identify and compare cytokine levels in GFP-ACM, OVER-ACM and MUT-ACM. Statistical significance was defined as (ns ≥ 0.05, * ≤ 0.05, ** ≤0.01, *** ≤ 0.001, **** ≤ 0.0001). Data is represented as mean ± SDEV.

2.6 Calcium Imaging of Human Primary Astrocytes

2.6.1 General Calcium Imaging Protocol

To quantify the responses of human primary astrocytes to various neurotransmitters, calcium transients were measured using a calcium imaging assay, enabling precise quantification of cellular responses based on calcium transients.

2.6.1.1 Seeding of Human Primary Astrocytes for Calcium Imaging

Astrocytes were cultured and passaged as described in section *2.1.1 General Passaging of Cell Lines Protocol*. For cell counting, 20 µL of cell suspension was mixed with 20 µL of 0.4 % Trypan Blue solution, loaded onto a dual-chamber cell counting slide (1450011, Bio-Rad Laboratories, UK), and counted using a TC20 Automated Cell Counter.

Cells were seeded into Greiner 12-well plates (665180, Greiner Bio-One, Germany) containing 19 mm coverslips pre-coated with poly-DL-ornithine hydrobromide (PDLO). PDLO coating was prepared by diluting a 2 % stock solution to 0.1 % in filter-sterilised (0.22 µm) deionised water, adding 1 mL to each coverslip, and incubating at 37 °C for 1h. Coverslips were then washed three times with filter-sterilised deionised water to remove excess PDLO and air-dried within class II Laminar flow cell culture hoods for at least 2 h before use.

Based on the live cell count, the suspension was diluted in astrocyte medium to achieve a cell density of approximately 6×10^4 cells per well on the day of imaging. 2ml of this suspension was added per well and left to incubate for at least 24 h to recover from the passaging before use.

2.6.1.2 Coverslip Preparation

Coverslips were removed from the incubator and taken out of the astrocyte medium before being washed three times with calcium imaging buffer (room temperature, RT, *see table 2-1*). The imaging buffer was then aspirated, and coverslips were incubated with one of three calcium indicators:

- Fluo-5 AM (1 µM) (F14222, Thermo Fisher Scientific, UK)
- Fluo-4 AM (10 µM) (F14201, Thermo Fisher Scientific, UK)
- Fura-2 AM (5 µM) (F1201, Thermo Fisher Scientific, UK)

Calcium indicators were prepared from frozen stock solutions dissolved in DMSO. For Fluo-5 AM, the DMSO stock also contained 20% Pluronic F-127. Stocks were defrosted immediately before use and diluted in calcium imaging buffer to the working concentrations indicated above.

Coverslips were incubated in the calcium indicator solution for 30 min in the dark and subsequently maintained in darkness for the remainder of the protocol. After incubation, coverslips were washed by flooding with 5 mL of calcium imaging buffer and incubated for a further 15 min at RT before imaging.

2.6.1.3 Superfusion System

Coverslips were mounted onto a closed bath imaging chamber (Warner Instruments, USA) using vacuum grease (59-TGZ0002, Oxford Instruments, UK). The perfusion chamber was attached to a PH-1 platform (64-0284, Warner Instruments, USA) providing clamping between the chamber and coverslips to create a watertight seal. The platform was mounted on a Leica DM IRB inverted fluorescence microscope.

Warner PE Tubing (Warner Instruments, USA) was connected to each end of the chambered slide, connecting the chamber to a gravity based superfusion apparatus and a vacuum pump to maintain continuous flow. Using this system, coverslips were continuously superfused throughout experiments at a flow rate of 2ml/min at room temperature.

At the start of each recording, calcium imaging buffer was superfused through the system for 30 seconds to establish baseline conditions, followed by an additional 2 minutes of calcium imaging buffer application, serving as the negative control. Neurotransmitters (*see table 2-4*) were then applied via superfusion for 2 min each; the neurotransmitters and the of their application varied between experiments. At the conclusion of each experiment, ionomycin (1 µM, a calcium ionophore that raises cytosolic calcium by promoting extracellular calcium entry) was applied for 2 min as a positive control.

Ionomycin and all Neurotransmitter used were prepared as described in *Table 2-4*. Frozen stock solutions were thawed immediately prior to use and diluted to the indicated working concentrations in calcium imaging buffer. All reagents were obtained from Sigma-Aldrich, UK.

Table 2-4: Preparation of neurotransmitter and ionomycin solutions for calcium imaging experiments. *Stock solutions were stored at −20 °C, thawed immediately before use, and diluted in calcium imaging buffer to the indicated working concentrations. All reagents were obtained from Sigma-Aldrich, UK.*

Reagent	Frozen stock (-20°C)	Working Concentration	Identifier
Histamine dihydrochloride (Histamine)	100mM (dissolved in deionised water)	1µM or 100µM	Cat# H7250

adenosine triphosphate (ATP) disodium salt hydrate	N/A	1µM or 100µM	Cat# A3377
L-Glutamic acid (Glutamate)	100mM (dissolved in deionised water)	100µM	Cat# G1251
Ionomycin	2mM (dissolved in ethanol)	1µM	Cat# I0634

2.6.1.4 Florescence Microscopy

Calcium imaging was performed on a Leica DM IRB Inverted Fluorescence Microscope, equipped with a 10x/0.30 NA objective. Excitation and emission wavelengths were 488 nm and 510 nm respectively. Images were acquired with a Hamamatsu High Resolution Digital CCD Camera system in conjunction with Andor iQ Live Cell Imaging Software. Images were taken at a rate of 1 frame per second (fps) or 0.5 fps if Fura-2 AM is used.

2.6.1.5 Image Analysis

Images were processes using FIJI Image J software. Data analysis was conducted using R (4.4.2) and R studio. Regions of interest (ROI) were drawn around astrocytes in the field of view. The mean grey value for each ROI was calculated. Data was normalised using the following calculation:

$$\Delta F/F = \frac{F_t - F_0}{F_0}$$

Where F0 was the average fluorescence of a 10 second period of buffer stimulation prior to the commencement of the experimental protocol, and F_t is the fluorescence intensity at time t.

2.6.2 Optimisation of Calcium Imaging Protocol

Several factors were carefully considered when optimising the calcium imaging assay to maximise astrocyte health and detection of changes in astrocyte calcium signalling. To achieve this, key variables within the protocol were systematically evaluated, as described below.

2.6.2.1 Optimisation of Astrocyte Response Thresholds

To quantify cellular responses, we assessed the useability of an automatic threshold to detect an astrocyte calcium transient. We optimised the following formula to define the response threshold:

$$\textit{Response Threshold} = \textit{Baseline} + (|\textit{Baseline}| \times x) + \textit{Stdev} \times y)$$

In this equation:

- Baseline: the average fluorescence intensity of three frames taken one frame before the start of each event.
- |*Baseline*| (absolute baseline): The positive value of the baseline, to ensure the scaling component of the equation is always positive.
- Stdev: standard deviation of the fluorescence signal over the same pre-event baseline period.
- x is the percentage increase above the absolute baseline.
- y is the multiple of the standard deviation (Stdev).

To optimise the automated data analysis, we systematically tested a range of parameter combinations:

- Percent increases above the baseline from 0% to 100%, in 10% increments
- Multiples of the standard deviation from 1 to 20.

In order to assess the automated threshold of a response, we compared the automated ranges against a gold standard. The gold standard was a response, as determined by eye, by an experienced observer. A positive response, as assessed by gold standard and automatic thresholding was given a classification of 1. A lack of a response was given a classification of 0. To assess the goodness of fit of the automated thresholds against our gold standard we used the following formula:

$$(\textit{Gold standard response [0 or 1]} - \textit{automated response [0 or 1]})^2$$

This measure of goodness of fit ranges from 0-1. It will measure 0 when the automated response matches the manual classification, and 1 when it does not. The average value of this goodness of fit was determined for each automatic threshold. The closer this value is to 0, the better the automated detection matches the gold standard. The automated threshold that produced the lowest average error was selected as the optimal statistical cut-off for defining a cellular response.

The optimal automatic threshold (as compared to gold standard) was determined for each calcium indicator that we used [Fura-2 AM, Fluo-4 AM, and Fluo-5 AM]. For each calcium indicator four independent experiments (N = 4) were compared.

2.6.2.2 Selection of Appropriate Calcium Indicator

To determine the most appropriate calcium indicator, the standard calcium imaging protocol (Section XYZ) was followed. Astrocytes were loaded with either Fluo-5 AM (1 µM), Fluo-4 AM (10 µM), or Fura-2 AM (5 µM) for 30 min, followed by a 15 min buffer incubation. Standard imaging was then performed, with sequential superfusion of 30s of calcium imaging buffer to establish baseline conditions followed by an additional

application of calcium imaging buffer (negative control), histamine or ATP (1 µM), and ionomycin (positive control).

2.6.2.2.1 Data Analysis

Numerical data was analysed using Prism version 10.0 (GraphPad Software), and appropriate statistical analysis (two-way ANOVA) was performed to evaluate the effect of calcium indicator choice on astrocyte response detection. Post hoc comparisons were performed using Tukey's multiple comparisons test. Statistical significance was defined as (ns ≥ 0.05, * ≤ 0.05, ** ≤0.01, *** ≤ 0.001, **** ≤ 0.0001). Data is represented as mean ± SDEV.

2.6.2.3 Optimisation of Coverslip Preparation

To determine if the surface astrocytes were seeded onto influenced cell health and responsiveness, astrocytes were seeded onto coverslips coated either with PDLO (as described in Section *2.6.1.2 Coverslip Preparation*) or gelatin.

Within a class II Laminar flow cell culture hood, Sterile 19mm glass coverslips were placed in 12-well plates. A 2% (w/v) gelatin solution was prepared in filter-sterilised (0.22 µm) deionised water. An excess of 80µl of the gelatin solution was spread over the coverslips before removing 40µl to ensure efficient coverage. Coverslips were left to incubate for 30 minutes then air-dried at RT for a minimum of 2 h before use.

Following coating, the standard calcium imaging protocol was performed. Astrocytes were loaded with Fura-2 AM (5 µM) for 30 min, followed by a 15 min buffer incubation. Standard imaging was then performed, with sequential superfusion of 30s of calcium imaging buffer to establish baseline conditions followed by an additional application of calcium imaging buffer (negative control), histamine or ATP (1 µM), and ionomycin (positive control).

2.6.2.3.1 Data Analysis

All numerical data was analysed using Prism version 10.0 (GraphPad Software), and appropriate statistical analysis (Multiple unpaired t tests) was performed to evaluate the effects of coverslip coating material on astrocyte responsivity. Statistical significance was defined as (ns ≥ 0.05, * ≤ 0.05, ** ≤0.01, *** ≤ 0.001, **** ≤ 0.0001). Data is represented as mean ± SDEV.

2.6.3 Calcium Imaging of Human Primary Astrocytes Treated with Astrocyte-Conditioned Media (ACM)

To investigate the impact of astrocyte-conditioned media (ACM) on healthy astrocytes, calcium imaging was used to measure changes in astrocyte responsivity after a 24h

incubation time in ACM from one of three conditions (GFP-control, OVER-GFAP or MUT-GFAP).

2.6.3.1 GFP-Control ACM vs Fresh Astrocyte Medium

Before investigating the effects of all three ACM treatments on naive astrocytes, a preliminary experiment was conducted to determine whether GFP-control ACM influences astrocyte responsiveness compared to fresh astrocyte medium.

Using the standard calcium imaging protocol (see section *2.6.1 General Calcium Imaging Protocol*), 24 h prior to imaging, spent astrocyte medium was replaced with 1 mL GFP-control ACM or fresh medium. Cells were loaded with Fluo-4 AM (10 µM) for 30 min, followed by a 15 min buffer incubation. During imaging, calcium imaging buffer was superfused for 30 s (baseline), followed by:

1. Calcium imaging buffer (negative control).
2. Histamine (1 µM), ATP (1 µM), and glutamic acid (100 µM) applied in alternating order.
3. Ionomycin (1 µM, positive control).

2.6.3.1.1 Data Analysis

Numerical data was analysed using Prism version 10.0 (GraphPad Software), and appropriate statistical analysis (Multiple unpaired t tests) was performed to evaluate the effect of GFP-ACM on Astrocyte responsivity in comparison to fresh astrocyte medium. Statistical significance was defined as (ns ≥ 0.05, * ≤ 0.05, ** ≤0.01, *** ≤ 0.001, **** ≤ 0.0001). Data is represented as mean ± SDEV.

2.6.3.2 Astrocyte Conditioned Media (ACM) Calcium Imaging Assay

The standard calcium imaging protocol was followed with the modification that, 24 h prior to imaging, spent astrocyte medium was replaced with 1 mL of GFP-ACM, OVER-ACM, or MUT-ACM. Cells were loaded with Fluo-4 AM (10 µM) for 30 min, followed by a 15 min buffer incubation. During imaging, calcium imaging buffer was superfused for 30 s (baseline), followed by:

1. Additional calcium imaging buffer (negative control)
2. Histamine (100 µM) and ATP (100 µM) in alternating order
3. Ionomycin (1 µM, positive control)

2.6.3.2.1 Data Analysis

Numerical data was analysed using Prism version 10.0 (GraphPad Software), and appropriate statistical analysis (ordinary one-way ANOVA) was performed to evaluate the effects of various ACM treatments on astrocyte responsivity to Histamine and ATP. Post hoc comparisons were performed using Tukey's multiple comparisons test. Statistical significance was defined as (ns ≥ 0.05, * ≤ 0.05, ** ≤0.01, *** ≤ 0.001, **** ≤ 0.0001). Data is represented as mean ± SDEV.

2.6.4 Calcium Imaging of Reactive-Like vs Quiescent-Like Human Primary Astrocytes

In order to establish the impact on phenotype shift from quiescent to reactive astrocyte on calcium signalling behaviour, an established model of quiescent state astrocytes was compared with the human primary astrocytes used throughout the thesis, which exhibit a reactive phenotype.

As detailed by White et al. (2024), ScienCell Human primary astrocytes (SC1800s) that have been split and cryopreserved as described in section *2.1.3 Human Primary Astrocyte Cell Line* were thawed and maintained in either regular Astrocyte medium (serum) or Astrocyte medium without 2% FBS supplementation (serum free). Human primary astrocytes cultured in Serum-Free astrocyte medium present similarities with in vivo quiescent astrocytes, whereas those cultured in astrocyte medium containing serum were found to display morphologies similar to human reactive astrocytes (White et al., 2024).

2.6.4.1 Cell Culture of Reactive-Like and Quiescent-Like Astrocytes for Calcium Imaging

Culture of both astrocyte phenotypes was conducted by the lab group of Mattea Finelli, University of Nottingham. The standard cell culture protocol was followed for these experiments (see section 2.4.1 General calcium imaging protocol) with the modification of either standard astrocyte medium or serum-free astrocyte medium was used to maintain cells depending on their designated phenotype group. Passaging was conducted using StemPro Accutase (A1110501, Thermo Fisher Scientific, UK) instead of trypsin.

Additionally, 19mm coverslips were coated overnight with Poly-L-Lysine Solution (PLL) (1.5 µg/mL 0403; ScienCell Research Laboratories, USA) in a tissue culture incubator. Coverslips were rinsed 3x with sterile deionised water and air-dried in the culture hood before use.

2.6.4.2 Coverslip Preparation and Imaging of Reactive-Like and Quiescent-Like Astrocytes

The standard calcium imaging protocol was then followed. Cells were loaded with Fluo-4 AM (10 µM) for 30 min, followed by a 15 min buffer incubation. During imaging, calcium imaging buffer was superfused for 30 s (baseline), followed by:

1. Additional calcium imaging buffer (negative control)
2. Histamine (100 µM), ATP (100 µM), or Glutamate (100 µM)
3. Ionomycin (1 µM, positive control)

2.6.4.2.1 Data Analysis

Numerical data was analysed using Prism version 10.0 (GraphPad Software), and appropriate statistical analysis (unpaired t test and multiple unpaired t tests) was performed to evaluate the effects astrocyte reactivity on responsivity to Histamine, ATP and Glutamate. Statistical significance was defined as (ns ≥ 0.05, * ≤ 0.05, ** ≤0.01, *** ≤ 0.001, **** ≤ 0.0001). Data is represented as mean ± SDEV.

2.7 Effect of Astrocyte-Conditioned Media (ACM) Treatment on Cortical Neuron Viability

To study the effects of astrocytic GFAP upregulation on the central nervous system (CNS), primary cortical neurons were cultured and treated with astrocyte-conditioned medium (ACM) to assess its impact on neuronal behaviour, axonal growth, and overall cell viability.

2.7.1 Culture of Mouse Primary Cortical Neurones

Mouse primary cortical neurons were cultured under aseptic conditions in Class II laminar flow hoods and maintained in a humidified incubator (37 °C, 5 % CO_2). Cells were grown in Neurobasal medium (Gibco) supplemented with 1 % (v/v) GlutaMAX and 2 % (v/v) B27 supplement.

2.7.2 Animals

C57BL/6J mice (Charles River, UK) were maintained in the Biomedical Services Unit, University of Nottingham, and handled in accordance with the Animals (Scientific Procedures) Act 1986 and institutional welfare guidelines.

2.7.3 Dissection of the Mouse Cortices

Pregnant adult female mice were euthanized using a Schedule 1 method by a trained individual. The abdomen was sprayed with 70% ethanol (diluted in deionised water) in preparation for the removal of the uterus. The uterus was cut away from the abdominal cavity and embryos were removed from the uterus and amniotic sac before being decapitated using scissors. Brains were extracted by midline incision of the skull and removal with an iris spatula, then transferred to Petri dishes containing HBSS. Under a dissection microscope, cortices were separated at the midline, meninges removed, and up to six cortices placed into a sterile nunc containing 2ml of HBSS.

2.7.4 Dissociation of the Mouse Cortices

In a tissue culture hood, cortices were dissociated into small fragments using forceps and digested in 200 µL trypsin (1 mg/mL in Dulbecco's phosphate-buffered saline, DPBS) and 20 µL DNase I (50 µg/mL in sterile water) at 37 °C for 30 min. Tissue breakdown was halted with 100 µL trypsin inhibitor (final concentration 5 % v/v diluted in DPBS) in supplemented Neurobasal medium. Tissue was transferred to 50 mL falcon tube containing 6 mL neurobasal medium and washed by allowing the tissue to settle, removing most of the medium, and adding fresh medium with 10 µL DNase I. The washing step was repeated once. Cells were then dissociated by gentle trituration using a 2 mL pipette until no visible clumps remained. The suspension was brought to 10 mL with supplemented neurobasal medium and centrifuged at 250 × g for 5 min to pellet the cells.

Medium was aspirated and the remaining Pellet was resuspended in 1 mL supplemented neurobasal medium per brain to yield a stock of approximately 1.2×10^7 cells/mL.

2.7.5 Preparation of Coated Coverslips

Glass coverslips (19 mm) were sterilized in 70 % ethanol and coated overnight at 37 °C with poly-L-ornithine (PLO) (0.05 mg/mL in deionised water). On the day of cell plating, coverslips were rinsed twice with sterile dH_2O and air-dried in the culture hood.

2.7.6 Cell Seeding

For medium-density cultures, the stock suspension was diluted 1:10 in supplemented medium, then further diluted 1:6 to achieve ~2×10^5 cells/mL. 1ml of this suspension was added per well of a 12 well plate. For low-density cultures, the 1:10 dilution was further diluted 1:8 to yield ~1.5×10^5 cells/mL. 1ml of this suspension was added per well of a 12 well plate. Plates were returned to the incubator and cultured for 24 h before further experimental use.

2.7.7 Conditioned Media Addition

24 hours after cell seeding, three types of astrocyte-conditioned medium (ACM) were concentrated using 5 kDa Vivaspin® 2 centrifugal concentrators (cat. no. VS02H11, Sartorius, Germany):

- GFP control ACM (GFP-ACM)
- GFAP-overexpressing ACM (OVER-ACM)
- GFAP ACM (MUT-ACM)

For each condition, 3.5 mL ACM was thawed from −80 °C at RT and concentrated 10-fold to 350 µL. Prior to use, centrifugal concentrators were sterilised by rinsing with 70%

ethanol. In 12-well plates, a 38 µL media change was performed per well, replacing spent Neurobasal medium with one of the three concentrated ACM preparations. Control wells received 38 µL fresh supplemented Neurobasal medium, corresponding to a total media replacement of 3.8%. The small amount of media change was conducted to reduce impact on cortical astrocytes by media change, as they are highly sensitive to changes in media. Plates were then returned to incubators.

2.7.8 Plate Fixing and Immunocytochemistry of Cortical Neurons

24h after the media change, 12-well plates were fixed using 4% PFA as described in section *2.2.1 Coverslip preparation and fixing* in preparation for ICC.

Cortical neurons were stained according to the ICC protocol described in *Section* 2.2 *Immunocytochemistry (ICC) General Protocol*. Following permeabilisation and blocking, anti–acetylated tubulin primary antibody was applied at a 1:200 dilution in blocking buffer and incubated overnight. The secondary antibody, anti–mouse Alexa Fluor 488, was applied at a 1:300 dilution in blocking buffer together with DAPI and incubated for 2h. Coverslips were mounted onto microscope slides using VECTASHIELD® mounting medium.

2.7.9 Cortical Neuron Immunocytochemistry (ICC) Image Analysis

Slides were imaged using Leica DM IRB inverted fluorescence microscope in conjunction with Andor iQ Live Cell Imaging Software. Image analysis was conducted using Fiji ImageJ software and the neuroanatomy SNT plugin (Arshadi et al., 2021) were used to trace and count individual projections, which could then be measured. DAPI stain was used to count the number of individual cells per FOV. 3 FOVs were randomly selected per coverslip, and measurements were averaged across all three.

Numerical data was analysed using Prism version 10.0 (GraphPad Software), and appropriate statistical analysis (One-way ANOVA) was performed in addition to Post hoc comparisons using Tukey's multiple comparisons test, in order to evaluate the effect of Astrocyte-conditioned media on cortical neuron viability and axonal growth. Statistical significance was defined as (ns ≥ 0.05, * ≤ 0.05, ** ≤0.01, *** ≤ 0.001, **** ≤ 0.0001). Data is represented as mean ± SDEV.

Chapter 3: Results

3.1 Lentiviral Transduction of Human Primary Astrocytes

To determine whether altered GFAP expression affects astrocyte proliferation, morphology, and signalling, human primary astrocytes were transduced to overexpress GFP tagged WT-GFAP (OVER-GFAP), the AxD-associated R79H GFAP variant ((MUT-GFAP) or a GFP control (GFP-control) plasmid. Production of these cellular models was necessary in order to collect there secretomes by harvesting their spent media. The aim of these experiments was to validate the models of modified GFAP expression, as well as determine the most appropriate time to harvest the Astrocyte-conditioned media (ACM).

Throughout these experiments two different concentrations of lentiviral particles were used (neat and a 1:5 dilution) to determine if particle concentration had a deleterious effect on cell viability (see section *2.3.2 Lentiviral Transduction 2)*.

3.1.1 PhaseFocus LiveCyte Image Acquisition

To assess whether GFAP overexpression or mutation alters astrocyte viability, proliferation, and morphology over time, longitudinal live-cell imaging was performed within 1h post-transduction. Phase contrast and fluorescence images were acquired every hour for 72h, data from every FOV per condition were averaged together and normalised to their baseline value *(see section 2.3.2.4 Transduced Astrocytes PhaseFocus LiveCyte Acquisition)*.

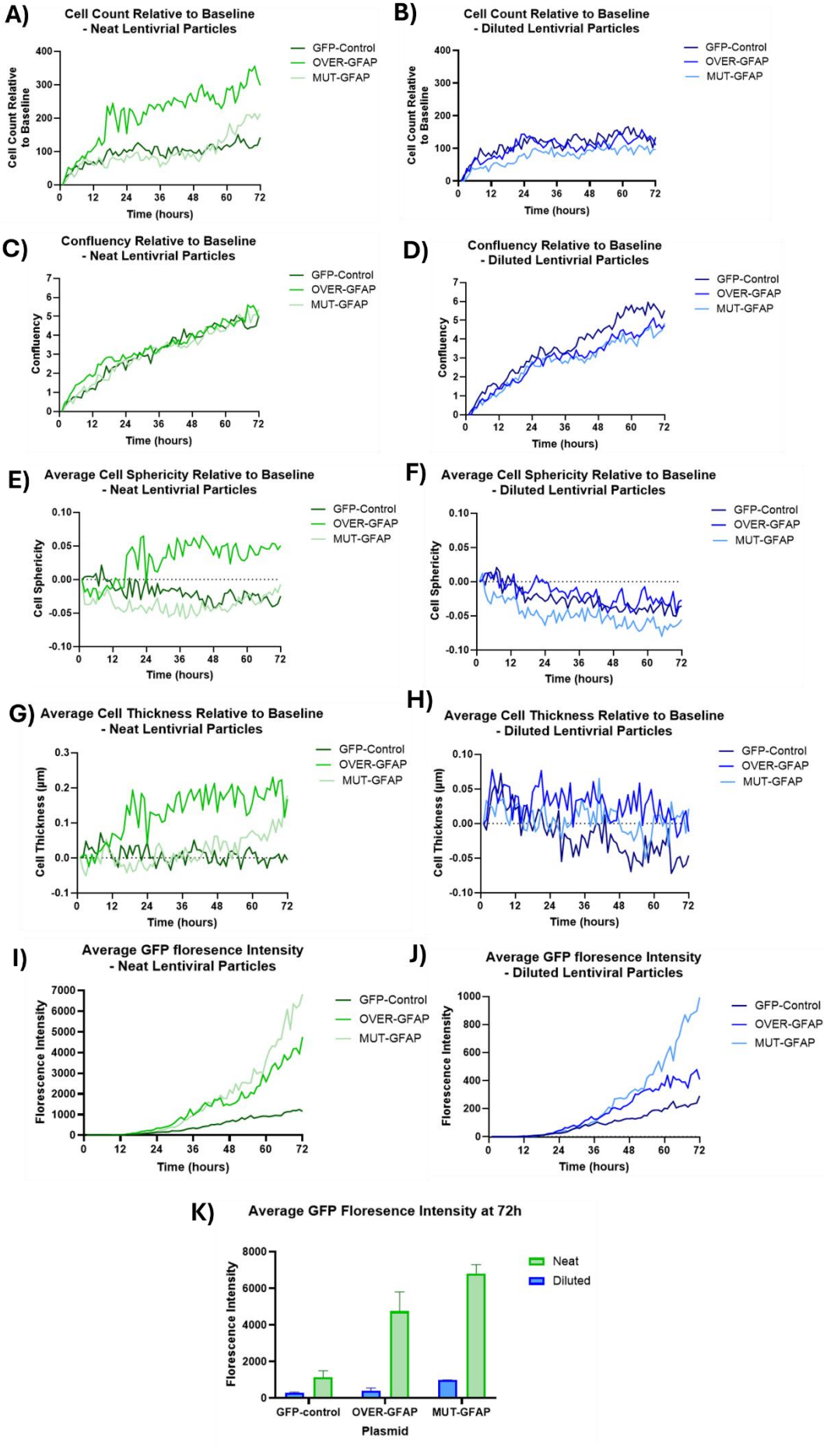
A)
Cell Count Relative to Baseline
- Neat Lentivrial Particles
Cell Count Relative to Baseline
Time (hours)
GFP-Control
OVER-GFAP
MUT-GFAP
B)
Cell Count Relative to Baseline
- Diluted Lentivrial Particles
C)
Confluency Relative to Baseline
- Neat Lentivrial Particles
Confluency
D)
Confluency Relative to Baseline
- Diluted Lentivrial Particles
E)
Average Cell Sphericity Relative to Baseline
- Neat Lentivrial Particles
Cell Sphericity
F)
Average Cell Sphericity Relative to Baseline
- Diluted Lentivrial Particles
G)
Average Cell Thickness Relative to Baseline
- Neat Lentivrial Particles
Cell Thickness (µm)
H)
Average Cell Thickness Relative to Baseline
- Diluted Lentivrial Particles
I)
Average GFP floresence Intensity
- Neat Lentiviral Particles
Florescence Intensity
J)
Average GFP floresence Intensity
- Diluted Lentiviral Particles
K)
Average GFP Floresence Intensity at 72h
Neat
Diluted
GFP-control
OVER-GFAP
MUT-GFAP
Plasmid

Figure 3-1: PhaseFocus LiveCyte analysis of astrocytes transduced with GFP-control (N=2) , OVER-GFAP (N=2), or MUT-GFAP (N=2) plasmids using neat or diluted lentiviral particles over a 72h time period. *Phase contrast and florescence images were captured every hour immediately after transduction using either neat (green) or 1:5 diluted (blue) lentiviral particles. All readings were normalised to baseline values (first measurements recorded).* ***(A, B)*** *Average cell count,* ***(C, D)*** *average confluency per FOV,* ***(E, F)*** *average cell sphericity* ***(G,H)*** *average cell thickness* ***(I, J)*** *Average GFP florescence intensity,* ***(K)*** *Average florescence intensity at 72h, data represent mean ± SD from duplicate experiments. Statistical analysis was not performed due to insufficient sample size (N).*

Results from the PhaseFocus Cell Analysis Toolbox (figure 3-1, A-H) revealed cell count and confluency steadily increased across all conditions (figure 3-1 A-D) however neat particle treatment resulted in a greater increase in cell count in OVER-GFAP and MUT-GFAP conditions than GFP-control. Quantitative analysis showed that at 72 h, the final cell count was 2.1-fold higher in OVER-GFAP and 1.5-fold higher in MUT-GFAP compared to GFP-control.

Morphological changes including astrocyte shape and cytoskeletal organisation were assessed using cell sphericity and thickness *(Figure 3-1 E–H*). In astrocytes, increased sphericity is commonly associated with retraction of fine processes resulting in a more rounded, hypertrophic morphology (Zou et al., 2019). Similarly, increased cell thickness reflects cytoskeletal remodelling and accumulation of structural proteins such as GFAP within the cell body (Lye-Barthel, Sun and Jakobs, 2013). In neat conditions, cell sphericity remained relatively unchanged in neat MUT-GFAP and GFP-control conditions across 72h, however cell sphericity increased in OVER-GFAP by 204.32% relative to GFP-control, suggesting WT-GFAP overexpression promotes cytoskeletal remodelling, specifically the loss of elongated, stellate morphology

In contrast, cell sphericity decreased across all three dilute particle conditions (GFP-control=-12.6-fold; OVER-GFAP=-10.3-fold; MUT-GFAP=-4.6-fold). When normalised to their baseline thickness (time 0h), cell thickness at 72 h was increased under neat conditions in both MUT-GFAP (+0.18 µm) and OVER-GFAP (+0.17 µm) relative to the GFP-Control group, which instead showed a slight decrease in thickness (–0.0055 µm). Meanwhile, in dilute particle conditions, thickness remained relatively stable in OVER-GFAP (-0.011µm) and MUT-GFAP (0.021µm) but decreased in GFP-control (–0.046 µm) indicating the concentration of lentiviral particles can impact the effects of GFAP expression changes on cell morphology.

GFP tracking of lentiviral transduction confirmed successful transduction across all groups regardless of particle concentration, with GFP florescence beginning to occur approximately 24h post transduction (figure 3-1 I-J). Fluorescence intensity was consistently higher under neat particle conditions, reinforced by 72 h endpoint measurements (figure 3-1 K); with an average increase of 396.44% for GFP-control, 1166.54% for OVER-GFAP, and 686.75% for MUT-GFAP relative to diluted conditions. Moreover, at both concentrations GFP-control florescence intensity (neat= 1151.96; dilute = 290.57) was markedly lower than OVER-GFAP (neat=4758.08; dilute=407.87) and MUT-GFAP (neat=6824.624; dilute=993.75). It is important to note GFP-control viral

plasmids contained mGFP rather than tGFAP (see section *2.3 Production of Astrocyte-Conditioned media (ACM)*), therefore transduction conditions are not directly comparable.

These results, indicate there are no deleterious effects of neat lentiviral particle concentration on astrocyte viability, therefore ACM, from astrocyte cultures transduced at neat concentration was selected for subsequent experiments. Additionally, it was determined 72h post-transduction is an appropriate time frame to collect ACM, as changes in transgene expression have occurred for sufficient time to induce changes in astrocyte phenotype.

3.1.2 Immunocytochemistry (ICC) of Transduced Astrocytes

After establishing that neat lentiviral transduction produced the most suitable astrocyte model, GFAP overexpression and astrocyte identity were validated by ICC using an additional transduced plate. Alongside the three transduction groups, an additional negative control group of naïve, Untransduced astrocytes was included. was added. Cells were fixed 48 h post-transduction and processed for ICC *(see section 2.3.2.6 Plate Fixing and Immunocytochemistry of Transduced astrocytes)*.

Cells were fixed at 48 h rather than 72 h (the time point used for ACM harvesting; see above section) to capture early GFAP and inflammatory protein expression while preserving optimal confluency for single-cell segmentation during ICC analysis. Notably, LiveCyte longitudinal imaging confirmed that 48h is sufficient time for robust lentiviral transgene expression to occur.

After imaging, a mean grey value of each cell ROI was calculated for each channel and an average background value subtracted, producing average fluorescence intensity readings for DAPI, GFP, GFAP, ALDH1L1 and TSPO. Due to the low number of repeats per condition statistical analysis was not conducted for this experiment. Data is represented as mean ± SDEV.

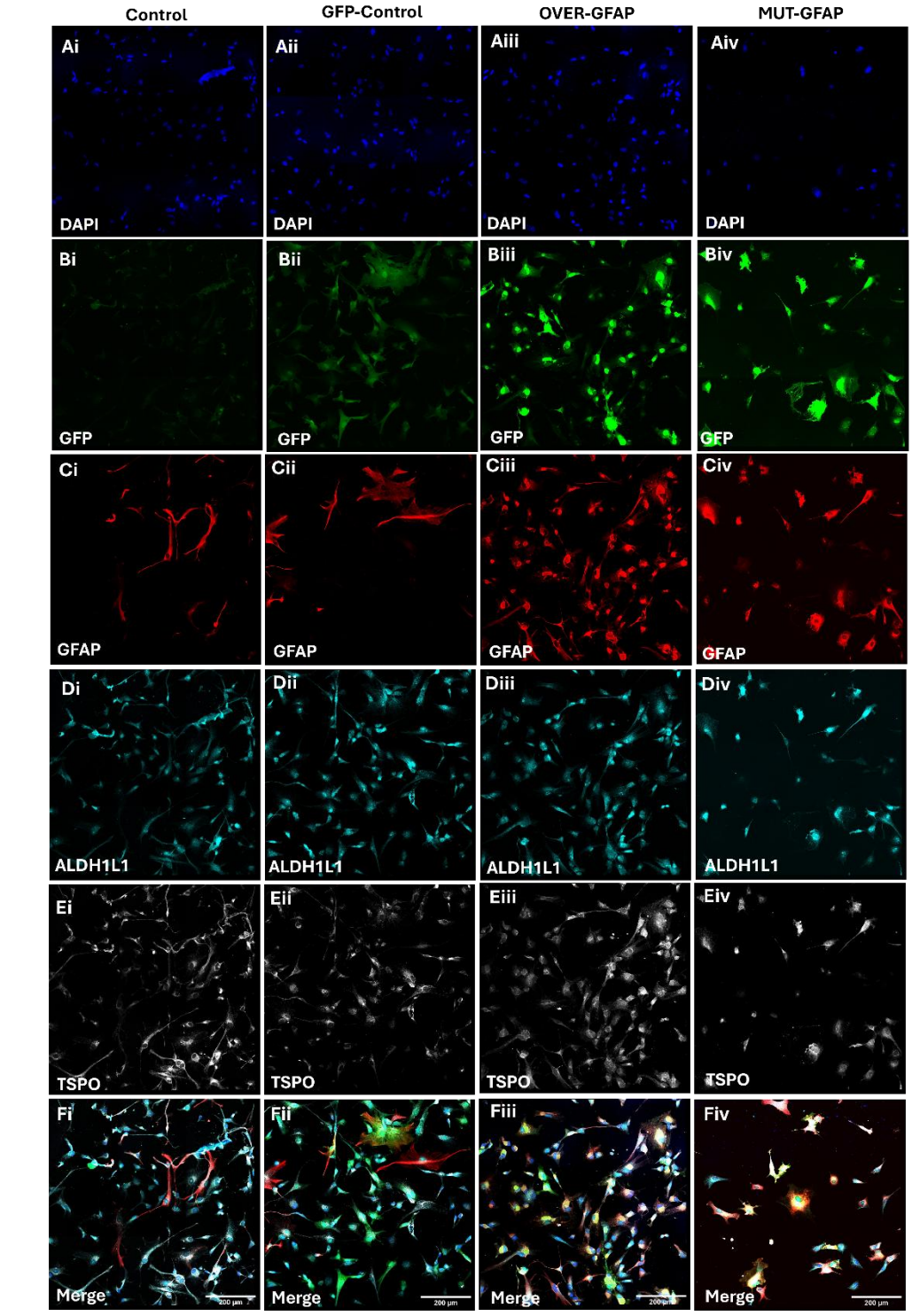
Control
GFP-Control
OVER-GFAP
MUT-GFAP
Ai
Aii
Aiii
Aiv
DAPI
Bi
Bii
Biii
Biv
GFP
Ci
Cii
Ciii
Civ
GFAP
Di
Dii
Diii
Div
ALDH1L1
Ei
Eii
Eiii
Eiv
TSPO
Fi
Fii
Fiii
Fiv
Merge
200 µm

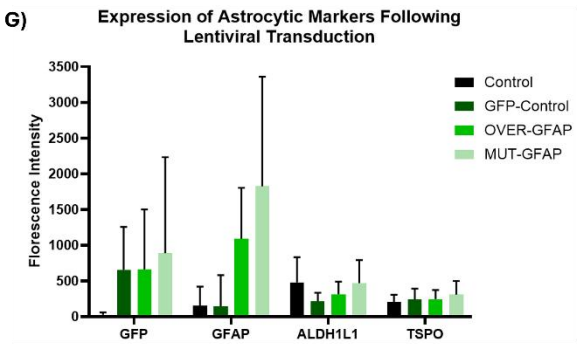
G)
Expression of Astrocytic Markers Following Lentiviral Transduction
Florescence Intensity
3500
3000
2500
2000
1500
1000
500
0
GFP
GFAP
ALDH1L1
TSPO
Control
GFP-Control
OVER-GFAP
MUT-GFAP

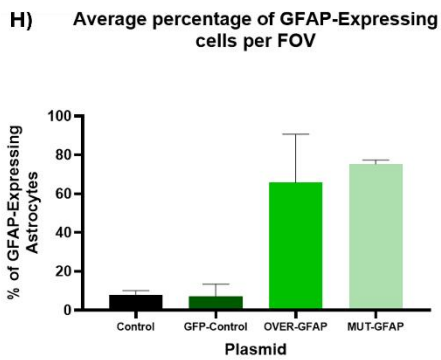
H)
Average percentage of GFAP-Expressing cells per FOV
% of GFAP-Expressing Astrocytes
100
80
60
40
20
0
Control
GFP-Control
OVER-GFAP
MUT-GFAP
Plasmid

Figure 3-2: Validation of GFAP-modified astrocyte models using ICC. *Astrocytes were fixed 48h post transduction with GFP-control (N=2), OVER-GFAP (N=3), or MUT-GFAP (N=2) plasmids. A negative control group of untransduced astrocytes (N=2) were also imaged. Cells were immunolabelled with GFAP (**Ci-Civ**), ALDH1L1(**Di-Div**), TSPO (**Ei-Eiv**). (**Ai-Aiv**) Cells were stained with DAPI to confirm the presence of astrocytes across all conditions, (**Bi-Biv)** GFP expression originating from lentiviral plasmids was also imaged, confirming successful transduction. (**G**) Average florescence intensity of each immunolabel was measured and the percentage of cells positively identified to be expressing GFAP per FOV were counted (**H**). data represent mean ± SD from duplicate experiments. Statistical analysis was not performed due to insufficient sample size (N). Images were taken at 10x magnification with scale bar representing 200 µm.*

DAPI nuclear staining (Figure 3-2 Ai–Aiv) alongside ALDH1L1 immunolabelling confirmed the presence of astrocytes across all conditions (Figure 3-2 Di–Div). GFP expression was detectable in transduced conditions (GFP-control, OVER-GFAP, and MUT-GFAP) but was largely absent in untransduced controls aside from autofluorescence (Figure 3-2 Bi–Biv), confirming successful transduction and expression. GFAP immunolabelling indicated increased expression in OVER-GFAP and MUT-GFAP groups compared to GFP-control, confirming the plasmid specific upregulation (Figure 3-2 Ci–Civ). Furthermore, the comparable GFAP expression between untransduced controls and GFP-control confirm changes in GFAP florescence cannot be attributed to the baseline process of lentiviral transduction methods. TSPO, which is upregulated in certain inflammatory conditions, showed relatively consistent expression across groups (Figure 3-2 Ei–Eiv). Merged images (Figure 3-2 Fi–Fiv) confirm colocalization of all markers, further validating astrocyte identity in all conditions.

Quantification of fluorescence intensity (Figure 3-2 G) supported these observations. GFP levels were markedly increased across transduced conditions compared to untransduced control (GFP-control= 27-fold; OVER-GFAP= 27-fold; MUT-GFAP= 36-fold). GFAP levels were only increased in OVER-GFAP (7.11-fold) and MUT-GFAP (11.8-fold) conditions, while GFP-control remained unchanged. ALDH1L1 expression fluctuated slightly between conditions (control=480.22 AU; GFP-control=215 AU; OVER-GFAP=314.97 AU; MUT-GFAP=470.29 AU), and TSPO remained broadly consistent (control=206.6 AU; GFP-control=241.14 AU; OVER-GFAP=245.53 AU; MUT-GFAP=307.52 AU).

Additionally, quantification of the percentage of GFAP-positive astrocytes per FOV (Figure3-2 H), revealed a substantial increase in the percentage of GFAP-expressing in OVER-GFAP (8.5-fold) and MUT-GFAP (9.8-fold) groups than untransduced control, whereas GFP-control remained unchanged.

It is to be noted, although Figure 3-2 may visually suggest reduced cell density in MUT-GFAP cultures, density differences in representative images reflect FOV selection variability rather than genuine reductions in cell count or viability. Furthermore, LiveCyte data *(see section 3.1.1 PhaseFocus LiveCyte Image Acquisition)* confirmed comparable cell numbers across all conditions at both the beginning and 48h into imaging - corresponding to the time point at which fixing of this plate occurred. Total cell counts were obtained from four randomly selected FOV at 1h post-transduction and again at 48

h. At 1h, cell counts were similar across groups (Control: 282; OVER: 283; MUT: 361), and by 48h all conditions showed steady increases (Control: 463; OVER: 399; MUT: 448), supporting the observation that cell density was comparable across all groups.

Overall, these results validate the effectiveness of the lentiviral transduction protocol to upregulate GFAP expression in astrocytes, however due to low sample sizes no statistical comparisons could be identified. Notably, no differences in other astrocyte/ inflammatory markers could by established between all four conditions.

3.2 The Effect of Astrocyte-conditioned Media (ACM) on CRISPR Edited TERT2 HUVECs E-selectin Expression

To investigate the presence of inflammatory mediators in astrocyte conditioned media, hTERT2 HUVECs (clone C8) previously generated by CRISPR–Cas9 engineering, as described by Ogrodzinski et al. (2023) were used.

To summarise briefly, HUVEC cells were genetically modified to express a HiBiT tag at the N-terminus of the endogenous E-selectin protein, an adhesion molecule upregulated on endothelial cells in response to inflammatory cytokines. Upon addition of the complementary fragment LgBiT, the HiBiT-tagged E-selectin reconstitutes the active luciferase enzyme, producing a luminescent signal proportional to the amount of E-selectin present on the cell surface.

By exposing these hTERT2HUVECs to astrocyte-conditioned media, I aimed to assess the communication between astrocytes and endothelial cells and whether astrocytes (GFAP-overexpressing, Mutant-GFAP) secrete factors which upregulate e-selectin expression.

3.2.1 Establishing TERT2 HUVEC Cell Viability in Astrocyte-Conditioned Media (ACM)

To ensure that ACM did not compromise endothelial viability, hTERT2 HUVEC viability was first assessed following exposure to GFP-control ACM.

To assess the effect of GFP-ACM on endothelial cell viability, hTERT2 HUVECs were incubated for 24 h with GFP-ACM diluted in standard HUVEC Medium 200 at concentrations ranging from 0 % to 100 % ACM in 10 % increments.

Cell viability was then measured using the PrestoBlue assay. PrestoBlue fluorescence corresponds to the reduction of resazurin in the presence of metabolically active cells. The resulting fluorescence intensity is proportional to the number of viable cells, providing an indirect quantitative measure of cell viability. Fluorescence intensity from the 0 % ACM condition (i.e.,100 % Medium 200) served as the positive control and were defined as representing 100% viability. Viability values for all other ACM dilutions were expressed as a percentage of this positive control to quantify the relative reduction in

metabolic activity induced by GFP-ACM. A background control (wells with no cells seeded) was included for each concentration, and its fluorescence was subtracted from the corresponding sample values.

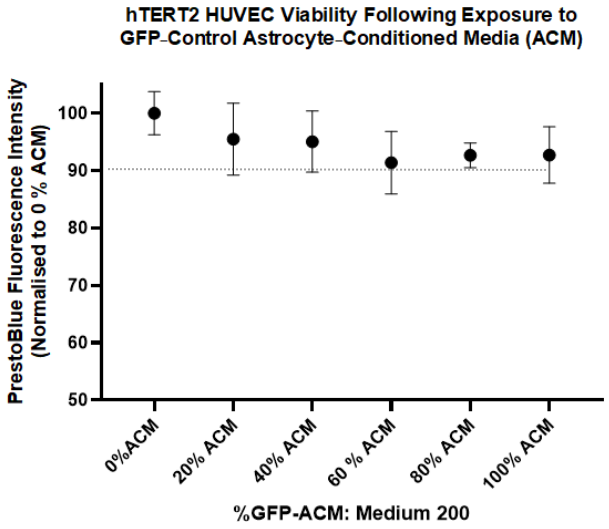

Figure 3-3: PrestoBlue assay to determine the effects of GFP-ACM on hTERT2 HUVECs cell viability. *hTERT2 HUVECs were treated for 24 h with varying concentrations of GFPcontrol ACM, and fluorescence intensity was measured using the PrestoBlue assay. PrestoBlue fluorescence is proportional to the number of metabolically active cells, providing a quantitative measure of cell viability. Values were normalised to the positive control condition (0 % GFP-ACM, 100 % Medium 200) and expressed as a percentage of this control. Data points represent mean ± SD from n = 5 replicates per condition. Dotted line indicates 90% viability of HUVEC cells.*

A one-way ANOVA revealed no statistically significant differences in viability between any ACM concentration and the positive control. Across all conditions, viability remained above 90 %, indicating that ACM, even at 100 % concentration, did not significantly compromise hTERT2 HUVEC metabolic activity (figure 3-3).

Given that 100 % ACM did not significantly reduce viability, this concentration was selected for subsequent assays to avoid dilution of any potential astrocyte derived factors within the ACM, thereby maximising assay sensitivity.

3.2.2 CRISPR Edited TERT2 HUVECs E-selectin Assay

After determining that 100% GFP-ACM does not significantly compromise HUVEC viability, the presence of inflammatory mediators within the astrocyte secretomes (within the astrocyte-conditioned media) could then be investigated.

Experiments were performed at two timepoints, 6-hours and 24-hours and using 5 experimental conditions. Each time point and experimental condition was assessed both for cell viability (measured by presto blue assay, see section *2.5.3.3 Fluorescence Detection*) and e-selectin expression (measured by luminescence, see section *2.5.3.2 Luminescence Detection*).

- Fresh astrocyte media (**negative control**)

- GFP control ACM (GFP-ACM)
- GFAP-overexpressing ACM (OVER-ACM)
- GFAP ACM (MUT-ACM)
- TNF-α (1nM) diluted in fresh astrocyte media (**positive control**)

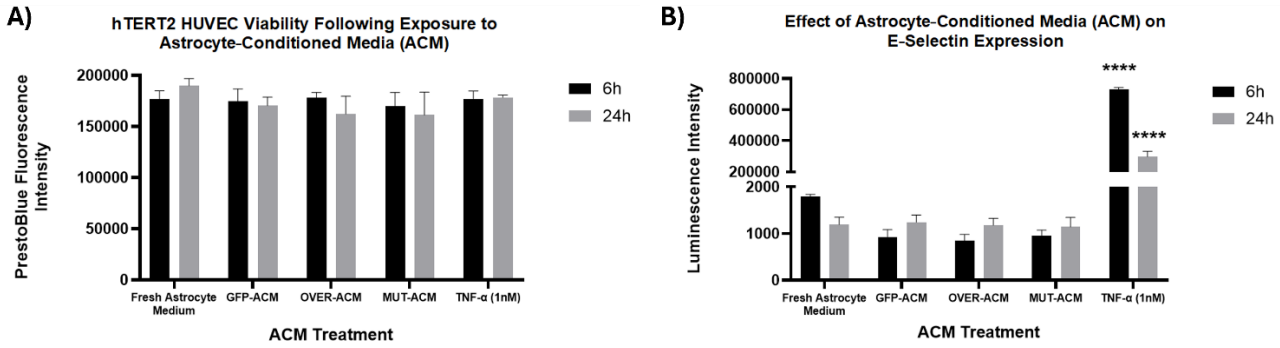

Figure 3-4: Effect of Astrocyte-Conditioned Media (ACM) on hTERT2 HUVEC Viability and E-Selectin Expression. *CRISPR-edited hTERT2 HUVECs were treated with Fresh Astrocyte Medium (negative control), GFP-ACM, OVER-ACM, MUT-ACM or TNF-α (1 nM; positive control) for 6 or 24 hours.* ***(A)*** *Cell viability was assessed via PrestoBlue fluorescence. No significant differences in viability were observed between treatments or time points (two-way ANOVA, $p > 0.05$).* ***(B)*** *E-selectin expression was quantified via luminescence following LgBiT addition. TNF-α significantly increased E-selectin expression compared to all other treatments at both time points (Tukey's post hoc, $p < 0.0001$), However, no significant differences were detected among ACM conditions or between 6 h and 24 h time points within each treatment ($p > 0.33$). Data represent mean ± SD, statistical significance was defined as **** ≤ 0.0001.*

A two-way ANOVA of the PrestoBlue Assay (figure 3-4 A) found florescence intensity was not significantly affected by any astrocyte-conditioned media (ACM) treatment or by incubation duration ($p > 0.05$). This was confirmed by a subsequent Post hoc Tukey's multiple comparisons which showed no significant differences between any pairwise comparisons among treatments or between the 6 h and 24 h time points ($p > 0.05$). These results indicate that no ACM conditions or TNF-α exposure compromised hTERT2-HUVECs viability across at both 6h and 24h, suggesting that HUVEC cell viability is not affected by any of the treatment conditions used and that any subsequent changes in luminescence seen from the e-selectin assay are unlikely to be due to changes in cell number or cell viability.

A two-way ANOVA followed by Tukey's multiple comparisons test was also performed on the E-selectin assay data (figure 3-4 B) to evaluate the effects of astrocyte-conditioned media (ACM) on E-selectin expression at 6 and 24 hours.

Multiple comparisons revealed that at both 6 h and 24 h, TNF-α treatment induced significantly higher luminescence compared with all other ACM treatments ($p < 0.0001$ for all comparisons). No significant differences were observed among Fresh Astrocyte Media, GFP-ACM, Over-ACM, or Mut-ACM groups at either time point ($p > 0.33$).

When comparing time points within each treatment, no significant changes in luminescence were detected between 6 h and 24 h for any condition ($p > 0.33$), except TNFα (all $p < 0.0001$), which remained consistently elevated across both time points.

These results indicate that, when analysed individually, none of the ACM treatments significantly altered E-selectin levels compared with negative control (fresh astrocyte medium) and luminescence intensity for all three ACM treated hTERT2-HUVEC conditions were significantly lower than the TNF-α positive control treatment at both time points.

3.3 Cytokine Profiling Array Results

To determine whether GFAP expression alters the astrocytic secretomes, cytokine profiling was performed on media collected from GFP control astrocytes (GFP-ACM), GFAP-overexpressing astrocytes (OVER-ACM), and mutant GFAP-expressing astrocytes (MUT-ACM) (see section *2.3 Production of Astrocyte-Conditioned media (ACM*)). The Proteome Profiler Human XL Cytokine Array Kit was used, with the capability of identifying 105 various cytokines, chemokines, and growth factors.

The mean pixel intensity of each dot was measured using FIJI software, background correction was then applied to each spot by subtracting the mean background pixel intensity, each cytokine was represented by two duplicate spots per membrane, which were averaged to generate a single value. Values were subsequently normalised to the average intensity of the positive control spots to account for membrane-membrane variation. The dots were then traced back to the original map of cytokines to identify the cytokine of interest (figure 3-5 A).

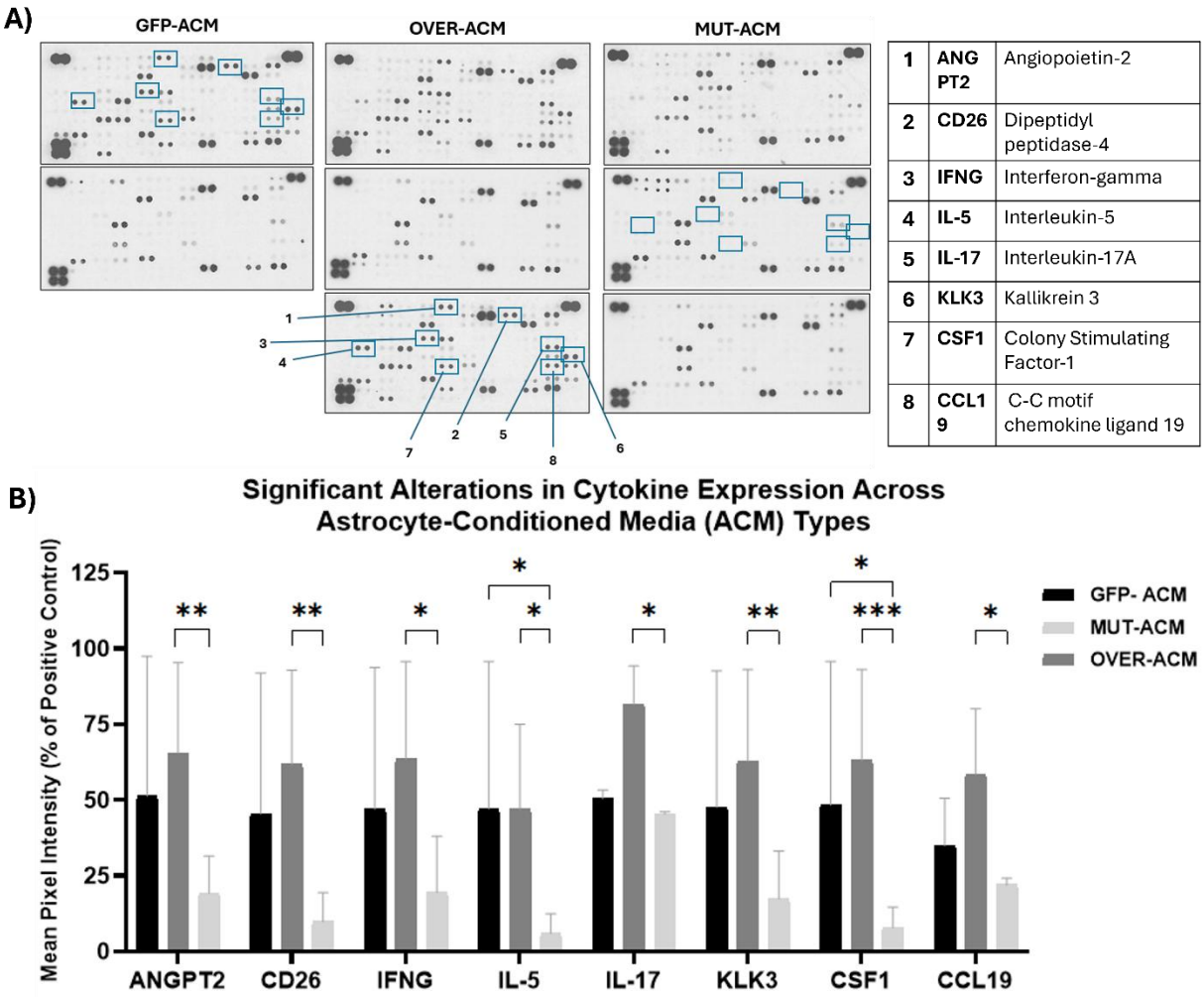

1	ANGPT2	Angiopoietin-2
2	CD26	Dipeptidyl peptidase-4
3	IFNG	Interferon-gamma
4	IL-5	Interleukin-5
5	IL-17	Interleukin-17A
6	KLK3	Kallikrein 3
7	CSF1	Colony Stimulating Factor-1
8	CCL19	C-C motif chemokine ligand 19

Figure 3-5: Cytokine profiling of astrocyte-conditioned media (ACM). *Cytokine expression was compared between GFP-ACM (N=2), OVER-ACM (N=3), and MUT-ACM (N=3) using a Proteome Profiler Human XL Cytokine Array. A total of 105 cytokines were probed, each represented by duplicate spots per membrane. (A) Representative raw array images are shown for each experimental replicate per ACM condition.* ***(B)*** *Of the 105 cytokines tested, 10 showed significant differences between conditions, with the corresponding spots indicated in* ***(A).*** *There was a significant decrease in MUT-ACM cytokine expression compared to OVER-ACM for 8 cytokines (ANGPT2: p=0.007; CD26: p= 0.002; IFNG: p=0.011; IL-5: p= 0.020; IL-17: p=0.046; KLK3: p=0.008; CSF1: p=0.001; CCL19: p=0.044). MUT-ACM also displayed consistently lower cytokine levels compared to GFP-ACM for two cytokines (IL-5: p= 0.042; CSF1: p=0.046). Data represent mean ± SEM.*

The numerical data was then analysed using a two-way ANOVA followed by a Post hoc Tukey's multiple comparison tests. Out of the 105 cytokines, 52 were detected in at least one of three ACM conditions, however only 8 were found to be significantly different between groups (Figure 3-5, A). MUT-ACM displayed consistently lower cytokine levels compared to OVER-ACM (ANGPT2: p=0.007; CD26: p= 0.002; IFNG: p=0.011; IL-5: p= 0.020; IL-17: p=0.046; KLK3: p=0.008; CSF1: p=0.001; CCL19: p=0.044). MUT-ACM also displayed consistently lower cytokine levels compared to GFP-ACM however only two of these comparisons reached statistical significance (IL-5: p= 0.042; CSF1: p=0.046). There is also a notable trend of increased cytokine expression in the OVER-ACM condition however this did not reach statistical significance.

These results confirm the presence of various cytokines across all three ACM conditions; however, only 8 of these cytokines significantly varied between groups. Nevertheless, A consistent trend was observed in which MUT-ACM displayed reduced cytokine expression compared to both GFP-ACM and OVER-ACM, whereas OVER-ACM exhibited increased cytokine levels compared with GFP-ACM, although not statistically significant. Importantly, these findings highlight that alterations in GFAP expression can alter astrocyte-derived signalling molecules, specifically that GFAP overexpression may increase specific cytokine levels, while mutant GFAP expression dampens it.

3.4 Calcium Imaging of Human Primary Astrocytes

3.4.1 Optimisation of Calcium Imaging Protocol Results

To establish a robust method for evaluating astrocyte signalling, a calcium imaging assay was optimised for human primary astrocytes. Calcium imaging is a florescence microscopy technique used for the visualisation and quantification of intracellular calcium levels, serving as an indication of cellular activity. Cells are loaded with calcium indicators, these fluorescent probes bind to free calcium ions and alter their fluorescence properties as a result, allowing real-time monitoring of calcium transients. In these experiments, this technique has been utilised to investigate human primary astrocyte activity (in vitro) in response to neurotransmitter stimulation. Neurotransmitters were delivered via continuous superfusion, ensuring stable experimental conditions and minimizing mechanical disturbances that could otherwise induce neurotransmitter independent calcium responses as depicted in *figure 3-6*.

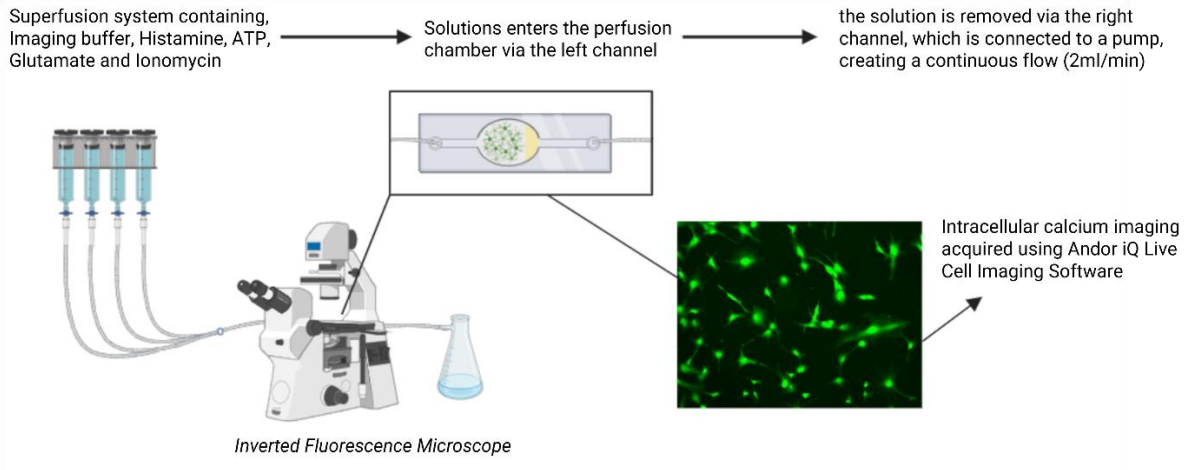

Figure 3-6: The Calcium Imaging superfusion system set-up. *Neurotransmitter solutions (histamine, ATP, glutamate, ionomycin, and buffer) were delivered into a chambered slide via the left channel of the superfusion system by turning syringe taps. Solutions were continuously superfused over cultured astrocytes and removed through the right channel, which is connected to a pump to maintain a constant flow rate of 2 mL/min, thereby minimising mechanical changes to the environment. Intracellular calcium signals were recorded at 1 fps (or 0.5 fps for Fura-2 AM imaging) using Andor iQ Live Cell Imaging Software on a Leica DM IRB inverted fluorescence microscope equipped with a 10×/0.30 NA objective. Excitation and emission wavelengths were set to 488 nm and 510 nm, respectively.*

3.4.1.1 Optimisation of Astrocyte Response Thresholds

Calcium imaging experiments can generate large data sets, with on average 50-80 cells imaged per coverslip. We therefore required an automated analysis method, which would be able to assess the responses of many hundreds of cells per experiment in a timely manner. We therefore used a subset of experiments (N=4 per calcium indicator) to determine an automated cutoff against a gold standard (visual detection of a response by an experienced observer, See section *2.6.2.1 Optimisation of Astrocyte Response Thresholds*).

This assessment of the automatic threshold vs gold standard was done for three different calcium indicators, all with different calcium binding affinity (Kd Ca^{2+}) characteristics; Fluo-5 AM (Kd = ~2300 nM), Fluo-4 AM (Kd = ~345 nM), Fura-2 AM (Kd = ~145-225 nM). In addition to differences in binding affinity, Fura-2 AM is a ratiometric indicator, whereas Fluo-4 AM and Fluo-5 AM are non-ratiometric. Fura-2 AM's ability to internally normalise for variations such as dye loading and photobleaching may lead to more stable and consistent signal measurements, which in turn could influence the gold standard threshold and its comparability to non-ratiometric indicators.

The optimal parameters for each indicator are illustrated in Figure 3-7. The response threshold was defined using the following equation as defined in section *2.6.2.1 Optimisation of Astrocyte Response Thresholds:*

$$\boldsymbol{Response\ Threshold = Baseline + (|Baseline| \times x) + Stdev \times y)}$$

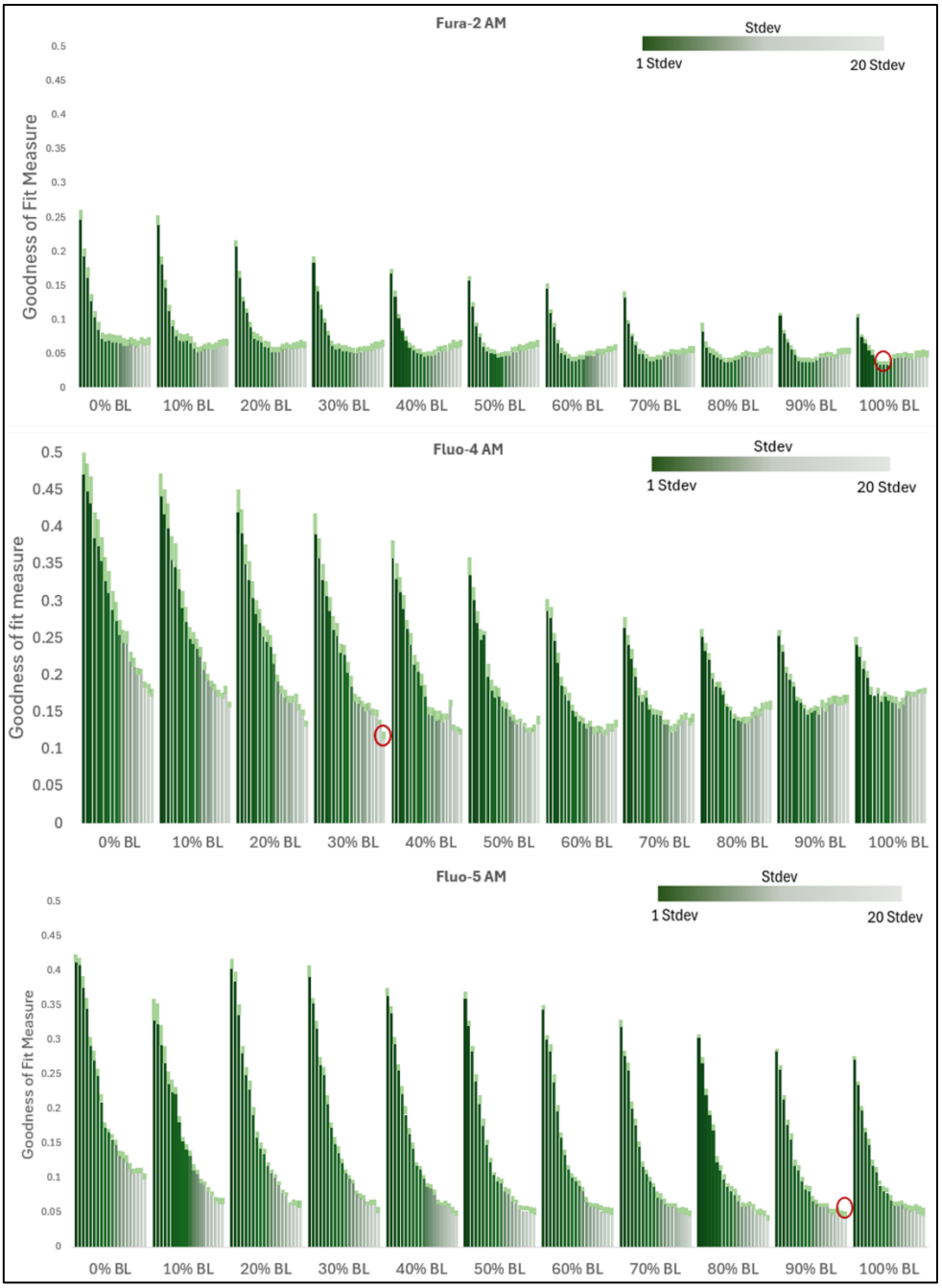

Figure 3-7: Optimisation of automated response detection parameters in Fura-2 AM, Fluo-4 AM and Fluo5-AM – loaded cells. *Graphs to show the goodness of fit measure automated and manually annotated ("gold standard") response classifications across varying threshold parameters. The x-axis represents the percentage increase above the baseline (BL) fluorescence ranging from 0% to 100%. Each bar within each group corresponds to increasing multiples of the standard deviation (Stdev), from 1 to 20 as indicated by the figure legend. The y-axis represents the mean squared error between the automated and manual classifications, with lower values indicating a better fit.*

The lowest point across all combinations—marked with a red circle—indicates the optimal threshold parameters. Error bars represent the standard deviation of the goodness-of-fit measure across four independent experiments (N = 4), exact values shown in table 3-1.

An increase in baseline and standard deviation initially produces a sharp increase in the overlap between the gold standard and the automated detection threshold (Figure 3-7). However, with the parameter ranges we selected, this improvement was followed in almost all cases by a decline in overlap. This is reflected in the upward trajectory of the goodness-of-fit value as baseline and standard deviation increase beyond their optimal values (Table 3-1).

The optimised parameters (table 3-1) were subsequently applied in the analysis of all calcium imaging data to ensure consistent and accurate response detection.

Table 3-1: Optimised parameters for automated response detection across different calcium indicators.

Calcium Indicator	Percent Increases Above the Baseline (x)	Multiples of the Standard Deviation (y)	Percentage Overlap (Between Gold Standard and Automated Analysis)
Fura-2 AM	100%	7, 8, 9	96.66%
Fluo-4 AM	30%	20	88.7%
Fluo-5 AM	80%	20	96.17%

Note: For Fura-2 AM, multiple values for y (7, 8, and 9) produced equivalently low error scores, and thus all were considered suitable. However, for consistency across experiments, a value of y = 7 was selected.

3.4.1.2 Selection of Appropriate Calcium Indicator Results

During calcium imaging the appropriate choice of calcium indicator is critical as different indicators vary in their calcium-binding affinities, and their effectiveness depends on the cell type, baseline calcium levels, and the magnitude of predicted responses. To identify the most suitable dye for astrocyte calcium imaging, three indicators with different calcium - binding affinities were compared.

Human Primary astrocytes were loaded with either Fura-2 AM (N=3), Fluo-4 AM (N=4) or Fluo-5 AM (N=4) as described in section *2.6.1.2 Coverslip preparation*. Calcium imaging was then performed, and astrocytes were stimulated with either histamine or ATP (1 µM), alongside calcium imaging buffer (negative control) or ionomycin (positive control). Image analysis was conducted as described in section *2.6.1.6 Image Analysis* and the parameters listed in *Table 3-1* were applied to detect astrocyte responses according to the specific calcium indicator used.

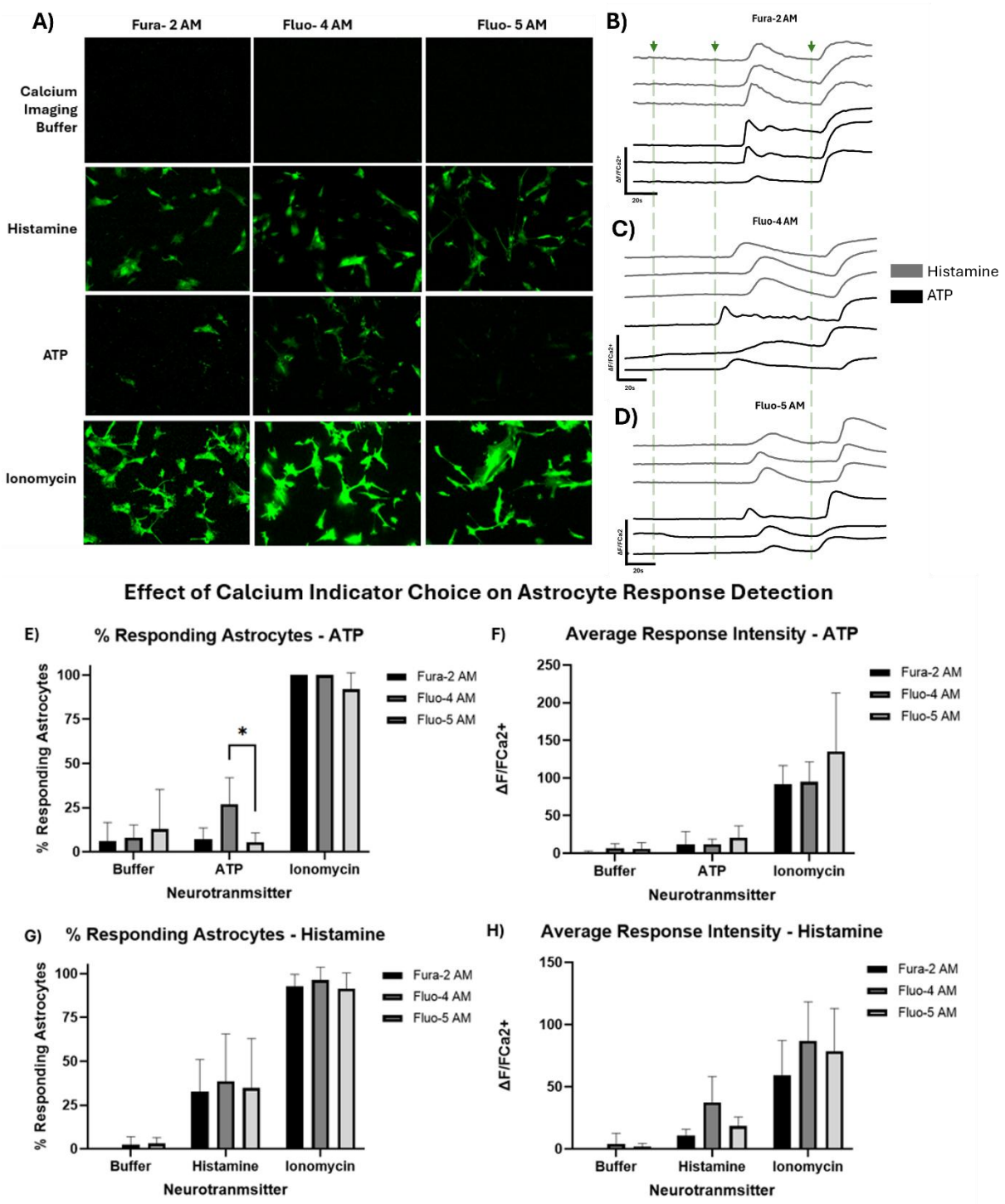

Figure 3-8: Comparison of calcium indicators for astrocyte calcium imaging. *Human primary astrocytes were loaded with Fura-2 AM (N=3), Fluo-4 AM (N=4), or Fluo-5 AM (N=4) and imaged using the standard calcium imaging protocol.* ***(A)*** *Representative fluorescence images showing peak calcium responses under each condition. Florescent values were normalised using the following equation: $\Delta F/F = (F_t-F_0)/F_0$. Where F_0 was the average fluorescence of a 10 second period of buffer stimulation prior to the commencement of the experimental protocol, and F_t is the fluorescence intensity at time t.* ***(B, C, D)*** *Florescent traces of single cell responses to Neurotransmitter application. Stimulants were applied in the following order: Calcium imaging buffer (negative control), Histamine or ATP and Ionomycin (positive control; all 1μM). Green dashed lines indicate the onset of each superfused stimulus. Each stimulus was applied for 2 minutes; however, only the first 60 seconds of the response were included in the analysis. Traces have been normalised using the same equation as* ***(A).*** *Average percentage of astrocytes responding per coverslip* ***(E, G)*** *and average response intensity (****F, H)*** *were measured.* ***(E, F)*** *depict experiments in which ATP was applied, alongside calcium imaging buffer and ionomycin.* ***(G, H)*** *follow the same experimental design however cells*

were stimulated with histamine instead of ATP. No significant differences were observed in response intensity, similarly no significant differences were detected between average percentage of responding astrocytes to histamine across all three indicators. However, a higher percentage of ATP- induced responses were detected by Fluo-4 compared to Fluo-5 (P = 0.0315, ***E****). Error bars represent mean ± SD. *p < 0.05.*

A two-way ANOVA showed that ionomycin reliably elicited a significantly higher percentage of responding astrocytes compared to calcium imaging buffer, ATP, and histamine ($p < 0.0001$). Consistent results were observed for response intensity, with ionomycin-induced responses significantly greater than those evoked by the other stimuli ($p < 0.0001$). Post hoc analysis using Tukey's multiple comparisons revealed that Fluo-4 AM detected a significantly higher percentage of astrocyte responses to ATP than Fluo-5 AM ($P = 0.0315$), as depicted in *figure 3-8 graph E*. No other significant differences were observed in either the percentage of responding astrocytes or response intensity among Fura-2 AM, Fluo-4 AM, and Fluo-5 AM for any of the neurotransmitters/ stimuli tested (all $P > 0.05$).

The high percentage of astrocyte responses to ionomycin (all above 90%) confirms Astrocyte viability and robust calcium responsiveness. Although not statistically significant, it is to be noted that Fura-2 AM produced consistently lower responses to the negative control calcium imaging buffer in both response intensity and percentage of responding cells. Additionally, standard deviation error bars for Fura-2 AM were consistently smaller than those for Fluo-4 AM and Fluo-5 AM, indicating lower variability between measurements.

Together, these results confirm ionomycin as a robust positive control for astrocyte calcium imaging, while also suggesting that Fluo-4 AM may offer advantages over Fluo-5 AM in detecting ATP-evoked responses, and Fura-2 AM provides less variation between measurements than the other two indicators.

3.4.1.3 Optimisation of Coverslip Preparation Results

Culturing astrocytes in 2D on coverslips differs significantly from their native environment, this may have an impact on cell behaviour and responsivity, as a result coverslips are often coated to support adhesion and cell viability. To investigate whether substrate coating affects astrocyte responses during calcium imaging, human primary astrocytes were cultured on glass coverslips coated with either poly-DL-ornithine hydrobromide (PDLO), a commonly used synthetic coating that promotes strong and consistent adhesion, or gelatin, a protein-based coating that provides extracellular matrix (ECM)-like properties for cell attachment.

After astrocyte seeding on either gelatin or PDLO coverslips standard calcium imaging protocol was followed. Cells were loaded with Fura-2 AM and astrocytes were stimulated with calcium imaging buffer (negative control), followed by histamine (1 µM) and then ionomycin (positive control). Image analysis was conducted as described in section *2.6.1.6 Image Analysis* and the parameters listed in *Table 3-1* appropriate for Fura-2 AM loaded cells were applied to determine astrocyte responses.

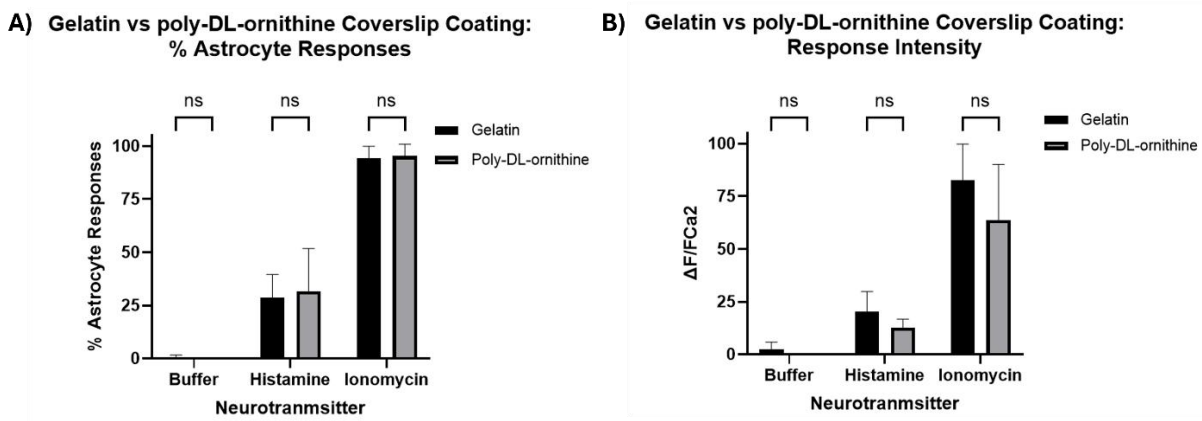

Figure 3-9: Effect of PDL- vs. Gelatin-Coated Coverslips on Astrocyte Calcium Responses. *Human primary astrocytes were cultured on 19 mm glass coverslips coated with poly-DL-ornithine (PDL) (N=4) or gelatin (N=4) and stimulated with calcium imaging buffer (negative control), histamine (1 µM), or ionomycin (1 µM, positive control). The percentage of responding astrocytes **(A)** and mean response intensity **(B)** were quantified. Data represent mean ± SD. Statistical comparisons were performed using multiple unpaired t-tests with FDR correction; no significant differences were detected between PDL- and gelatin-coated coverslips for any condition ($p > 0.05$).*

Comparisons between PDLO- and gelatin-coated coverslip calcium responses were performed using Multiple Unpaired t tests, with multiple comparisons corrected using a false discovery rate (FDR) adjustment. No significant differences were observed between gelatin- and PDLO-coated coverslips for either the percentage of responding astrocytes (figure 3-9 A; buffer: $p = 0.13$; histamine: $p = 0.80$; ionomycin: $p = 0.82$; all $p > 0.4$) or average response intensity (figure 3-9 B; buffer: $p = 0.17$; histamine: $p = 0.19$; ionomycin: $p = 0.28$; all $p > 0.2$).

Mean values indicated a trend toward higher average response intensity of astrocytes grown on gelatin-coated coverslips compared with PDLO for all three Stimulants (buffer, Histamine, Ionomycin) however this was not statistically significant.

These findings suggest that coverslip coating (PDLO vs. gelatin) did not significantly alter astrocyte responsivity to neurotransmitter stimulation or control conditions, and that PDLO was a suitable to continue using as coating substrate of choice.

3.4.2 Calcium Imaging of Human Primary Astrocytes Treated with Astrocyte-Conditioned Media (ACM) Results

To determine whether secretomes derived from GFAP-modified astrocytes alter astrocyte calcium responsivity, healthy astrocytes were treated with ACM prior to calcium imaging; ultimately mimicking the presence of these unhealthy astrocytes by using their secretomes within the media. Calcium imaging was then used to measure changes in astrocyte responsivity after a 24h incubation in ACM from one of three conditions (GFP-control, OVER-GFAP or MUT-GFAP).

3.4.2.1 GFP-Control ACM Treatment Effect on Calcium Signalling Compared to Fresh Astrocyte Medium

Before evaluating the effects of the three ACM treatments (GFP-control, OVER-GFAP or MUT-GFAP), we first assessed whether GFP-control ACM (GFP-ACM) significantly impacted astrocyte responsivity compared to fresh astrocyte medium. This step ensured that any subsequent differences observed were attributable to the conditioned media itself, rather than arising from media collection and cell treatment procedures.

Standard seeding and calcium imaging protocol was followed except for 24h prior to imaging spent astrocyte medium was replaced with 1ml of fresh astrocyte medium or GFP-ACM collected from **lentiviral transduction 1** (see section 2.3.1 *Lentiviral Transduction 1*). Astrocytes were loaded with Fluo-4 AM and sequentially stimulated with calcium imaging buffer (negative control), histamine or ATP (1 µM) in rotating order, glutamate (100 µM), and ionomycin (positive control). Due to notable order effects in neurotransmitter application, only the first neurotransmitter applied was included in the analysis. Image analysis was conducted as described in section *2.6.1.6 Image Analysis* and the parameters listed in *Table 3-1* appropriate for Fura-4 AM loaded cells were applied to determine astrocyte responses.

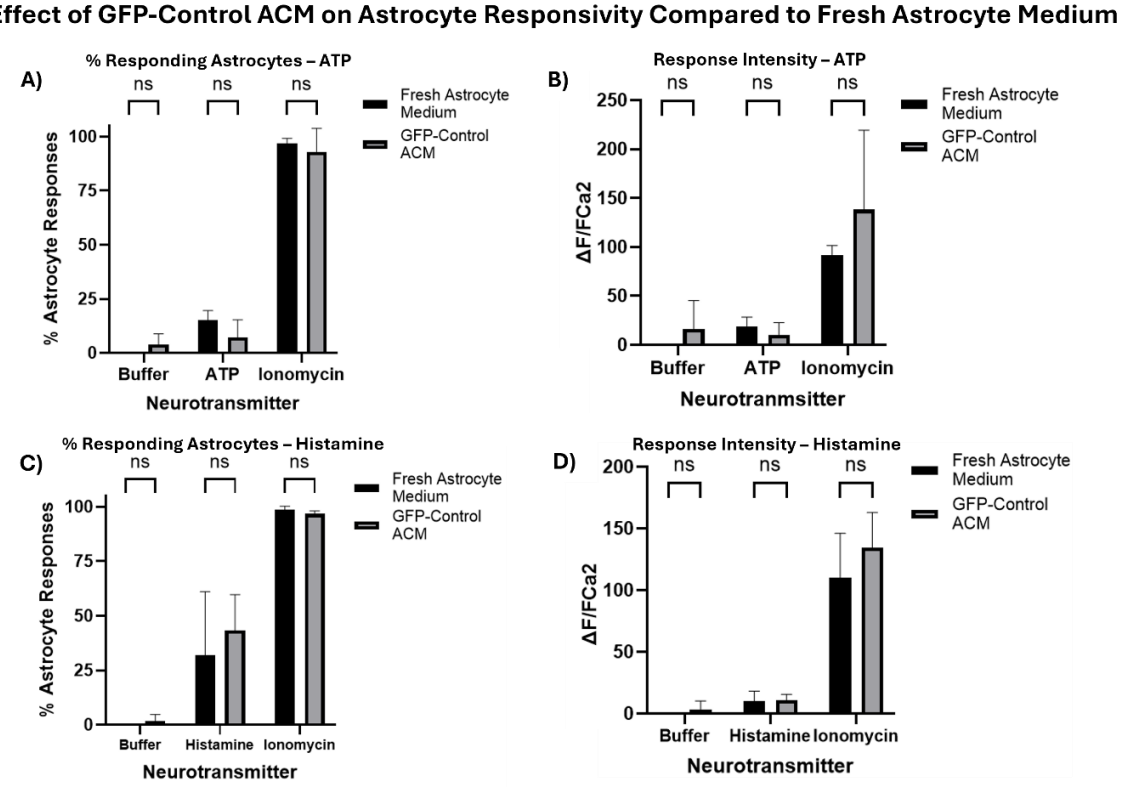

Figure 3-10: Comparing astrocyte responsivity to ATP and Histamine (1µM) after 24h incubation in 1ml of GFP-control ACM or fresh astrocyte medium. *Calcium imaging buffer was applied as a negative control and Ionomycin (1µM) at the end of each experiment (positive control). The average percentage of responding astrocytes per coverslip (**A, C**) and mean response intensity (**B, D**) were quantified for both ATP (**A, B**) and histamine (**C, D**). Data represent mean ± SD. Statistical comparisons were performed using multiple unpaired t-tests with FDR correction; no significant differences were detected between fresh astrocyte medium (N=4) and GFP-control ACM (N=4) for any condition, for both the percentage of astrocytes responding and response intensity (p > 0.05).*

All comparisons between conditions were performed using Multiple unpaired, parametric t-tests. To account for multiple comparisons, a False Discovery Rate (FDR) correction was applied. No significant differences were observed between GFP- ACM and fresh medium for any stimulus in regard to the average percentage of astrocytes responding per coverslip and average response intensity (see figure 3-10).

Specifically, the percentage of responding astrocytes was similar across all stimuli (buffer: $p = 0.17$; ATP: $p = 0.14$; histamine: $p = 0.53$; ionomycin: $p = 0.52$; all $q > 0.25$). Average fluorescence intensity also showed no significant differences (buffer: $p = 0.31$; ATP: $p = 0.30$; histamine: $p = 0.53$; ionomycin: $p = 0.09$; all $q > 0.27$).

These results indicate GFP-ACM does not significantly alter the percentage of responding astrocytes or the average response intensity compared to fresh astrocyte medium. These findings confirm that subsequent experiments using mutant GFAP ACM (MUT-ACM) or overexpressed wild-type GFAP (OVER-ACM) reflect the effects of the ACM itself as opposed to media collection or handling.

3.4.2.2 Effects of Astrocyte Conditioned Media (ACM) Treatment on Calcium Signalling

Having established that GFP-ACM treatment does not significantly alter calcium signalling in healthy astrocytes compared to fresh astrocyte medium, we next investigated whether ACM from astrocytes with altered GFAP expression impacts astrocyte responsivity. Standard seeding and calcium imaging protocol was followed except for 24h prior to imaging spent astrocyte medium was replaced with 1ml of ACM from one of three astrocyte conditions:

- GFP control ACM (GFP-ACM)
- overexpressed wild-type GFAP ACM (OVER-ACM)
- Mutant GFAP ACM (MUT-ACM)

ACM was collected from **lentiviral transduction 1** (see section 2.3.1 *Lentiviral Transduction 1*).

Astrocytes were loaded with Fluo-4 AM and sequentially stimulated with calcium imaging buffer (negative control), histamine or ATP (1 µM) in rotating order, ionomycin (positive control) was applied last. Due to notable order effects in neurotransmitter application, only the first neurotransmitter applied was included in the analysis. Image analysis was conducted as described in section *2.6.1.6 Image Analysis* and the parameters listed in *Table 3-1* appropriate for Fura-4 AM loaded cells were applied to determine astrocyte responses.

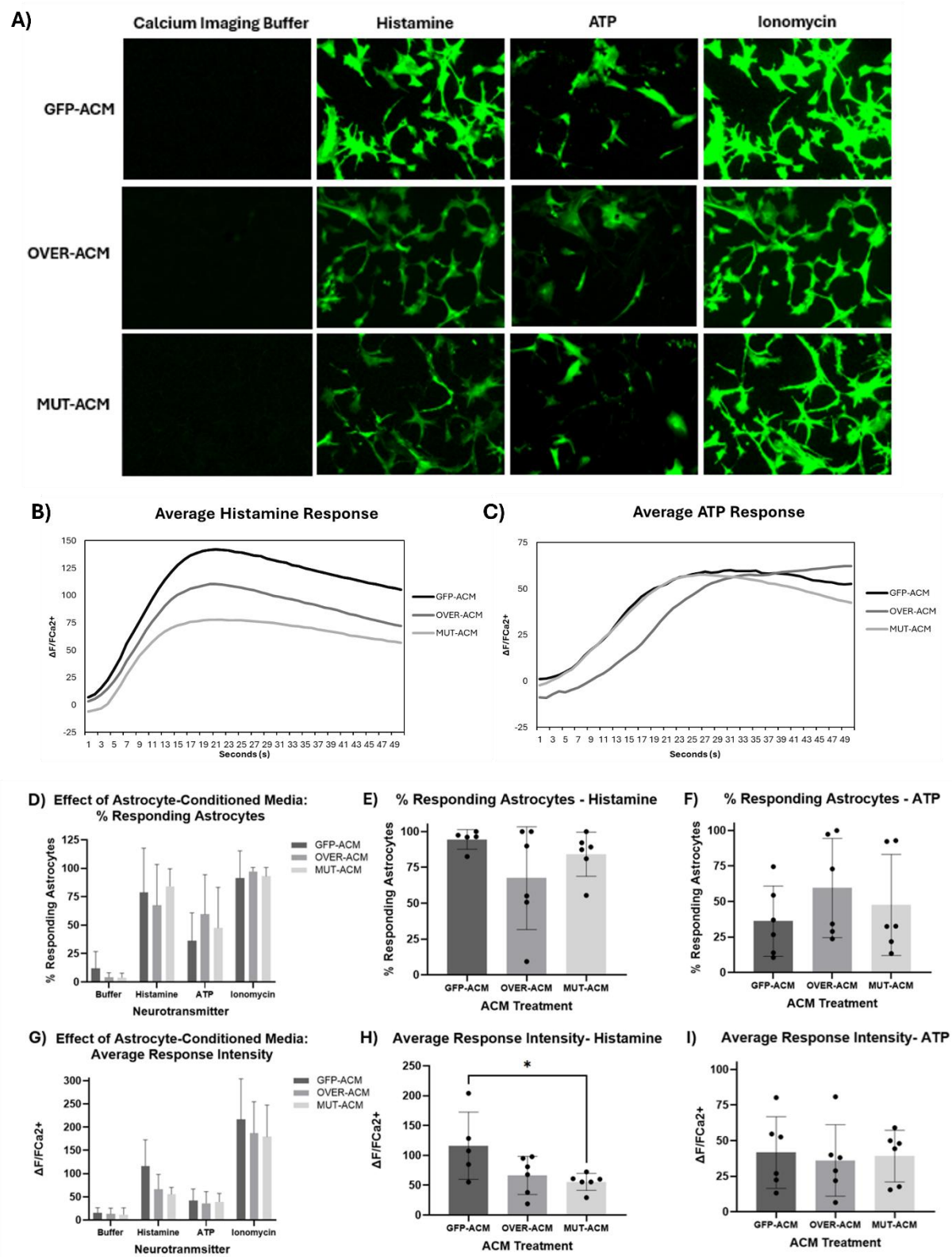

Figure 3-11: The effect of astrocyte-conditioned media (ACM) on astrocyte responsivity. *Human primary astrocytes were incubated for 24 h with GFP-ACM (N=5), OVER-ACM (N=6) or MUT-ACM (N=6), and calcium imaging was performed. Calcium imaging buffer (negative control), histamine or ATP (100μM), and ionomycin (positive control) were each superfused over cells for 2 minutes.* ***(A)*** *Representative fluorescence images showing peak calcium responses under each condition. Florescent values were normalised using the following equation: $\Delta F/F = (F_t-F_0)/F_0$. Where F_0 was the average fluorescence of a 10 second period of buffer stimulation prior to the commencement of the experimental protocol, and F_t is the fluorescence intensity at time t.* ***(B, C)*** *Time-course traces showing the average histamine* ***(B)*** *and ATP* ***(C)*** *evoked responses across treatments, Florescence intensity was normalised using the same*

*equation as **A**. **(D, G)** Ionomycin reliably induced strong calcium transients across all conditions, confirming astrocyte viability. **(D, E, F)** show the average percentage of cells responding per coverslip to ATP and Histamine stimulation. No significant differences were observed between ACM treatments in the percentage of astrocytes responding. (**G, H, I)** display the average response intensity to ATP or histamine stimulation. **(H)** histamine-evoked response intensity was significantly reduced in astrocytes treated with MUT-ACM compared to GFP-ACM. **(I)** in contrast, no significant differences in ATP-evoked response intensity were found between ACM treatment. Data are presented as mean ± SD with individual data points shown. *p < 0.05.*

Across all conditions, ionomycin reliably induced robust calcium transients, confirming cell viability and effective dye loading (Figure 3-11, D and G). All comparisons were performed using a one-way ANOVA, which revealed no significant differences between ACM treatment in average percentage of astrocytes responding per coverslip to ATP (P=0.471) or histamine (P=0.193) (Figure 3-11, E and F). Similarly, no significant differences were detected between treatments in average response intensity to ATP stimulation (p = 0.91; Figure 3-11, I).

However, a significant effect of ACM treatment was observed for histamine-induced response intensity (P < 0.05) (Figure 3-11, H). Post hoc Tukey's multiple comparisons test showed that MUT-ACM significantly reduced histamine response intensity compared to GFP-ACM (p = 0.040), while no significant difference was observed between GFP-ACM and OVER-ACM or between OVER-ACM and MUT-ACM (both P > 0.05).

These findings indicated ACM from astrocytes expressing a mutant variant of GFAP selectively impairs responsiveness to histamine, while responses to ATP remain unaffected.

3.4.3 The Effect of Astrocyte Reactivity on Calcium Signalling Behaviour

Astrocytes undergo a vast set of functional, morphological and genetic changes when shifting from a quiescent to reactive phenotype, known as astrogliosis. To investigate the impact of astrocyte reactivity on astrocytes signalling in vitro, calcium imaging was performed using an established model of reactive and quiescent human primary astrocytes by White et al. (2024).

Astrocytes cultured either with FBS serum (reactive) or without serum (quiescent) as described in *section 2.6.4 Calcium Imaging of Reactive-Like vs Quiescent-Like Human Primary Astrocytes*. Both conditions were than imaged following the standard, calcium imaging protocol measure changes in astrocyte responsivity to various neurotransmitters. Astrocytes were loaded with Fluo-4 AM and sequentially stimulated with calcium imaging buffer (negative control) followed by either histamine, ATP or Glutamate (100 µM). Ionomycin (positive control) was applied last. Image analysis was conducted as described in section *2.6.1.6 Image Analysis* and the parameters listed in *Table 3-1* appropriate for Fura-4 AM loaded cells were applied to determine astrocyte responses.

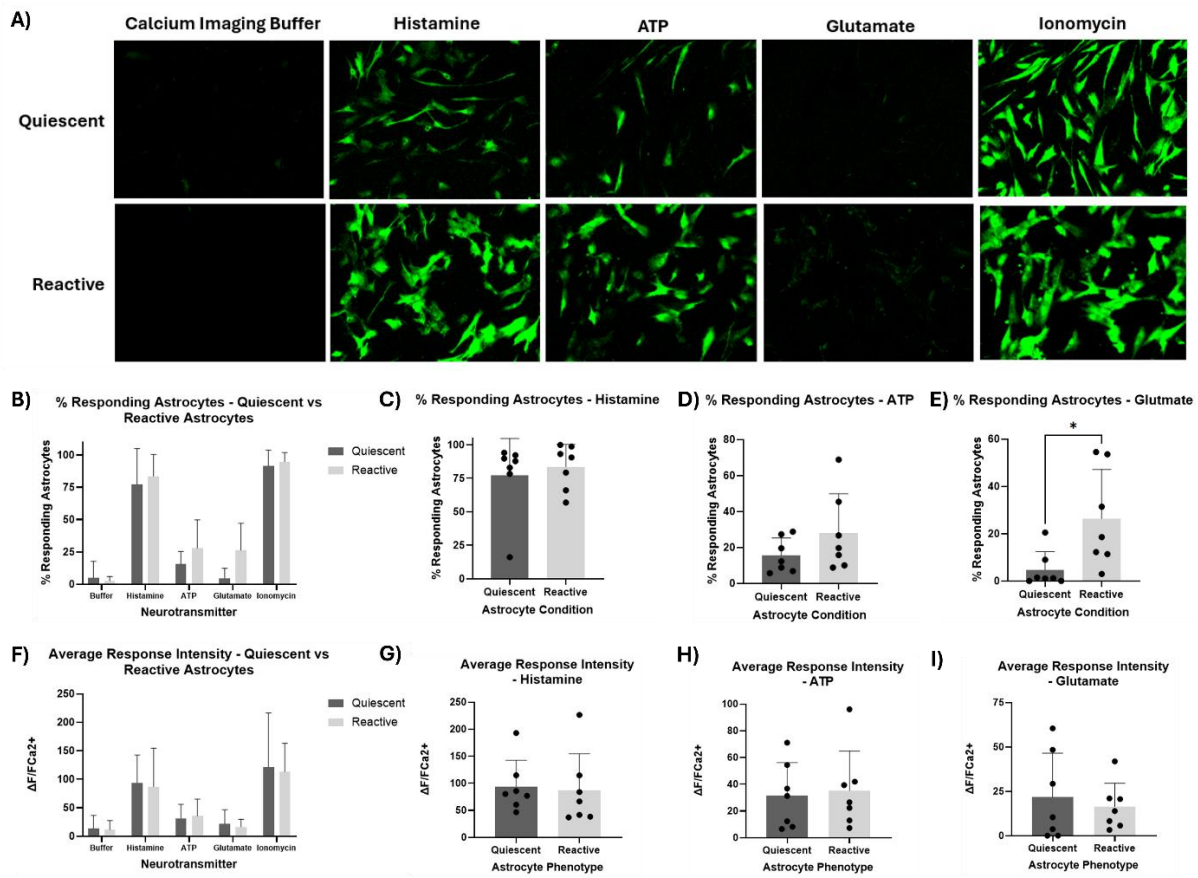

Figure 3-12: Comparing calcium signalling of quiescent and reactive astrocytes. *Human primary astrocytes were cultured using astrocyte medium containing FBS serum (reactive) or without serum (quiescent) and calcium imaging was performed. Calcium imaging buffer (negative control) was superfused followed by to histamine, ATP or Glutamate (100μM; all N=7). Ionomycin was superfused last as a positive control.* ***(A)*** *Representative fluorescence images showing peak calcium responses to stimulants under both conditions. Florescent values were normalised using the following equation:* $\Delta F/F = (F_t\text{-}F_0)/F_0$. *Where* F_0 *was the average fluorescence of a 10 second period of buffer stimulation prior to the commencement of the experimental protocol, and* F_t *is the fluorescence intensity at time t.* ***(B, F)*** *Ionomycin reliably induced strong calcium transients across all conditions, confirming astrocyte viability.* ***(C, D, E)*** *show the average percentage of cells responding per coverslip to histamine, ATP, and glutamate stimulation.* ***(G, H, I)*** *display the average response intensity to histamine, ATP and glutamate stimulation. No significant differences were observed between quiescent and reactive astrocytes when using multiple unpaired t tests, however when compared individually using an unpaired t test, reactive astrocytes had a significant increase in average percentage of responding astrocytes compared to quiescent astrocytes (p=0.0237;* ***E)*** *Data are presented as mean ± SD with individual data points shown. *p < 0.05.*

Comparisons between quiescent and reactive astrocytes were performed using Multiple Unpaired t tests for each stimulus independently, with multiple comparisons corrected using a false discovery rate (FDR) adjustment. No significant differences were observed between quiescent and reactive astrocytes for either the percentage of responding astrocytes (buffer: p = 0.412; histamine: p = 0. 622; ATP: p = 0. 210; Glutamate: p= 0.033; ionomycin: p = 0. 292; all q > 0.15; *figure 3-12 B*) or average response intensity (buffer: p = 0. 678; histamine: p = 0. 827; ATP: p = 0. 805; Glutamate: p= 0.624; ionomycin: p = 0. 724; all q > 0.83; *figure 3-12 F*).

It is to be noted that reactive astrocytes showed a general trend toward a larger percentage of astrocyte responses across all three neurotransmitters (Figure 3-12 C–E), however these differences did not reach statistical significance ($p > 0.05$) when analysed

with Multiple Unpaired t tests. Conversely, individual t tests of neurotransmitters identified a significant difference of percentage of responding astrocytes to glutamate (p= 0.0237) (*see figure 3-12 D*).

Figure 3-12A depicts Representative fluorescence images showing peak calcium responses to each stimulant per condition. However, these images also support the phenotype shift between the two conditions, with reactive astrocytes exhibiting a hypertrophic morphology with shorter projections compared to quiescent astrocytes which have longer, thinner projections.

Overall, these results indicate that while overall responsivity remains relatively similar between quiescent and reactive astrocytes, there is some evidence to indicate a slight increase in percentage of astrocyte responses in reactive astrocytes, particularly to glutamate stimulation.

3.5 Effect of Astrocyte-Conditioned Media (ACM) Treatment on Cortical Neuron Viability Results

To study the effects of astrocytic GFAP upregulation on the central nervous system (CNS), primary cortical neurons were cultured and treated with astrocyte-conditioned medium (ACM) to assess its impact on neuronal behaviour, axonal growth, and overall cell viability. Due to cortical neurons high sensitivity to media changes, ACM media was concentrated 10-fold, and a 3.8% media change was performed. Media was replaced with either GFP-ACM, OVER-ACM or MUT-ACM harvested from lentiviral transduction 1 (see section *2.3 Production of Astrocyte-Conditioned media (ACM))* 24h after cortical neurons were seeded.

3.5.1 The Effect of Astrocyte-Conditioned Media (ACM) On Cortical Neurons

24h after ACM media treatment cortical neurons seeded on 19mm coverslips in 12 well plates were fixed, and immunocytochemistry was performed (see section *2.7.9 plate fixing and immunocytochemistry)*. Acetylated tubulin was immunolabelled in addition to DAPI staining, to allow for visualisation of neuron structure and axon projections. individual projections could then be measured and DAPI stain was used to perform a cell count per FOV. For each coverslip, 3 FOVs were imaged, and the measurements were averaged to generate a single N. Three coverslips were analysed per condition (N = 3).

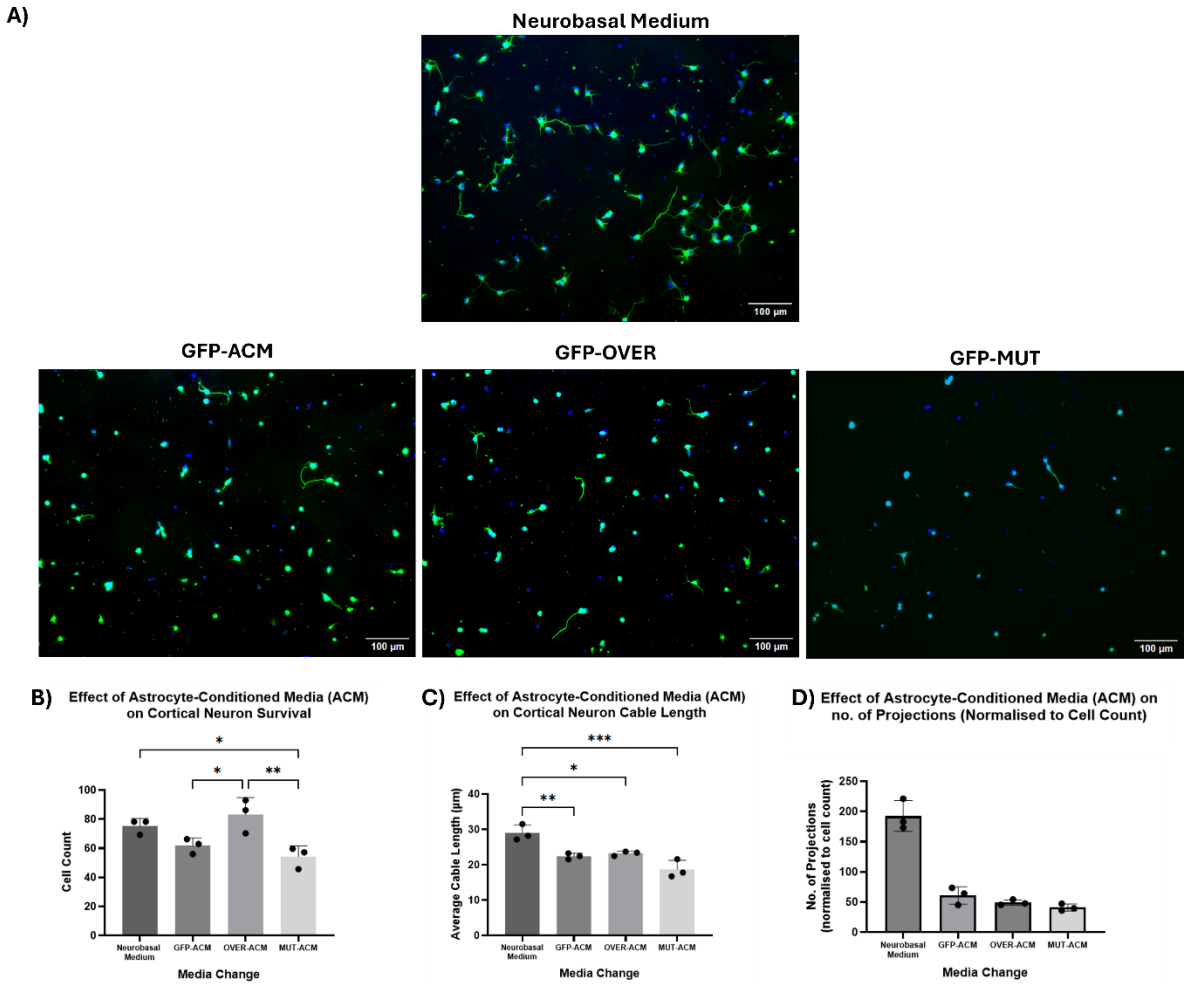

Figure 3-13*: the effect of astrocyte conditioned media (ACM) on cortical neuron viability and axonal growth.** *Cortical neurons underwent a 3.8% media change of either GFP-ACM, OVER-ACM, MUT-ACM or neurobasal medium (control).* ***(A) *After 24 hours coverslips were fixed and immunolabelled for acetylated tubulin (green) and DAPI (blue) stained to visualise cell structure. Example FOVs from each media condition, show a significant decrease in the number of projections in ACM conditions compared to neurobasal medium control.* ***(B)*** *The effect of ACM on the average cell count, one-way ANOVA followed by Post Hoc Tukey test revealed MUT-ACM treated coverslips cell count significantly decreased compared to neurobasal medium (p=0.0041), cell count of cortical neurons treated with OVER-ACM was significantly greater than both GFP-ACM (p=0.0410) and MUT-ACM (p=0.0084).* ***(C)*** *All three ACM conditions had significantly shorter average projection lengths compared to neurobasal medium control (GFP-ACM: p=0.0090; OVER-ACM: p=0.0185; MUT-ACM: p=0.0005).* ***(D)*** *all ACM treatments were found to have a lower average number of projections compared to neurobasal medium (all p<0.0001,) however no significant differences were found between ACM conditions (p>0.05). Data are presented as mean ± SD with individual data points shown.*

A One-way ANOVA was performed in addition to Post hoc comparisons using Tukey's multiple comparisons test, to evaluate the effect of ACM on cortical neuron cell count, average length of projections (cable length) and number of projections, which has been normalised to the corresponding neuronal cell count to account for variability in cell density between coverslips. The analysis revealed a significant decrease is cell count of cortical neurons treated with MUT-ACM compared to neurobasal medium (p=0.0041), cell count of cortical neurons treated with OVER-ACM was significantly greater than both GFP-ACM (p=0.0410) and MUT-ACM (p=0.0084) (figure 3-13 B).

All three ACM were found to have significantly shorter average projection length compared to neurobasal medium control (figure 3-13 C; GFP-ACM: p=0.0090; OVER-ACM: p=0.0185; MUT-ACM: p=0.0005). Despite no significant differences between the ACM groups themselves (p>0.05), notably each comparison varied in thresholds, with MUT-ACM having the lowest P value, followed by GFP-ACM and then OVER-ACM. This pattern is consistent with the trend observed across cell count, where OVER-ACM appeared to better support cortical neuron viability than GFP-ACM, while MUT-ACM was associated with the poorest neuronal outcomes.

Additionally, all ACM treatments were found to have a lower average number of projections compared to neurobasal medium (all p<0.0001) however no significant differences were found between ACM conditions (figure 3-13 D; p>0.05).

These results suggest a significant deleterious effect of ACM on cortical neurons, even absent of changes in GFAP expression. Additionally, these results indicate a trend where OVER-ACM increasing cell viability and axonal growth compared to GFP-ACM whereas MUT-ACM appears to have the most detrimental effects on cell viability and axonal growth compared to both GFP-ACM and OVER-ACM.

Chapter 4: Discussion

The overall aim of the work described in this thesis was to determine the effect of altered GFAP expression and GFAP variants on astrocyte function as well as the broader impact on CNS pathology. To achieve this, we developed a cultured human astrocyte model of WT GFAP overexpression, Mutant GFAP expression (using the patient-derived R79H variant; associated with severe AxD) and a GFP-control. The secretomes from these astrocytes could then be harvested, as conditioned media from the cultured cells, and profiled, to identify potential changes in astrocytic signalling mechanisms. This conditioned media was subsequently applied to various cell types including endothelial cells, cortical neurons, and healthy astrocytes to investigate how dysregulated GFAP expression and mutations modify astrocyte communication with the surrounding CNS.

This research identifies R79H GFAP expression as a key driver of CNS dysfunction in AxD via maladaptive astrocyte communication. Three key take-home messages surface from this project. First, the AxD-associated R79H GFAP mutation fundamentally alters astrocyte signalling, dampening calcium-dependent communication and impairing cytokine secretion, thereby shifting astrocytes from a homeostatic, supportive state toward a maladaptive secretory phenotype. Second, these signalling changes extend beyond just pathogenic astrocytes, impairing astrocyte–neuron interactions, resulting in reduced neuronal viability and suppressed axonal growth, notably, these effects were not observed between astrocyte-endothelial interactions. Third, these pathological effects are mechanistically distinct from non-pathological WT GFAP upregulation, which in several contexts preserved or even enhanced neurotrophic support. Together, these findings depict AxD as a disorder of impaired astrocyte communication and reduced trophic support, as a direct result of mutant GFAP aggregation. This breakdown in astrocyte support likely underlies the progressive neurodegeneration exhibited in patients.

Thus, these experiments not only offer insight into astrocyte driven inflammatory mechanisms but also begin to uncover the underlying mechanisms of AxD and how these changes link to the observed clinical symptoms, with an end goal of identifying potential therapeutic targets that point towards restoring astrocyte signalling and homeostatic function to stabilise CNS networks.

4.1 In Vitro Model of Alexander Disease and GFAP Over Expression in Astrocytes

To investigate the secretome profile of astrocytes with altered GFAP expression, it was necessary to establish a suitable in vitro model of GFAP overexpression. Three models were generated using lentiviral transduction: astrocytes over expressing WT-GFAP

(OVER-GFP), astrocytes over expressing the R79H mutant variant of GFAP (MUT-GFAP) and a GFP-control. The R79H mutant variant is frequently seen in severe cases of AxD, particularly in neonatal and juvenile onset. These models can then be used to distinguish how GFAP expression alters the expression of various astrocytic and inflammatory markers, particularly in the context of AxD pathology. Additionally, these models enable the harvesting of astrocyte conditioned media (ACM). This media contains molecules secreted by the transduced astrocytes, allowing analysis of their secretome, providing insight into signalling mechanisms between astrocytes and other CNS cells.

PhaseFocus LiveCyte analysis combined with immunocytochemistry (ICC) confirmed that lentiviral transduction with neat and 1:5 diluted viral particle concentrations effectively produced astrocyte populations overexpressing wild-type or mutant GFAP without compromising overall cell viability, no deleterious effects were observed at either lentiviral concentration, and astrocytes transduced with undiluted particles were selected as an appropriate model.

GFP tracking provided evidence of successful transduction, with expression becoming detectable around 24h and steadily increasing throughout the experiment. This trend in GFP expression determined 72h post transduction as a suitable time period to harvest ACM, giving astrocytes sufficient time to exhibit changes in signalling molecules and protein expression as a result of GFAP upregulation.

LiveCyte imaging demonstrated that GFP reporter signal became detectable by approximately 24h post-transduction, supporting the widely established timeline that lentiviral-mediated transgene expression becomes robust within 48–72 h (Seo et al., 2026). Thus, a 72h window before ACM collection allows sufficient time for viral integration, transgene expression, and subsequent GFAP accumulation. Increased GFAP expression has been reported as early as 12 h, with maximal induction observed by 24 h following stimulation in mouse primary astrocytes (Brahmachari, 2006), indicating that GFAP cytoskeletal remodelling develops progressively as opposed to immediately.

In addition to GFAP dynamics, a 72h time point is necessary to capture downstream effects of GFAP-mediated activation, particularly cytokine secretion. Time courses of cytokine release in astrocytes vary significantly between signalling molecules, with pro-inflammatory cytokines such as TNF-α and IL-6 showing early production around 6–8 h post-stimulation (Semple, Frugier and Morganti-Kossmann, 2010; Seo et al., 2026). In contrast, other cytokines and chemokines including Interferon-gamma-inducible protein 10 kDa (IP-10) and Monocyte chemoattractant protein-1 (CCL-2) peak at approximately 48 h, while early IL-6 secretion is cleared and followed by later secondary release (van Kralingen et al., 2013). Selecting a 72h ACM collection time therefore captures both early and delayed astrocyte inflammatory signalling, ensuring that ACM reflects a functionally altered astrocyte phenotype driven by sustained GFAP overexpression rather than transient early responses.

Live-cell imaging over 72 hours revealed that neat lentiviral particles led to over a 2-fold increase in cell count in OVER-GFAP and MUT-GFAP conditions compared to the 1:5 dilution. These findings suggest that neat particle concentration did not have a negative effect on cell count or confluency, in fact the results indicate increased proliferation of OVER-GFAP astrocytes compared to GFP-control and MUT-GFAP. Changes to cell morphology were also observed, with cell sphericity and thickness increasing in neat OVER-GFAP and MUT-GFAP, in contrast diluted lentiviral particles led to a decrease in cell thickness and sphericity. This suggests that viral concentration directly impacts the behaviour and morphology changes induced by increased GFAP expression.

The increase in cell count was particularly great in neat OVER-GFAP than both MUT-GFAP and GFP-ACM; At 72 h, the final cell count was 2.1-fold higher in OVER-GFAP and 1.5-fold higher in MUT-GFAP relative to GFP-control. This increased proliferation could be related to changes in astrocyte reactivity, with increased proliferation being observed in conditions with upregulated GFAP expression after CNS injury (Levison et al., 2000), and in the presence of inflammatory cytokine such as IL-6 which induce proliferation in previously resting astrocytes (Levison et al., 2000). Furthermore, the observed increases in cell thickness and sphericity in neat OVER-GFAP and MUT-GFAP astrocytes provide mechanistic insight into GFAP-driven cytoskeletal remodelling. Increased sphericity and thickness reflect a shift away from the typical elongated, stellate morphology towards a more hypertrophic astrocyte phenotype, a hallmark of astrocyte reactivity, as reviewed by Sofroniew and Vinters (2009). This transition is driven by reorganisation and accumulation of intermediate filament networks particularly GFAP (Lye-Barthel, Sun and Jakobs, 2013).

In the context of this project, these morphological changes occurred selectively in GFAP-modified conditions and not GFP-control astrocytes, indicating that GFAP accumulation alone is sufficient to induce structural changes consistent with a reactive-like state. Notably, hypertrophied astrocyte states have been associated with aberrant neurogenesis following injury and reduced extension of glial projections across lesion sites (Robinson, Apgar and Shapiro, 2016), suggesting diminished neurotrophic capacity of astrocytes with this phenotype. It is important to note that increased sphericity of astrocytes in cell culture can also indicate poor cell health, however the increased confluency and proliferation tracking contradict this theory. Together, these findings support the interpretation that OVER-GFAP and MUT-GFAP astrocytes undergo GFAP-mediated cytoskeletal modifications, adopting a structurally reactive-like phenotype, which has previously been linked to diminished neuronal support.

Additionally, as the neat particle condition demonstrated the most robust transduction efficiency in the LiveCyte experiments, ICC analysis focused on the undiluted conditions only, and the 1:5 dilution was not included. ICC analysis further validated LiveCyte results, showing a clear relationship between GFP fluorescence and increased GFAP

expression in both OVER-GFAP and MUT-GFAP astrocytes, while GFP-control and untransduced cells showed similar low GFAP expression (OVER-GFAP = 7.11-fold; MUT-GFAP=11.8-fold increase relative to untransduced control). Not only did the fluorescence intensity of GFAP labelling increase but also the percentage of GFAP expressing cells , (from ~7.5% in control conditions to ~70% percent in OVER/MUT conditions) meanwhile GFP- control astrocytes showed baseline levels of GFAP expression similar to that of untransduced controls (7.2% GFAP positive astrocytes) despite a 27-fold increase in GFP, confirming lentiviral transduction had occurred. The comparable immunolabelling between negative control and GFP-control eliminates the potential for lentiviral transduction itself to influence GFAP upregulation.

Notably, baseline GFAP expression was relatively low, with only ~7.5% of astrocytes expressing GFAP despite it being a well-established marker of astrocytes and inflammation (Yang and Wang, 2015). This observation puts into question of the accuracy and representativeness of the human primary astrocytes at the basis of this model, given that a key cytoskeletal protein is widely undetectable. However, these findings are not unique, as multiple studies have highlighted the heterogeneity of GFAP expression. For example, Cahoy et al. (2008) noted most astrocytes in the cortical gray matter express GFAP at low or undetectable levels by immunolabelling, suggesting that GFAP may not be a reliable marker of astrocyte identity in the absence of more universal markers such as ALDH1L1.

Expression of ALDH1L1, remained consistent across groups. ALDH1L1 is an enzyme that belongs to the aldehyde dehydrogenase superfamily and is expressed uniformly regardless of reactive phenotypes (Cahoy et al., 2008). Similarly, TSPO, an inflammatory marker in certain neurodegenerative conditions including AD (Tournier et al., 2023), did not show significant differences between conditions, suggesting no identifiable changes in mitochondrial mediated homeostatic changes, due to TSPO's location on the outer mitochondria membrane of astrocytes (Tournier et al., 2023). This suggests that increased GFAP expression alone may be insufficient to drive TSPO upregulation and additional inflammatory simuli is required. Alternatively, the experimental timeframe may have been insufficient for changes in TSPO expression to manifest previous; this theory is supported by previous research which found TSPO was upregulated by sustained (one month) cytokine stimulation in mice (Ceyzériat et al., 2023). This could suggest increased GFAP expression alone is not sufficient to upregulate TSPO expression, alternatively these changes may require more time to take hold.

Although these experiments demonstrate the effectiveness of these (mutant) GFAP overexpression models, statistical conclusions cannot be drawn due to small sample sizes (N=2). Nevertheless, the extensive datasets generated from this experiment followed consistent trends across conditions, collectively strengthening the validity of the results. Overall, these findings validate successful over expression of GFAP in the

majority of cells 72h post transduction, establishing this timepoint as a suitable time to collect ACM.

4.2 Cytokine Profiling of Astrocyte-Conditioned Media (ACM)

To distinguish how GFAP expression alters astrocyte signalling and cytokine release, a cytokine array was conducted on each of the three types of ACM collected: overexpressing WT GFAP (OVER-ACM), overexpressing the R79H GFAP variant (MUT-ACM) or a GFP-control (GFP-ACM). This array permitted the specific cytokine profiling of ACM composition, allowing for both characterisation and direct comparison of cytokine expression across conditions. The cytokine array revealed that of 105 cytokines tested, 52 were detected in at least one of three ACM conditions, these included common trophic factors (e.g., BDNF, FGF-2, HGF, VEGF) interleukins (e.g, IL-8, IL-11, IL-32) and inflammatory markers (e.g. IFNG, YKL40, petraxin 3). Although the number of cytokines detected in each condition remained relatively similar, it is to be noted only 42 cytokines were detected in MUT-ACM compared to 47 in OVER-ACM and 48 in GFP-ACM. Additionally, only 8 of the 52 cytokines detected (ANGPT2, CD26, IFNG, IL-5, IL-17, KLK3, CSF1, CCL19) were found to be significantly different between conditions. For all these cytokines, MUT-ACM had significantly lower levels than OVER-ACM. OVER-ACM in turn showed a general trend of increased cytokine levels compared to control. However, this elevation did not reach statistical significance. A significant decrease in MUT-ACM levels compared to GFP-ACM was found for both IL-5 and CSF1:

- **Angiopoietin-2 (ANGPT2)** = Acts as a natural antagonist for angiogenesis, the formation of new blood vessels (Maisonpierre et al., 1997). A downregulation of ANGPT2 can enhance blood vessel formation, whilst upregulation is reported to increase BBB permeability as well as induce endothelial cell death (Nag et al., 2005). However, an imbalance between ANGPT1 and ANGPT2 is crucial in maintaining vascular and homeostatic stability (Shi and Mansour, 2023). For example, Sie et al. (2009) reported a correlation between ANGPT1/ANGPT2 balance and the survival time of glioblastoma patients.
- **Dipeptidyl peptidase-4 (CD26)** = A glycoprotein, expression in astrocytes increases significantly during inflammation. Functionally, it cleaves neuropeptides, cytokines, and chemokines, determining their subsequent activation or inactivation (Chitadze et al., 2021). DPP4 is a known marker of inflammation, and its downregulation is linked to an attenuation of inflammatory responses in the CNS (Sim et al., 2023). However, rat studies have reported increased DPP4 astrocytic expression during inflammation however no change in a neuropathic condition, suggesting context-specific regulation (Kornél Király et al., 2018). It has been speculated that reduced DPP4 expression could prolong the activity of peptides normally degraded by DPP4 as reviewed by Ou,

O'Leary and Broxmeyer (2013), however this hypothesis requires further investigation.

- **Interferon-gamma (IFNG)** = Believed to have a neuroprotective role in the CNS, due to its involvement in activation of the STAT3 and ERK pathways in reactive astrocytes and promotion of IL-6 secretion (Sun et al., 2017). Abd-El-Basset, Rao and Alsaqobi (2020) reported IFNG increased cortical neuron survival in mouse stab wound brain injury. Moreover, blocking IFNG signalling in astrocytes led to greater demyelination and prolonged symptoms of neuroinflammation in transgenic mice (Hindinger et al., 2012).
- **Interleukin-5 (IL-5)** = Whilst astrocytes themselves do not respond to IL-5, they release IL-5 in response to inflammatory indicators such IFNG (Sawada et al., 1993). IL-5 is an anti-inflammatory cytokine traditionally known for its role in the growth, differentiation, and activation of eosinophils (white blood immune cells) (Ettore Dolcetti et al., 2024) as well as inducing proliferation and cellular metabolism of microglial cells (Liva and de Vellis, 2001), further contributing to the immune response and inflammation. A downregulation of IL-5 may lead to an impaired neuroimmune response and indicates an overall dampening of astrocyte crosstalk.
- **Interleukin-17A (IL-17)** = Pro-inflammatory factor in neurodegenerative diseases. IL-17A has been reported to induce excitotoxicity by inhibiting the uptake of glutamate by astrocytes (Kostic et al., 2017). IL-17A signalling can also upregulate other inflammatory signalling cascades, such as inducing high levels of SOCS3 in astrocytes, which can inhibit axonal regeneration (Zhou et al., 2022).
- **Kallikrein-3 (KLK3)** = There is little evidence to suggest that Astrocytes secrete or express KLK3 specifically, however KLK3 has been observed to breakdown Extracellular Matrix (ECM) proteins including collagen I and fibronectin, contributing to prostate cancer progression, as reviewed by Wenta et al. (2024). In the context of astrocyte dysfunction, increased KLK3 levels may indicate impaired structure integrity or remodelling of not only the astrocytic microenvironment but also alterations in astrocytes themselves, particularly in relation to changes in GFAP expression.
- **Colony Stimulating Factor-1 (CSF1)** = Elevated CSF1 protein promotes microglial proliferation and induces neuroinflammation (Imai and Kohsaka, 2002). Whilst a downregulation of CSF1 could be associated with a shift towards a more quiescent astrocyte phenotype, it has also been reported to impair macrophage and microglia survival, proliferation, and differentiation in mice, resulting in impaired brain structure and premature death (Erblich et al., 2011). Additionally, remyelination was severely impaired in Csf1 deficient mice (Wylot et al., 2019).
- **C-C Motif Chemokine Ligand 19 (CCL19)** = Plays a crucial role in immune cell trafficking and regulation of immune responses. CCL19 has been observed to

enhance T cell proliferation by inducing maturation of dendritic cells, ultimately increasing the production of proinflammatory cytokines (Marsland et al., 2005).

Because cytokine concentration in ACM can be influenced by astrocyte density and viability, it was necessary to determine whether the reduced cytokine signal observed in MUT-ACM could be attributed to differences in cell number as opposed to GFAP-induced functional changes. ACM for this experiment was collected following lentiviral transduction 1 procedure *(see section 2.3.1 Lentiviral Transduction 1*) meaning ACM was only harvested at the point of routine passaging. Consequently, all ACM was collected from cultures at approximately 70% confluency. This standardisation ensures that equivalent astrocyte densities contributed to each ACM condition.

Furthermore, LiveCyte analysis of proliferation dynamics and overall confluency *(see Section 3.1.1 PhaseFocus LiveCyte Image Acquisition)* demonstrated near-identical increases in confluency relative to baseline across all groups. This indicates that any potential variations in proliferation or cell death would not have a significant impact on cell density between conditions at the time of ACM collection. Therefore, the reduced cytokine expression observed in MUT-ACM is unlikely to result from lower cell density and instead reflects GFAP-dependent changes in astrocyte cytokine secretion.

A downregulation of cytokines present in MUT-ACM suggests weakened astrocyte communication with other glial cells and immune cells, leading to impaired regulation of immune responses, microglial activation and chemokine processing. Furthermore, the downregulation of KLK3 suggests potential remodelling of the astrocytic microenvironment, likely linked to AxD GFAP mutations. These hypo-responsive astrocytes fail to induce appropriate inflammatory or homeostatic responses; whilst this could reduce chronic inflammation, it also suggests CNS dysfunction extending beyond just astrocytic cells and underscores the need for a healthy balance of reactive astrocyte function within the CNS.

In contrast, the increase in cytokine levels such as IL-17 observed in OVER-ACM reflects the expected effects of GFAP upregulation, as a hallmark of astrocyte reactivity and inflammation. Together, these findings indicate that AxD GFAP mutations disrupt multiple aspects of astrocyte function, including astrocyte crosstalk with the CNS intercellular communication and appropriate maintenance of the neuronal microenvironment, rather than simply driving chronic reactivity, ultimately contributing to neurodegeneration.

Notably, although 52 cytokines were detected, many common inflammatory mediators such as TNF-α were not detected. While its expression did not reach statistical significance, YKL-40 was also identified in GFP-ACM and OVER-ACM but not MUT-ACM, despite being frequently seen in chronic neuroinflammatory conditions and reactive astrocytes (Bonneh-Barkay et al., 2010). Additionally, Markel Olabarria et al. (2015) found

upregulation of many inflammatory mediators in hippocampal and spinal cord tissue of an AxD mouse mode, including chemokines such as CXCL10 and CCL2, indicating GFAP mutations can elicit an inflammatory environment in vivo. In contrast, our results present an overall trend toward downregulation and absence of many secreted inflammatory factors in MUT-ACM relative to GFP and OVER-ACM, suggesting our in vitro model of AxD astrocytes may be insufficient in generating the amplified inflammatory response observed in vivo. This discrepancy may reflect the complexity of cell–cell interactions in the CNS, where astrocyte cross-talk with microglia and other immune cells is essential for driving neuroinflammation.

Alternatively, this absence of inflammatory cytokines could reflect methodological limitations, such as degradation during freeze–thaw cycles as opposed to true depletion of these cytokines in ACM. Interestingly, preliminary investigation of intracellular YKL-40, (data not shown) indicated, via ICC, that intracellular YKL-40 expression was not substantially upregulated in any ACM condition. We aim to explore this observation further in future research, using immunolabelling techniques such as western blotting to clarify its expression.

Results from this cytokine array however displayed large variability across replicates, raising questions about the reliability of the array. Although each positive control value represented the mean of six replicate spots, the absolute intensities of the positive control signals still varied markedly between membranes (approximately 20–40% between repeats). This variation could stem from variation within the exposure, development and scanning procedure of the array. Because all cytokine signals were normalised to these positive controls, this variability may propagate into the normalised data. Additionally, this variability could also stem from the low sample sizes due to the high cost of the array kit. Nevertheless, the data provide preliminary but important insights into the composition of ACM and the effects of GFAP mutations on cytokine signalling. Future research would aim to validate some of the key findings using alternative techniques, for example ELISAs.

4.3 Optimisation of a Robust Calcium Imaging Assay for Primary Astrocyte Cultures

In order to evaluate the effects of Astrocyte-conditioned media (ACM) on astrocyte calcium signalling, it was first necessary to establish a reliable and robust method for quantifying calcium transients, ensuring confidence in any subsequent findings.

4.3.1 Determining the Most Appropriate Calcium Indicator for Astrocyte Calcium Transients

Fluorescent detection of calcium signalling provides a widely applicable method for quantifying cellular communication, extending beyond just astrocyte research. A key

element of its versatility is the ability to optimise and tailor experimental conditions to specific cell types and contexts, particularly through the vast options of calcium indicators for imaging intracellular calcium transients. In these optimisation experiments we explored the effectiveness of three frequently used calcium indicators, each with different calcium binding affinity (Kd Ca^{2+}) characteristics; Fluo-5 AM (Kd = ~2300 nM), Fluo-4 AM (Kd = ~345 nM), Fura-2 AM (Kd = ~145-225 nM).

Results showed Fluo-4 AM detected significantly more astrocyte responses to ATP than Fluo-5 AM, these results coincide with the literature where Fluo-4 AM is frequently used in the calcium imaging of astrocytes specifically, both in vitro (James et al., 2011) and in vivo (Ding, 2012). In contrast Fluo-5 AM, with a lower binding affinity is not often cited in astrocyte studies, due to its appropriateness for measuring larger transients where Fluo-4 AM or Fura-2 AM would saturate.

Fura-2 AM is also a dye frequently used for detecting small rapid responses, similar to those measured during the optimisation experiments. Additionally, Fura-2 AM's ratiometric properties permit the normalisation of variations such as dye loading and photobleaching, resulting in more stable and consistent signal measurements. Constraints of the imaging system meant one limitation of using a ratiometric dye is imaging could be captured at 0.5 fps at the fastest, as opposed to 1 fps for the non ratiometric dyes, due to the rapidity of responses it was determined that Fluo-4 AM was the most appropriate dye for detecting the size and speed of astrocyte responses.

4.3.2 Optimising Coverslip Substrate Coating for Calcium Imaging Astrocyte Cultures

Substrate coating of glass coverslips was also assessed as a potential factor influencing astrocyte behaviour, adhesion and viability - which could influence calcium signalling. The in vitro environment is observed to strongly impact cellular behaviour, often differing markedly from the native CNS environment. Studies have identified surface topography to significantly suppress cell adhesion, growth, and proliferation with an increase in surface micro/nano roughness (Kunzler et al., 2007). However, the intensity of the impact of surface topography varies greatly between cell types.

Astrocytes are frequently cultured on positively charged polymers such as poly-D-ornithine (PDO) and Poly-D-Lysine to promote cell adhesion by increasing the surface charge (Harnett, Alderman and Wood, 2007). Gelatin is another popular substate coating due to its ECM-like qualities and has been reported to enhance stem cell proliferation more effectively than fibronectin, collagen, or laminin coated plates (Mogha, Iyer and Majumder, 2023). Additionally, recent studies have found that surface topography can alter astrocyte phenotype. Hu et al. (2021) observed astrocytes exhibit an activated phenotype when grown using soft hydrogels however stiff hydrogels can lead to an inactive phenotype. Additionally, they found softening of the stiff hydrogels can restore

astrocyte activation, reinforcing the importance of ensuring substrate coating of coverslips isn't hindering reactive astrocyte behaviours (ibid).

In this experiment, however, no significant differences in calcium response intensity or the percentage of astrocyte responses per FOV were observed between astrocytes grown on PDO and those grown on gelatin, when stimulated with histamine. Histamine was chosen as a suitable neurotransmitter for these experiments as it elicits larger and more widespread responses than ATP, as observed in previous experiments, allowing for easier detection of response changes. Based on these results, PDO was determined suitable to continue using as the coating substrate of choice.

2.3.3 Developing an Automated Response Detection for Calcium Imaging Analysis

A major challenge in calcium imaging experiments is reliably detecting individual cellular responses for such large dataset. Manual determination of individual cellular responses, while this was considered our gold standard, is not only inherently subjective but also time-consuming. By establishing an automated response detection thresholds for each calcium indicator based off the stimulants frequently used in our experiments, this study provides thorough analysis of the most appropriate parameters tailored to our cell line, perfusion system and stimulants used, rather than relying solely on assumptions drawn from current literature.

When designing an automated threshold, a cut-off based on both the overall intensity of the pre-stimulus baseline as well as the standard deviation of the signal (also measured in the pre-stimulus period) was included. It was deemed necessary to use a combination of these parameters to avoid over-reliance on just one factor. For example, overreliance on the standard deviation could prove problematic in conditions where variability is inherently high, thus skewing response detection. In contrast, relying solely on a baseline intensity cut off could easily lead to false response interpretations in experiments where the standard deviation varies substantially or where there are even very small amounts of signal drift. By integrating both factors, the thresholding helps to balance automated threshold sensitivity and prevent the overreliance on either one of the parameters.

We, therefore, systematically tested a rage of automated cutoffs derived from baseline intensity and the standard deviation of the baseline combinations. These classifications were compared to our gold standard assessment of what should be considered a response (experimenter observation). Therefore, each event in experimental datasets was determined by a binary outcome (response/ no response) of whether a given response is considered a true stimulus response based on the gold standard classification and by a range of automatic cut offs. This process permitted us to determine the reliability of the automated analysis in replicating manual experimenter assessment of responses.

The results showed a nonlinear pattern of response detection accuracy. Increasing baseline and standard deviation values initially improved the overlap between automated and manual response detection, but beyond the optimal range this overlap steadily declined. Additionally, the need for methodical optimisation for each calcium indicator specifically is emphasised by the results which showed each indicator had different optimal parameters (see *table 3-1*) as a result of their different calcium-binding affinity and indicator properties.

For Fluo-4 AM our indicator of choice (see section *4.1.1 Determining the Most Appropriate Calcium Indicator for Astrocyte Calcium Transients*) the optimal cut off chosen was 30% above baseline and 20x the standard deviation. This cut off resulted in a 88.7% overlap between our gold standard visual assessment of the data and the automated cut off. Fluo-4 AM

Overall, this optimisation framework establishes a thoroughly defined parameters, appropriate for detection astrocyte responses to various stimulants, thus ensuring the analyses of subsequent experiments is unbiased and reproducible. The systematic analysis of parameter thresholds on astrocyte response detection, ensures confidence in calcium transient quantification and comparability across experimental conditions.

4.4 The Effect of Astrocyte-Conditioned Media (ACM) on CNS Function

Conditioned media from control astrocytes in culture plus overexpressed WT GFAP and mutant GFAP was used to investigate how the secretome from these cells influenced the behaviour of healthy CNS cells – other astrocytes, endothelial cells and cortical neurons. The cytokine profiling gave insight into various signalling molecules which are crucial within the CNS for communication and inflammation regulation and suggested that the cytokine profile of astrocytes overexpressing mutant GFAP was significantly different from control cells.

The aim of these experiments was to identify the impact of GFAP expression in astrocytes on the CNS, specifically how changes in GFAP expression in astrocytes can impact function, viability and responsivity of healthy astrocytes, cortical neurons and endothelial cells, giving insight into dysfunction that could occur in the CNS as a result of astrocyte dysfunction.

4.4.1 The Effect of Astrocyte-Conditioned Media (ACM) on Astrocyte Calcium Signalling

After optimising a calcium imaging assay to quantify and characterise astrocyte function in response to various neurotransmitters, the assay was then used to assess changes in astrocyte responsivity after treatment with control (GFP-ACM), GFAP overexpressing (OVER-ACM) and mutant GFAP (MUT-ACM) astrocyte secretomes. This method allowed

us to determine if GFAP expression influences calcium signalling within astrocytes this is particularly important as calcium signalling is a crucial mechanism in the maintenance of neuronal microenvironments.

Establishing the effect of control ACM (GFP-ACM) treatment on astrocyte responsivity compared to fresh astrocyte medium was a crucial preliminary experiment, ensuring that GFP-ACM was an appropriate control, and to establish any changes in astrocyte calcium signalling was a result of secretomes within the media as opposed to the use of naive ACM itself. No significant differences in astrocyte responsivity were found between both groups, confirming any subsequent changes in astrocyte responsivity in ACM treated astrocytes were a result of changes in secretome profile rather than the producing and treating cell with naive ACM.

Following this experiment astrocytes were treated with GFP-ACM, OVER-ACM-or-MUT-ACM and calcium imaged, results showed a significant decrease in response intensity of MUT-ACM treated astrocytes to histamine stimulation compared to GFP-ACM. Notably OVER-ACM response intensity also decreased compared to GFP-ACM however this did not reach statistical significance. Moreover, these changes in response intensity were not seen during ATP stimulation. These results suggest a selective dampening of astrocyte response intensity as a result of incubation in media containing MUT-ACM secretomes, affecting Histamine stimulation but not ATP.

4.4.1.1 The Effects of Astrocyte Conditioned Media on Calcium Signalling in the Context of Current Literature

Whilst the current literature rarely focuses on changes in response intensity specifically, it does identify increased calcium signalling as a result of reactive astrogliosis, such as Delekate et al. (2014), who observed astrocytic hyperactivity, specifically single-cell transients and calcium waves is upregulated during reactive astrogliosis around surrounding plaques in an in vivo mouse model of Alzheimer's Disease (AD). Nevertheless, there is a plethora of studies which contradict these findings, suggesting hypoactivity in astrocyte signalling is a hallmark of AD pathology, particularly in early stages of the disease.

For example, somatosensory cortical astrocytes in an AD mouse model exhibited a severe reduction of Ca2+ signalling closely associated with decreased endoplasmic reticulum Ca2+ concentration at the onset of plaque deposition (Lia et al., 2023). A reduction in Ca2+ and reduced expression of the calcium sensor stromal Interaction Molecule 1 (STIM1), located in the ER was also noted (Lia et al., 2023). This indicates a relationship between reduced calcium signalling and potential disruption of internal calcium transient generation, which is crucial for Gliotransmission. Impaired Gliotransmission not only reduces communication between astrocytes but decreases their collective ability to be able to modulate neuronal microenvironments, which could lead to neurotoxicity and ultimately neuronal death.

This finding is supported by (Shah et al., 2022), who identified dysfunction in CNS network activity and functional connectivity in early stages of AD in mice. neuronal hyperactivity was accompanied with decreased astrocyte calcium signalling. Notably Recovery of astrocytic calcium activity normalised neuronal hyperactivity, as well as seizure susceptibility. These results indicate a relationship between dampened calcium signalling and hyperactivity of neurons, supporting the theory that a loss of astrocytic control over neuronal microenvironments is a contributing factor to neuronal death. Additionally, these results suggest that hyperactivity in neurons which risks excitotoxicity and maladaptive signalling, stems from dampened communication between astrocytes.

Interestingly, increased calcium signalling reduced seizures, this is relevant in the context of AxD as seizures are a common symptom of AxD, particularly in neonatal onset of the disease, which is frequently caused by the R79H variant - the same variant our MUT-ACM producing astrocytes express.

Whilst these studies do not focus on calcium signalling AxD models specifically, they offer insight into the potential impact of dampened astrocyte signalling, and how the consequential CNS dysfunction fits into the typical Pathology observed in AxD patients. However, it is still widely unclear on the underlying cause of dampened astrocyte signalling, whilst the reduced cytokine levels in ACM offer one explanation, this is an oversimplified model which cannot shed light on potential changes in calcium receptor expression or where specifically these signalling models can act on astrocytes to drive a maladaptive change in communicative behaviour.

4.4.1.2 Neurotransmitter Stimulation

ATP and histamine were selected as Neurotransmitter stimulants for these experiments due to their physiological relevance and distinct signalling pathways in astrocytes.

ATP is a well-studied gliotransmitter, which is highly prevalent is astrocytic signalling acting on both purinergic (P2Y) and ionotropic (PX2) receptors (Lezmy, 2023). ATP induced calcium responses are a key signalling mechanism at the tripartite synapse, with current literature highlighting that extracellular ATP can elicit robust calcium transients in cultured astrocytes (Goenaga et al., 2023). Choi et al. (2021) showed this calcium increases could be significantly attenuated when inhibiting calcium re-loading into the ER using thapsigargin. This also supports the belief that ATP acts through the release of calcium from internal stores, via purinergic receptors, making it a reliable indicator of astrocytic responsivity and network signalling.

In contrast, histamine, is a less frequently used neurotransmitter used in astrocyte studies, nevertheless it plays an important role in the inflammatory response. Studies have confirmed histamine can induce elevated Ca^{2+} levels in reactive astrocytes via H1 receptors (Inagaki et al., 1991). However, astrocytes express multiple subtypes of histamine receptor (H1R, H2R, and H3R), which are upregulated in response to histamine

stimulation (Xu et al., 2018). Additionally, Xu et al. (2018) found histamine stimulation suppressed the secretion of TNF-α and IL-1β, and these effects could be attenuated by histamine receptor antagonists. The effects of histamine were completely abolished by either an H1R or H3R antagonist, while an H2R antagonist attenuated the effects partly. Not only does this confirm the relevance of histamine in astrocyte signalling behaviour but offers a potential consequence of dampened histamine responsivity in AxD astrocyte models, that being a downregulation of histamine receptors and decreased suppression of proinflammatory cytokine release.

Ionomycin is a calcium ionophore and was included at the end of every experiment as a positive control, due to its ability to transport Ca^{2+} directly across the plasma membrane, regardless of calcium receptor activation (Liu and Hermann, 1978). This positive control confirms which astrocytes in the culture are capable of generating calcium transients and were successfully loaded with our calcium indicator dye. No changes were observed in astrocyte responses to ionomycin suggesting that any differences observed between ACM treatments were a genuine reflection of astrocyte signalling alternations, as opposed to impaired cell viability or failed dye loading.

4.4.2 Effect of Astrocyte-conditioned media (ACM) on the E-selectin expression of TERT2 HUVECS

To distinguish how GFAP expression alters astrocyte signalling at the BBB, this assay explored the effects of GFP-ACM, OVER-ACM and MUT-ACM on E-selectin expression in CRISPR edited TERT2 HUVEC endothelial cells. This assay provides a readout of endothelial cell reactivity to astrocyte produced stimuli as well as indirect measurements of pro inflammatory cytokine levels in astrocyte secretomes. While HUVECs are not neurovascular cells, they provide a suitable model to investigate astrocyte-endothelial interactions at the BBB and how GFAP expression may impact vascular inflammation.

As endothelial cells and astrocytes are maintained in different medium, we conducted an experiment to estimate the maximal amount of astrocyte media that HUVECs could be exposed to without compromising endothelial cell viability. The PrestoBlue viability assays confirmed that all concentrations of ACM (even undiluted) did not significantly compromise HUVEC metabolic activity. All future experiments therefore were able to use 100% ACM of various experimental conditions to assess the effect of ACM on endothelial cell E-selectin expression and viability. This ensured that any observed effects on E-selectin expression would be attributable to astrocyte-derived factors, rather than the ACM itself.

The E-selectin assay revealed ACM did not significantly impact on cell viability or E-selectin expression. While TNF treatment (used as a positive control) substantially

increased E-selectin expression, the various ACM conditions (control etc) did not cause an observable change in E-selectin expression or cell survival, either at 6 or 24h.

E-selectin is exclusively expressed in endothelial cells, under typical conditions E-selectin expression is very low, however in response to inflammatory cytokines its expression is rapidly increased, peaking within hours of stimulation and returning to baseline levels within 24 hours (Huang and Eniola-Adefeso, 2012). E-selectin directly mediates the adhesion of leukocytes along blood vessels, making them key players in maintaining BBB integrity during injury or disease (Lin et al., 2006).

The strong TNF-α response observed during the assay underscores the capacity of our platform to measure changes in HUVEC E-selectin expression when stimulated by pro-inflammatory cytokines. The observed absence of a response to the conditioned media was surprising as we expected ACM in our model to contain substantial cytokines. However endothelial activation is believed to be selective, with some cytokines such as IL-4 and 13 being reported to have no effect on E-selectin expression, even shortening its expression window to TNF-α (Etter et al., 1998). Notably, the cytokine positively identified 52 different cytokines in at least one of the three ACM conditions, however many common inflammatory mediators such as TNF-α were not detected This could offer insight into the lack of HUVEC E-selectin response observed in this experiment. It is entirely possible that ACM contains cytokines or other signalling molecules which endothelial cells are less responsive to or that ACM does not contain a high enough concentration of secretomes to effectively stimulate a response from HUVEC cells. Ultimately, the absence of HUVEC responses to ACM could reflect either a true absence of these cytokines in ACM or methodological limitations, such as degradation during freeze–thaw cycles or the sensitivity of our assay.

There is evidence to suggest storage of samples at −80 °C can result in cytokine degradation; however, the current literature is contradictory, and the effects vary considerably between individual cytokines. For example, analysis of 27 cytokines in Human intraocular fluid revealed several cytokines, including IL-2, IL-10, IL-12 and Platelet-Derived Growth Factor-BB declined significantly with long-term storage at −80 °C, with measurable losses occurring as early as three months after collection (Felfeli et al., 2023). In contrast, Kordulewska et al. (2021) reported minimal degradation of many inflammatory cytokines in plasma and serum stored at −80 °C, including IL-4, IL-6, IL-10, IL-13 and TNF-α. Additionally, they found −80 °C storage improved stability during multiple freeze-thaw cycles when compared with samples stored at −20 °.

Despite this, such studies do not exclude the possibility that partial cytokine degradation during −80 °C storage of ACM contributed to the unexpectedly low abundance of certain inflammatory mediators in the context of this project. Thus, future work should prioritise minimising -80 storage time to ensure that observed signalling deficits truly reflect the consequences of R79H GFAP expression.

Moreover, while both the selectin expression assay and the endothelial cell survival assay were highly reproducible, further work is required to contextualise these findings within broader endothelial function by comparing these results to other platforms. For example, western blots of adhesion molecule expression (e.g., E-selectin, ICAM-1, VCAM-1) could provide additional insight into the validity of our findings. As the e-selectin expression assay used in this experiment was done via a plate reader in a 96 well format a more spatially selective approach could have helped improve our readouts. For example ICC could be used to assess whether only subsets of endothelial cells are capable responding to ACM, e.g. by probing for the upregulation of adhesion molecules or other angiogenic or inflammatory markers on a cell-by-cell basis. If only small subsets of HUVECs show responses to ACM, these responses may be lost during bulk measurements of E-selectin expression. Additionally, future research may benefit from the concentration of the ACM secretome using spin columns (as described in *section 2.7.7 Conditioned media addition*), allowing us to apply higher concentrations of the astrocyte secretomes which perhaps would reflect in vivo expression levels more accurately. For example, in vivo astrocytes may secrete paracrine factors in very close proximity to endothelial cells for sustained periods of time, as opposed to being diluted in astrocyte media.

In addition, these assays could be conducted in more representative neuro-endothelial cells; for example, human brain microvascular endothelial cells (HBMECs) may offer a promising alternative endothelial cell model.

Ultimately, this E-selectin assay showed ACM from GFP-control, OVER-GFAP, or MUT-GFAP astrocytes did not induce TERT2 HUVEC activation, despite their significant responsivity to pro-inflammatory stimuli such as TNF-α. These findings imply that either ACM lacks sufficient concentrations of E-selectin–inducing cytokines, or that cytokines present with the ACM do not elicit HUVEC responses. These finding may also indicate technical limitations within the methodology including cytokine degradation during storage and thawing or insufficiently concentrated secretomes, highlighting the need for further experimentation to pinpoint how GFAP expression and mutations impact astrocyte–endothelial crosstalk.

4.4.3 The Effect of Astrocyte-Conditioned Meida (ACM) on Cortical Neuron Viability and Axonal Growth

To assess effect of astrocyte GFAP expression at the tripartite synapse, cortical neurons were treated with control (GFP-ACM), GFAP overexpressing (OVER-ACM) or mutant GFAP (MUT-ACM) astrocyte secretomes. This method allowed us to determine if GFAP dysregulated expression in astrocytes influences cortical neuron viability and axonal

growth, giving insight into how astrocyte dysfunction impacts neuromodulation/ neuronal microenvironments.

Results demonstrated that all ACM conditions significantly impaired neuronal outcomes compared to neurobasal medium (negative control), indicated by significantly shorter projections and reduced numbers of processes. Previous culture and maintenance of these cortical neurons has indicated their survival is greatly compromised when cultured with antibiotics or FBS. Notably, ACM contains both 2% FBS and 1% penicillin/streptomycin, therefore it is expected that the astrocyte media itself (even in the absence of secretomes) would have negatively impacted cortical neuron viability. Additionally, media changes have been observed to have deleterious effects on these cells, whilst an attempt was made to minimise these effects by concentrating the ACM 10-fold, it appears a combination of media change and baseline media composition may have led to a universal impairment of neuronal outcomes.

Nevertheless, significant results were still identified between ACM treatments: MUT-ACM presented the strongest deleterious effects in neuronal viability, with the lowest cell count and greatest decrease in average projection length. In contrast, OVER-ACM had a significantly higher cell counts than both GFP-ACM and MUT-ACM. Additionally, whilst all ACM groups had significantly reduced projection length compared to control neurobasal medium, longer average projections were observed in OVER-ACM compared to GFP-ACM, suggesting a partial restorative effect of astrocyte GFAP overexpression on neuronal outcomes.

These findings suggest secretomes from MUT-GFAP expressing astrocytes (as seen in AxD) exert neurotoxic effects on cortical neurons, impairing neuronal viability and supressing neuronal communication via axonal degeneration. Astrocytes have a well-established role in neuronal support and maintenance of the neuronal environment (Clarke and Barres, 2013); thus it is possible that MUT-ACM has reduced levels of neurotrophic factors which would normally promote neuronal growth and survival under deleterious conditions such as exposure to FBS, antibiotics and media changes.

In contrast, OVER-ACM displayed restorative effects, indicating that GFAP overexpression can enhance the release of neurotrophic factors relative to GFP-control and MUT-GFAP astrocytes. Although, GFAP upregulation is a hallmark of reactive astrocytes and chronic inflammation, this does not necessarily mean OVER-ACM astrocytes adopt a neurotoxic “A1” reactive phenotype. Instead, the observed neurotrophic effects may reflect signalling behaviours associated closer to “A2” astrocytes, which encourage synaptogenesis, axonal growth and neuroprotection.

Notably, in a rat model of AxD, Berman et al. (2025) reported a reduced expression of synaptic and mitochondrial proteins, in addition to reduced hippocampal long-term potentiation and are cognitive impairment. This supports the dampening of astrocyte

signalling seen observed during media profiling and the reduced axon and neuronal viability seen after ACM treatment, consistent with a loss-of-function mechanisms directly caused by mutant GFAP expression.

Together, these findings, alongside recent studies, support the hypothesis that AxD pathology may be driven by a loss of critical astrocyte support as a oppose to a neurotoxic gain-of-function. The observed deleterious effects of MUT-ACM on neuronal viability and axonal growth further illude to mutant GFAP carrying astrocytes have failed to provide sufficient metabolic, homeostatic and neurotrophic support in the CNS.

4.5 Calcium Signalling in Quiescent vs Reactive Astrocyte Phenotypes

It should be noted that the astrocytes which we used for our AxD cell culture model were grown in medium containing FBS. However, recent work from our collaborators has shown that this primary astrocyte model, grown in FBS, shows a number of hallmarks of reactive astrocytes including increased inflammatory markers (GFAP, Vimentin), hypertrophic morphology and altered extracellular vesicle profiles. Instead, the same astrocytes grown without serum, showed a far more quiescent phenotype as shown by reduced GFAP expression and displayed molecular profiles indicative of quiescent astrocytic function (White et al., 2024). We therefore explored the different astrocyte grown in conditions (with and without serum) using our calcium imaging paradigm, in order to inform future experiments using our AxD model and calcium imaging. This experiment also further validates the effectiveness of the optimised calcium imaging assay for astrocyte populations.

Similar to the other calcium imaging experiments, cells were stimulated with ATP and histamine, however the decision was made to explore glutamate stimulation, due to its key role as a gliotransmitter as well as it's prevalence at the tripartite synapse (Lalo et al., 2011). Results showed a general trend toward a larger percentage of astrocyte responses across all three neurotransmitters in the reactive condition compared to quiescent astrocytes; however, only glutamate stimulation reached statistical significance.

This selective upregulation of calcium responses in reactive astrocytes is supported by recent studies showing that the glutamate-sensitive receptor mGluR5 is upregulated in reactive, which enhances their responsiveness to glutamate signalling (Danjo et al., 2022). Current literature also illustrates elevated calcium signalling and astrocyte signalling during neuroinflammation, as reviewed by Shigetomi et al. (2019). Together these findings offer insight into the underlying mechanisms that facilitate selective upregulation in calcium signalling as a consequence of astrogliosis. Additionally, in the context of current literature, these finding emphasise the heterogeneity of astrocyte

populations and how influential context, including reactivity state, is in shaping astrocyte signalling behaviour.

Importantly, our finding that astrocyte calcium transients are influenced by the presence of serum in the culture medium suggests that future experiments using the AxD astrocyte model should be conducted in serum-free conditions. This approach may sharpen the differences between experimental groups, as the control condition would represent truly quiescent astrocytes in the absence of serum. In contrast, both GFAP upregulation and mutant GFAP expression may drive a more reactive phenotype under experimental conditions. At present, our control cultures may already display a reactive state due to serum exposure. Therefore, future studies should not only be performed in serum-free conditions but should also include an additional serum-containing control group, in order to further disentangle the impact of serum on astrocyte reactivity.

Notably, these findings support the robustness of the calcium imaging assay itself, being able to detect significant differences in glutamate stimulation responses in addition to ATP and histamine. This also emphasises the versatility of the assay, allowing for the detection and quantification of calcium signalling across astrocyte reactivity states, which is crucial for exploring heterogeneity in the context of neuronal disease pathology. Lastly, these results support the efficacy of the established in vitro model of astrocyte phenotypes developed by White et al. (2024).

4.6 Limitations

The findings of these experiments provide valuable insights into GFAP driven astrocyte dysfunction and the wider impact this has on the CNS, however there are several limitations to be acknowledged, which highlight areas of focus for future research.

4.6.1 Sample Sizes

Many of these experiments suffer from small sample size, limiting statistical power of the results, such as the cytokine array, or preventing the possibility of statistical analysis completely as seen in the development of GFAP over expression astrocyte models. Additionally, astrocyte populations were observed to be widely heterogenous, which is reflected in large standard deviation values in experiments such as calcium imaging. This meant although consistent trends were identified not all of these trends reached statistical significance and would have benefitted from lager sample sizes.

Future experiments should therefore not only include larger sample sizes but could also investigate the use of ICC as a way to identify subsets of astrocytes which may be impacted by an experimental condition. As astrocytes are highly variable it would be beneficial to overlap results from for example calcium imaging experiments with an ICC

profile of the astrocytes to investigate whether changes in calcium transients for example are only observed in an ICC defined subpopulation of astrocytes.

4.6.2 Limitations of Astrocyte Models for GFAP Overexpression

Whilst in vitro models enabled us to avoid the complexities and ethical constraints of in vivo work, our models lack the physiological context of in vivo models. Whist the collection of ACM allowed for us to explore the crosstalk of different cells in the CNS whilst simultaneously avoiding the complexities of co culture, the findings from these experiments have limited spatial context due to their oversimplification of CNS communication. Nevertheless, a simplified model of modified GFAP expression allowed us to focus on specific signalling pathways and isolate specific cellular interactions in order to generate hypotheses on the underlying mechanisms of astrocyte driven CNS dysfunction. Future experiments may explore complex and more three dimensional co-culture models in which astrocytes with or without GFAP mutation can be added to otherwise health CNS cells, to reveal the more complex consequences of GFAP mutations.

Certain characteristics of the human primary astrocytes used in these experiments contradict in vivo phenotypes of these cells. White et al. (2024) found when comparing quiescent-like and reactive-like astrocytes GFAP expression per astrocyte was significantly higher in the quiescent-like condition, despite a plethora of research supporting GFAP as a key hallmark of astrocyte reactivity. Furthermore, these astrocytes appeared to be more responsive to histamine than both ATP and glutamate during calcium signalling despite ATP and glutamate being highly prevalent gliotransmitters in the CNS compared to histamine. Lastly, the cytokine array revealed markedly low levels of TNF-α, despite ACM being derived from three different models of reactive astrocytes. These discrepancies raise further questions about the reliability of these cells in capturing reactive astrocyte phenotypes as observed in vivo. Future experiments could compare results from these human primary cells with other astrocytes including primary cells derived from rodents and iPSC derived astrocytes, potentially even derived from patient populations.

One explanation for these inconsistencies is the influence of 2D monoculture conditions on astrocyte phenotype. Culturing astrocytes on flat, rigid substrates can direct cells toward a flattened phenotype, indicating altered cytoskeletal organisation (Balasubramanian et al., 2016). Because GFAP is a key component of the astrocytic intermediate filament network, this suggests GFAP expression may also be altered as a result of these structural changes.

Moreover, 2D monoculture alone has been shown to impact astrocyte phenotype. Balasubramanian et al. (2016) found 2D culture systems favour homogeneous co-

expression of GFAP and the calcium-binding protein S100β, a marker of mature astrocytes, whereas 3D environments preserve cellular heterogeneity and promote co-expression of GFAP with developmental markers such as nestin while reducing S100β expression. This indicates that 2D culture alone is sufficient to dictate astrocytic protein expression. In the context of the astrocyte model utilised in this project, culture-induced phenotypic drift may contribute to low GFAP expression in reactive like astrocytes and help explain why signalling and cytokine profiles sometimes differed from expectations.

Moreover, this study focuses solely on the R79H variant of GFAP seen in AxD, this mutation was selected due to its prevalence and association with the most severe form of the disease, however there are over 100 mutations have been reported with different variations being associated to different age of onset of AxD. For example, other variants such as R416W are more prominent in adult onset (Yoshida et al., 2011), making our model less relevant for adult AxD patients as different GFAP mutation may impact astrocyte functions differently and to different extents/ severity. Future studies could include a comparison or more or less severe variants and variants associated with adult vs juvenile onset. In addition, our approach could be an ideal way to assess the phenotype of variants of unknown significance, which are genetic mutations found in the GFAP gene for which it is not yet clear whether it is pathogenic or benign.

4.6.3 Limitation of Endothelial and Neuronal Cell Models

Findings from species models, such as applying human primary astrocyte secretome on mouse cortical neurons, may be skewed by species incompatibilities. A key consideration is the differing receptor expression and signalling mechanisms between species. For example, Tarassishin, Suh and Lee (2014) compared human and mouse astrocytes, and found human astrocytes lack CD14 expression and, whilst IL-1 induced both neurotoxic and neurotrophic astrocyte responses in humans, mouse astrocytes exhibited predominantly neurotoxic responses. This highlights the issue that cytokines present within the human ACM may interact differently with mouse neuronal receptors than they would human neurons. Consequently, observed changes in neuronal viability and axonal growth in these cross-species experiments may reflect species-specific incompatibilities as opposed to human biological mechanisms of astrocyte–neuron communication. Whilst cross species models remain valuable for exploring CNS dysfunction and probing for signalling pathways of interest, these results should be interpreted with caution due to their reduced physiological relevance to the human CNS. Future experiments should therefore seek to validate key findings using human iPSC-derived neuronal models, to provide more physiologically applicable insight into astrocyte–neuron interactions.

Similarly, the use of HUVECs instead of neurovascular endothelial cells to distinguish how GFAP expression alters astrocyte signalling at the BBB imposes limitations on the applicability of these results. HUVECs are primary cells extracted from human umbilical cord and despite their frequent use in endothelium models and research, they lack the specialised barrier properties of neurovascular endothelial cells. For example, Man et al. (2008) observed transfected human brain microvascular endothelial cells (THBMECs) exhibited significantly lower solute permeability than HUVECs and were more restrictive for mononuclear cell migration than HUVECs. Moreover, T-lymphocyte migration in vitro was facilitated by chemokine CCL5 in THBMECs but not in HUVECs, highlighting not only the functional differences between HUVEC and THBMECs which may impact cell responsiveness to astrocyte signalling. Consequently, the lack of responsiveness of HUVECs observed in these experiments may not represent the full impact of GFAP derived astrocyte dysfunction on astrocyte-endothelial communication at the BBB. Future studies should therefore prioritise the use of neurovascular endothelial cells astrocytes to accurately recapitulate reactive astrocyte interactions at the BBB.

These finding may also indicate technical limitations within the methodology including cytokine degradation during storage and thawing or insufficiently concentrated secretomes, highlighting the need for further experimentation to pinpoint how GFAP expression and mutations impact astrocyte–endothelial crosstalk.

4.6.4 Calcium Imaging of Astrocyte Limitations

Whilst the optimised calcium imaging provided replicable and robust findings on astrocyte responsivity to various neurotransmitters, the assay only focuses on brief, individual stimulation. In vivo calcium signalling of astrocytes can occur over a prolonged period of time, with calcium transients manifesting as multiple waves as opposed to isolated peaks. calcium influxes occur from both ionotropic and metabotropic receptors and propagate across astrocyte networks over time. Our optimised calcium assay does not offer insight into cell fatigue as well as how GFAP expression impacts response frequency and intensity over prolonged and repeated stimulation. Many studies describe aberrant calcium signalling in neurodegenerative disease models (A.M. Baraibar et al., 2024), however research into prolonged stimulation has been less extensively investigated. Observing these signalling behaviours could reflect the regulation of Gliotransmission seen during periods of elevated neuronal activity and neuroinflammatory conditions (Cendra Agulhon et al., 2012). Ultimately, the single-stimulus design of the assay does not account for the cumulative effects of neurotransmitter stimulation and how GFAP induced astrocyte dysfunction may impact prolonged calcium signalling.

Despite limitations being identified in cellular model integrity and methodological reliability, these results provide a robust preliminary base for future experiments on a

widely under researched AxD, as well as astrocyte-driven CNS dysfunction and the impact of GFAP expression on astrocytic signalling mechanisms.

4.7 Future Directions

4.7.1 Further Characterisation of GFAP-Driven Alterations in Astrocytic Calcium Signalling

It would be interesting to calcium image astrocytes transduced to over express WT GFAP, R79H mutant GFAP and their GFAP control directly, as opposed to imaging astrocytes which have been treated with the ACM from these cells. This would allow us to investigate the direct impact of GFAP expression on calcium signalling behaviours, expanding the overall picture we have begun to explore in this project. Due to the GFP expressed in these cells and the calcium indicators used in this project being stimulated using the same fluorescence channel wavelength (488nm), this experiment would require a re-optimisation of our established calcium imaging protocol, finding a different calcium indicator which would allow us to avoid the issue of GFP signal interfering with ca transient signals. Rhod-2 AM is a potential calcium indicator, which has successfully been used in recent studies for the calcium imaging of astrocytes (Lakshmini Balachandar et al., 2020).

During this project we began to overlap function and neurochemical readouts by performing ICC on regions which had previously been calcium imaged (data not shown), however this work remains unfinished due to time constraints. Future research could include looking into this overlap further to identify a relationship between astrocyte responsivity and the expression/ upregulation of various astrocytic markers including translocator proteins and common receptors (e.g., EAAT1/2). This allows us to investigate the observed heterogeneity within astrocyte cultures in this project more closely, as previous studies have already identified correlations between enhanced Ca^{2+} signals and GFAP upregulation in a model of AxD (Saito et al., 2018).

4.7.2 Refinement of Astrocyte – Endothelial Interactions Models

The limitations identified in this project call for a refinement of our current model of astrocyte- endothelial communication. Whilst CRISPR Edited TERT2 HUVECs are valuable cells to use due to their genetically modified HiBiT tag at the N-terminus of the endogenous E-selectin protein, they lack specialised barrier properties connected to neurovascular endothelial cells. Therefore, treating an endothelial cell line more closely associated with the BBB with ACM could provide additional physiological relevance to results. As previously discussed, human brain microvascular endothelial cells (HBMECs) are a promising alternative; these cells have already been used in previous research to explore the effects of astrocyte secretome on the BBB properties (Siddharthan et al.,

2007). Future studies using HBMECs could help to contextualise our current, permitting a more accurate insight of how altered GFAP expression in astrocytes influences neurovascular function.

4.8 Concluding Remarks

This project provides insight into the impact of GFAP expression-derived changes in astrocyte function and the wider implications this has on CNS function. Using transduced human primary astrocytes of WT GFAP over expression (OVER-GFAP), R79H mutant variant expression (MUT-GFAP) and a GFP-control has permitted the investigation of changes in astrocyte signalling behaviours and the various consequences this change in expression has on endothelial, neuronal and naïve astrocyte cells.

The experiments conducted during this project exhibited a consistent theme of a deleterious effect of the R79H variant on not only astrocyte signalling within populations but also cytokine expression, which in turn appeared to have maladaptive effects on cortical neuron viability and axonal growth. These findings support the hypothesis that mutant GFAP has a dampening effect on astrocytes ability to provide homeostatic, metabolic and neurotrophic support to the surrounding CNS. Whilst the exact mechanisms behind these changes are unclear, they offer insight into the progressive neurodegeneration and CNS integrity exhibited in AxD patients.

In contrast, astrocytes that over expressed WT GFAP appeared to exhibit similar behaviours that closely align with the neuroprotective ‘A2’ reactive phenotype. Specifically, upregulation of neuroprotective cytokines as well as increased proliferation observed not only within astrocyte populations but also cortical neuron cultures, where OVER-ACM treatment restored cell count compared to both GFP-control and MUT-ACM. This also suggests that whilst GFAP is a hallmark of astrocyte reactivity it does not solely determine where astrocytes fall along the spectrum of astrogliosis phenotypes.

Together, the results of this project suggest AxD pathology is far more complex than a toxic gain-of-function and may instead include a loss of crucial astrocyte support throughout the CNS, underscored by a breakdown of astrocytic communication. These findings imply therapeutic targets should focus less on reducing prolonged inflammation and instead target the restoration of astrocyte homeostatic support. These findings highlight the importance of distinguishing between GFAP mutations and WT GFAP upregulation when looking into AxD pathology, as in this project the experimental outcomes differed greatly despite both alterations resulting in an over expression of GFAP.

Beyond the context of AxD, the results of these experiments reinforce the central role of astrocytes in maintaining neuronal microenvironments, and how dysfunction in astrocytes can induce a cascade of deleterious and inflammatory effects which drive neurodegeneration.

In conclusion, this project has provided a detailed insight into GFAP-driven astrocyte dysfunction and the broader implications this has regarding CNS dysfunction. This thesis has provided a solid platform for future investigations into the impact of altered GFAP expression in not just AxD but other inflammatory conditions where a chronic upregulation of GFAP expression is observed. The cellular models and optimised assays produced in these experiments provide a necessary foundation for future research necessary to deepen our understanding on the molecular mechanisms behind AxD and neurodegeneration, with the end goal of identifying therapeutic targets and improve clinical outcomes.

Bibliography

A.M. Baraibar, Colomer, T., A. Moreno-García, A. Bernal-Chico, E. Sánchez-Martín, C. Utrilla, Serrat, R., E. Soria-Gómez, A. Rodríguez-Antigüedad, Araque, A., Matute, C., Marsicano, G. and Mato, S. (2024). Autoimmune inflammation triggers aberrant astrocytic calcium signaling to impair synaptic plasticity. *Brain Behavior and Immunity*, 121, pp.192–210. doi:https://doi.org/10.1016/j.bbi.2024.07.010.

Abd-El-Basset, E.M., Rao, M.S. and Alsaqobi, A. (2020). Interferon-Gamma and Interleukin-1Beta Enhance the Secretion of Brain-Derived Neurotrophic Factor and Promotes the Survival of Cortical Neurons in Brain Injury. *Neuroscience Insights*, 15. doi:https://doi.org/10.1177/2633105520947081.

Absinta, M., Maric, D., Gharagozloo, M., Garton, T., Smith, M.D., Jin, J., Fitzgerald, K.C., Song, A., Liu, P., Lin, J.-P., Wu, T., Johnson, K.R., McGavern, D.B., Schafer, D.P., Calabresi, P.A. and Reich, D.S. (2021). A lymphocyte–microglia–astrocyte axis in chronic active multiple sclerosis. *Nature*, 597(7878), pp.709–714. doi:https://doi.org/10.1038/s41586-021-03892-7.

Alexander, W.S. (1949). Progressive Fibrinoid Degeneration of Fibrillary Astrocytes Associated with Mental Retardation in a Hydrocephalic Infant. *Brain*, 72(3), pp.373–381. doi:https://doi.org/10.1093/brain/72.3.373.

Álvaro Viedma-Poyatos, González-Jiménez, P., Pajares, M.A. and Pérez-Sala, D. (2022). Alexander disease GFAP R239C mutant shows increased susceptibility to lipoxidation and elicits mitochondrial dysfunction and oxidative stress. *Redox Biology*, 55, pp.102415–102415. doi:https://doi.org/10.1016/j.redox.2022.102415.

Andersen, J.V. (2025). The Glutamate/GABA-Glutamine Cycle: Insights, Updates, and Advances. *Journal of Neurochemistry*, [online] 169(3). doi:https://doi.org/10.1111/jnc.70029.

Araque, A., Carmignoto, G., Haydon, Philip G., Oliet, Stéphane H.R., Robitaille, R. and Volterra, A. (2014). Gliotransmitters Travel in Time and Space. *Neuron*, 81(4), pp.728–739. doi:https://doi.org/10.1016/j.neuron.2014.02.007.

Araque, A., Parpura, V., Sanzgiri, R.P. and Haydon, P.G. (1999). Tripartite synapses: glia, the unacknowledged partner. *Trends in Neurosciences*, 22(5), pp.208–215. doi:https://doi.org/10.1016/s0166-2236(98)01349-6.

Arshadi, C., Günther, U., Eddison, M., Harrington, K.I.S. and Ferreira, T.A. (2021). SNT: a unifying toolbox for quantification of neuronal anatomy. *Nature Methods*, [online] 18(4), pp.374–377. doi:https://doi.org/10.1038/s41592-021-01105-7.

Balasubramanian, S., Packard, J.A., Leach, J.B. and Powell, E.E. (2016). Three-Dimensional Environment Sustains Morphological Heterogeneity and Promotes

Phenotypic Progression During Astrocyte Development. *Tissue Engineering Part A*, 22(11-12), pp.885–898. doi:https://doi.org/10.1089/ten.tea.2016.0103.

Balestrino, M., Aitken, P.G. and Somjen, G.G. (1986). The effects of moderate changes of extracellular K+ and Ca2+ on synaptic and neural function in the CA1 region of the hippocampal slice. *Brain research*, [online] 377(2), pp.229–39. doi:https://doi.org/10.1016/0006-8993(86)90863-2.

Berman, R.F., Matson, M.R., Bachman, A.M., Lin, N.-H., Coyne, S., Frelka, A., Pearce, R.A., Messing, A. and Hagemann, T.L. (2025). GFAP mutation and astrocyte dysfunction lead to a neurodegenerative profile with impaired synaptic plasticity and cognitive deficits in a rat model of Alexander disease. *eNeuro*, [online] 12(3), pp.ENEURO.0504-24.2025. doi:https://doi.org/10.1523/ENEURO.0504-24.2025.

Bjørnsen, L.P., Hadera, M.G., Zhou, Y., Danbolt, N.C. and Sonnewald, U. (2013). The GLT-1 (EAAT2; slc1a2) glutamate transporter is essential for glutamate homeostasis in the neocortex of the mouse. *Journal of Neurochemistry*, 128(5), pp.641–649. doi:https://doi.org/10.1111/jnc.12509.

Bonneh-Barkay, D., Wang, G., Starkey, A., Hamilton, R.L. and Wiley, C.A. (2010). In vivo CHI3L1 (YKL-40) expression in astrocytes in acute and chronic neurological diseases. *Journal of Neuroinflammation*, 7(1), p.34. doi:https://doi.org/10.1186/1742-2094-7-34.

Brahmachari, S. (2006). Induction of Glial Fibrillary Acidic Protein Expression in Astrocytes by Nitric Oxide. *Journal of Neuroscience*, 26(18), pp.4930–4939. doi:https://doi.org/10.1523/jneurosci.5480-05.2006.

Brenner, M. (2014). Role of GFAP in CNS injuries. *Neuroscience Letters*, 565, pp.7–13. doi:https://doi.org/10.1016/j.neulet.2014.01.055.

Brenner, M., Johnson, A.B., Boespflug-Tanguy, O., Rodriguez, D., Goldman, J.E. and Messing, A. (2001). Mutations in GFAP, encoding glial fibrillary acidic protein, are associated with Alexander disease. *Nature Genetics*, 27(1), pp.117–120. doi:https://doi.org/10.1038/83679.

Brown, A.M. and Ransom, B.R. (2007). Astrocyte glycogen and brain energy metabolism. *Glia*, 55(12), pp.1263–1271. doi:https://doi.org/10.1002/glia.20557.

Bush, T.G., Puvanachandra, N., Horner, C.H., Polito, A., Ostenfeld, T., Svendsen, C.N., Mucke, L., Johnson, M.H. and Sofroniew, M.V. (1999). Leukocyte Infiltration, Neuronal Degeneration, and Neurite Outgrowth after Ablation of Scar-Forming, Reactive Astrocytes in Adult Transgenic Mice. *Neuron*, 23(2), pp.297–308. doi:https://doi.org/10.1016/s0896-6273(00)80781-3.

Cahoy, J.D., Emery, B., Kaushal, A., Foo, L.C., Zamanian, J.L., Christopherson, K.S., Xing, Y., Lubischer, J.L., Krieg, P.A., Krupenko, S.A., Thompson, W.J. and Barres, B.A. (2008). A

transcriptome database for astrocytes, neurons, and oligodendrocytes: a new resource for understanding brain development and function. *The Journal of neuroscience : the official journal of the Society for Neuroscience*, [online] 28(1), pp.264–78. doi:https://doi.org/10.1523/JNEUROSCI.4178-07.2008.

Cendra Agulhon, Sun, M.-Y., Murphy, T.E., Myers, T.G., Lauderdale, K. and Fiacco, T.A. (2012). Calcium Signaling and Gliotransmission in Normal vs. Reactive Astrocytes. *Frontiers in Pharmacology*, 3. doi:https://doi.org/10.3389/fphar.2012.00139.

Ceyzériat, K., Nicolaides, A., Amossé, Q., Fossey, C., Cailly, T., Fabis, F., Garibotto, V., Escartin, C., Tournier, B.B. and Millet, P. (2023). Reactive astrocytes mediate TSPO overexpression in response to sustained CNTF exposure in the rat striatum. *Molecular brain*, [online] 16(1), p.57. doi:https://doi.org/10.1186/s13041-023-01041-x.

Che, J., Sun, Y., Deng, Y. and Zhang, J. (2024). Blood-brain barrier disruption: a culprit of cognitive decline? *Fluids and Barriers of the CNS*, 21(1). doi:https://doi.org/10.1186/s12987-024-00563-3.

Chitadze, G., Wehkamp, U., Janssen, O., Brüggemann, M. and Lettau, M. (2021). The Serine Protease CD26/DPP4 in Non-Transformed and Malignant T Cells. *Cancers*, 13(23), p.5947. doi:https://doi.org/10.3390/cancers13235947.

Chitnis, T. and Weiner, H.L. (2017). CNS inflammation and neurodegeneration. *Journal of Clinical Investigation*, [online] 127(10), pp.3577–3587. doi:https://doi.org/10.1172/jci90609.

Choi, J.V., Tchernookova, B.K., Kumar, W., Kiedrowski, L., Goeke, C., Guizzetti, M., Larson, J., Kreitzer, M.A. and Malchow, R.P. (2021). Extracellular ATP-Induced Alterations in Extracellular H+ Fluxes From Cultured Cortical and Hippocampal Astrocytes. *Frontiers in Cellular Neuroscience*, 15. doi:https://doi.org/10.3389/fncel.2021.640217.

Clarke, L.E. and Barres, B.A. (2013). Emerging roles of astrocytes in neural circuit development. *Nature Reviews Neuroscience*, 14(5), pp.311–321. doi:https://doi.org/10.1038/nrn3484.

Corkrum, M., Covelo, A., Lines, J., Bellocchio, L., Pisansky, M., Loke, K., Quintana, R., Rothwell, P.E., Lujan, R., Marsicano, G., Martin, E.D., Thomas, M.J., Kofuji, P. and Araque, A. (2020). Dopamine-Evoked Synaptic Regulation in the Nucleus Accumbens Requires Astrocyte Activity. *Neuron*, 105(6), pp.1036-1047.e5. doi:https://doi.org/10.1016/j.neuron.2019.12.026.

Correale, J. and Villa, A. (2009). Cellular elements of the blood-brain barrier. *Neurochemical Research*, [online] 34(12), pp.2067–2077. doi:https://doi.org/10.1007/s11064-009-0081-y.

Danjo, Y., Shigetomi, E., Hirayama, Y.J., Kobayashi, K., Ishikawa, T., Fukazawa, Y., Shibata, K., Takanashi, K., Parajuli, B., Shinozaki, Y., Kim, S.K., Nabekura, J. and Koizumi, S. (2022). Transient astrocytic mGluR5 expression drives synaptic plasticity and subsequent chronic pain in mice. *Journal of Experimental Medicine*, 219(4). doi:https://doi.org/10.1084/jem.20210989.

Darabid, H., St-Pierre-See, A. and Robitaille, R. (2018). Purinergic-Dependent Glial Regulation of Synaptic Plasticity of Competing Terminals and Synapse Elimination at the Neuromuscular Junction. *Cell Reports*, 25(8), pp.2070-2082.e6. doi:https://doi.org/10.1016/j.celrep.2018.10.075.

Delekate, A., Füchtemeier, M., Schumacher, T., Ulbrich, C., Foddis, M. and Petzold, G.C. (2014). Metabotropic P2Y1 receptor signalling mediates astrocytic hyperactivity in vivo in an Alzheimer's disease mouse model. *Nature Communications*, 5(1). doi:https://doi.org/10.1038/ncomms6422.

Ding, S. (2012). In Vivo Imaging of Ca2+ Signaling in Astrocytes Using Two-Photon Laser Scanning Fluorescent Microscopy. *Humana Press eBooks*, [online] pp.545–554. doi:https://doi.org/10.1007/978-1-61779-452-0_36.

Doengi, M., Hirnet, D., Coulon, P., Pape, H.-C., Deitmer, J.W. and Lohr, C. (2009). GABA uptake-dependent Ca^{2+} signaling in developing olfactory bulb astrocytes. *Proceedings of the National Academy of Sciences*, 106(41), pp.17570–17575. doi:https://doi.org/10.1073/pnas.0809513106.

Eng, L.F., Ghirnikar, R.S. and Lee, Y.L. (2000). Glial Fibrillary Acidic Protein: GFAP-Thirty-One Years (1969–2000). *Neurochemical Research*, 25(9/10), pp.1439–1451. doi:https://doi.org/10.1023/a:1007677003387.

Erblich, B., Zhu, L., Etgen, A.M., Dobrenis, K. and Pollard, J.W. (2011). Absence of Colony Stimulation Factor-1 Receptor Results in Loss of Microglia, Disrupted Brain Development and Olfactory Deficits. *PLoS ONE*, 6(10), p.e26317. doi:https://doi.org/10.1371/journal.pone.0026317.

Escartin, C., Galea, E., Lakatos, A., O'Callaghan, J.P., Petzold, G.C., Serrano-Pozo, A., Steinhäuser, C., Volterra, A., Carmignoto, G., Agarwal, A., Allen, N.J., Araque, A., Barbeito, L., Barzilai, A., Bergles, D.E., Bonvento, G., Butt, A.M., Chen, W.-T., Cohen-Salmon, M. and Cunningham, C. (2021). Reactive astrocyte nomenclature, definitions, and future directions. *Nature Neuroscience*, [online] 24(3), pp.1–14. doi:https://doi.org/10.1038/s41593-020-00783-4.

Etter, H., Althaus, R., Eugster, H.P., Santamaria-Babi, L.F., Weber, L. and Moser, R. (1998). IL-4 and IL-13 downregulate rolling adhesion of leukocytes to IL-1 or TNF-alpha-activated endothelial cells by limiting the interval of E-selectin expression. *Cytokine*, [online] 10(6), pp.395–403. doi:https://doi.org/10.1006/cyto.1997.0308.

Ettore Dolcetti, Buttari, F., Bruno, A., Azzolini, F., Gilio, L., Borrelli, A., Caprio, V.D., Lauritano, G., Galifi, G., Gambardella, S., Rosangela Ferese, Giardina, E., Rovella, V., Furlan, R., Finardi, A., Musella, A., Balletta, S., Mandolesi, G., Centonze, D. and Bassi, M.S. (2024). An IL-5 Single-Nucleotide Polymorphism Influences Neuroinflammation and Prospective Disease Activity in Multiple Sclerosis. *International Journal of Molecular Sciences*, [online] 25(16), pp.9108–9108. doi:https://doi.org/10.3390/ijms25169108.

Fan, Y.-Y. and Huo, J. (2021). A1/A2 astrocytes in central nervous system injuries and diseases: Angels or devils? *Neurochemistry International*, [online] 148, p.105080. doi:https://doi.org/10.1016/j.neuint.2021.105080.

Felfeli, T., Park, J., Nestor, B., Altomare, F., Rai, A.S., Mandelcorn, E.D., Chow, D.R. and Wong, D.T. (2023). Evaluating the long-term biological stability of cytokine biomarkers in ocular fluid samples. *BMJ open ophthalmology*, [online] 8(1), p.e001346. doi:https://doi.org/10.1136/bmjophth-2023-001346.

Feng, D., Zhou, J., Liu, H., Wu, X., Li, F., Zhao, J., Zhang, Y., Wang, L., Chao, M., Wang, Q., Qin, H., Ge, S., Liu, Q., Zhang, J. and Qu, Y. (2022). Astrocytic NDRG2-PPM1A interaction exacerbates blood-brain barrier disruption after subarachnoid hemorrhage. *Science Advances*, [online] 8(39). doi:https://doi.org/10.1126/sciadv.abq2423.

Frost, G.R. and Li, Y.-M. (2017). The role of astrocytes in amyloid production and Alzheimer's disease. *Open Biology*, 7(12), p.170228. doi:https://doi.org/10.1098/rsob.170228.

Gagliardi, D., Wade, C., Tucci, A., Houlden, H., Chataway, J., Barkhof, F. and Lynch, D.S. (2024). Analysis of GFAP variants in UK Biobank suggests underdiagnosis or incomplete penetrance of adult-onset Alexander disease. *Journal of Neurology, Neurosurgery & Psychiatry*, p.jnnp-2024-335089. doi:https://doi.org/10.1136/jnnp-2024-335089.

Gawdi, R. and Emmady, P.D. (2020). *Physiology, Blood Brain Barrier*. [online] PubMed. Available at: https://pubmed.ncbi.nlm.nih.gov/32491653/.

Giovannoni, F. and Quintana, F.J. (2020). The Role of Astrocytes in CNS Inflammation. *Trends in Immunology*, [online] 41(9), pp.805–819. doi:https://doi.org/10.1016/j.it.2020.07.007.

Goenaga, J., Araque, A., Paulo Kofuji and Herrera, D. (2023). Calcium signaling in astrocytes and gliotransmitter release. *Frontiers in Synaptic Neuroscience*, 15. doi:https://doi.org/10.3389/fnsyn.2023.1138577.

Guttenplan, K.A., Weigel, M.K., Prakash, P., Wijewardhane, P.R., Hasel, P., Rufen-Blanchette, U., Münch, A.E., Blum, J.A., Fine, J., Neal, M.C., Bruce, K.D., Gitler, A.D., Chopra, G., Liddelow, S.A. and Barres, B.A. (2021). Neurotoxic reactive astrocytes induce cell death via saturated lipids. *Nature*. doi:https://doi.org/10.1038/s41586-021-03960-y.

Hagemann, T.L., Gaeta, S.A., Smith, M.A., Johnson, D.A., Johnson, J.A. and Messing, A. (2005). Gene expression analysis in mice with elevated glial fibrillary acidic protein and Rosenthal fibers reveals a stress response followed by glial activation and neuronal dysfunction. *Human Molecular Genetics*, 14(16), pp.2443–2458. doi:https://doi.org/10.1093/hmg/ddi248.

Hansen, D.V., Hanson, J.E. and Sheng, M. (2017). Microglia in Alzheimer's disease. *Journal of Cell Biology*, [online] 217(2), pp.459–472. doi:https://doi.org/10.1083/jcb.201709069.

Harnett, E.M., Alderman, J. and Wood, T. (2007). The surface energy of various biomaterials coated with adhesion molecules used in cell culture. *Colloids and Surfaces B: Biointerfaces*, 55(1), pp.90–97. doi:https://doi.org/10.1016/j.colsurfb.2006.11.021.

Hemmer, K., Fransen, L., Vanderstichele, H., Eugeen Vanmechelen and Heuschling, P. (2001). An in vitro model for the study of microglia-induced neurodegeneration: involvement of nitric oxide and tumor necrosis factor-α. *Neurochemistry International*, 38(7), pp.557–565. doi:https://doi.org/10.1016/s0197-0186(00)00119-4.

Hindinger, C., Bergmann, C.C., Hinton, D.R., Phares, T.W., Parra, G.I., Hussain, S., Carine Savarin, Atkinson, R.D. and Stohlman, S.A. (2012). IFN-γ Signaling to Astrocytes Protects from Autoimmune Mediated Neurological Disability. *PLOS ONE*, 7(7), pp.e42088–e42088. doi:https://doi.org/10.1371/journal.pone.0042088.

Hu, Y., Huang, G., Tian, J., Qiu, J., Jia, Y., Feng, D., Wei, Z., Li, S. and Xu, F. (2021). Matrix stiffness changes affect astrocyte phenotype in an in vitro injury model. *NPG Asia Materials*, [online] 13(1), pp.1–15. doi:https://doi.org/10.1038/s41427-021-00304-0.

Huang, R.B. and Eniola-Adefeso, O. (2012). Shear Stress Modulation of IL-1β-Induced E-Selectin Expression in Human Endothelial Cells. *PLoS ONE*, 7(2), p.e31874. doi:https://doi.org/10.1371/journal.pone.0031874.

Hughes, E.G., Maguire, J.L., McMinn, M.T., Scholz, R.E. and Sutherland, M.L. (2004). Loss of glial fibrillary acidic protein results in decreased glutamate transport and inhibition of PKA-induced EAAT2 cell surface trafficking. *Molecular Brain Research*, 124(2), pp.114–123. doi:https://doi.org/10.1016/j.molbrainres.2004.02.021.

II, F.W., Perry, A. and J Lennerz (2006). Neuropathology for the Neuroradiologist: Rosenthal Fibers. *AJNR: American Journal of Neuroradiology*, [online] 27(5), p.958. Available at: https://pmc.ncbi.nlm.nih.gov/articles/PMC7975751/.

Imai, Y. and Kohsaka, S. (2002). Intracellular signaling in M-CSF-induced microglia activation: Role of Iba1. *Glia*, 40(2), pp.164–174. doi:https://doi.org/10.1002/glia.10149.

Inagaki, N., Fukui, H., Ito, S., A Yamatodani and Wada, H. (1991). Single type-2 astrocytes show multiple independent sites of Ca2+ signaling in response to histamine. *Proceedings*

of the National Academy of Sciences, [online] 88(10), pp.4215–4219. doi:https://doi.org/10.1073/pnas.88.10.4215.

Jalal, P.J., Urbanowicz, R.A., Horncastle, E., Pathak, M., Goddard, C., Saeed, A., Mason, C.P., Ball, J.K., Irving, W.L., McClure, C.P., King, B.J. and Tarr, A.W. (2019). Expression of human ficolin-2 in hepatocytes confers resistance to infection by diverse hepatotropic viruses. *Journal of Medical Microbiology*, 68(4), pp.642–648. doi:https://doi.org/10.1099/jmm.0.000935.

James, L.R., Andrews, S., Walker, S., de Sousa, P.R.S., Ray, A., Russell, N.A. and Bellamy, T.C. (2011). High-Throughput Analysis of Calcium Signalling Kinetics in Astrocytes Stimulated with Different Neurotransmitters. *PLoS ONE*, 6(10), p.e26889. doi:https://doi.org/10.1371/journal.pone.0026889.

Jones, J.A., Kong, L., Hanna, M.G., Hoffman, B., Krencik, R., Bradley, R.H., Hagemann, T.M., Choi, J., Doers, M.E., Dubovis, M., Mohammad Amin Sherafat, Bhattacharyya, A., Kendziorski, C., Anjon Audhya, Messing, A. and Zhang, S.-C. (2018). Mutations in GFAP Disrupt the Distribution and Function of Organelles in Human Astrocytes. *Cell Reports*, 25(4), pp.947-958.e4. doi:https://doi.org/10.1016/j.celrep.2018.09.083.

Kamphuis, W., Middeldorp, J., Kooijman, L., Sluijs, J.A., Kooi, E.-J., Moeton, M., Freriks, M., Mizee, M.R. and Hol, E.M. (2014). Glial fibrillary acidic protein isoform expression in plaque related astrogliosis in Alzheimer's disease. *Neurobiology of Aging*, 35(3), pp.492–510. doi:https://doi.org/10.1016/j.neurobiolaging.2013.09.035.

Katerina Akassoglou, Bauer, J., Kassiotis, G., Manolis Pasparakis, Lassmann, H., Kollias, G. and Probert, L. (1998). Oligodendrocyte Apoptosis and Primary Demyelination Induced by Local TNF/p55TNF Receptor Signaling in the Central Nervous System of Transgenic Mice. *American Journal of Pathology*, 153(3), pp.801–813. doi:https://doi.org/10.1016/s0002-9440(10)65622-2.

Kondo, T., Funayama, M., Miyake, M., Tsukita, K., Era, T., Osaka, H., Ayaki, T., Takahashi, R. and Inoue, H. (2016). Modeling Alexander disease with patient iPSCs reveals cellular and molecular pathology of astrocytes. *Acta Neuropathologica Communications*, 4(1). doi:https://doi.org/10.1186/s40478-016-0337-0.

Kordulewska, N.K., Topa, J., Tańska, M., Cieślińska, A., Fiedorowicz, E. and Jarmołowska, B. (2021). Stability of interleukin-1β, -4, -6, -8, -10, -13, interferon-γ and tumor necrosis factor-α in human sera after repetitive freeze-thaw cycles and long storage. *Journal of Pharmaceutical and Biomedical Analysis*, 196, p.113900. doi:https://doi.org/10.1016/j.jpba.2021.113900.

Kornél Király, Márk Kozsurek, Lukácsi, E., Barta, B., Alán Alpár, Tamás Balázsa, Lechan, R.M., Judit Szabon, Zsuzsanna Helyes, Kata Bölcskei, Valéria Tékus, Zsuzsanna Tóth, Pap, K., Gerber, G. and Puskár, Z. (2018). Glial cell type-specific changes in spinal dipeptidyl

peptidase 4 expression and effects of its inhibitors in inflammatory and neuropatic pain. *Scientific Reports*, 8(1). doi:https://doi.org/10.1038/s41598-018-21799-8.

Kostic, M., Zivkovic, N., Cvetanovic, A., Stojanovic, I. and Colic, M. (2017). IL-17 signalling in astrocytes promotes glutamate excitotoxicity: Indications for the link between inflammatory and neurodegenerative events in multiple sclerosis. *Multiple Sclerosis and Related Disorders*, 11, pp.12–17. doi:https://doi.org/10.1016/j.msard.2016.11.006.

Kuhn, J. and Cascella, M. (2020). *Alexander Disease*. [online] PubMed. Available at: https://www.ncbi.nlm.nih.gov/books/NBK562242/.

Kunzler, T.P., Christoph Huwiler, Drobek, T., Janos Vörös and Spencer, N.D. (2007). Systematic study of osteoblast response to nanotopography by means of nanoparticle-density gradients. *Biomaterials*, 28(33), pp.5000–5006. doi:https://doi.org/10.1016/j.biomaterials.2007.08.009.

Lakshmini Balachandar, Montejo, K.A., Castano, E., Perez, M., Moncion, C., Chambers, J.W., Lujan, J.L. and Diaz, J.R. (2020). Simultaneous Ca^{2+} Imaging and Optogenetic Stimulation of Cortical Astrocytes in Adult Murine Brain Slices. *Current Protocols in Neuroscience*, [online] 94(1). doi:https://doi.org/10.1002/cpns.110.

Lalo, U., Yuriy Pankratov, Vladimir Parpura and Alexei Verkhratsky (2011). Ionotropic receptors in neuronal–astroglial signalling: What is the role of 'excitable' molecules in non-excitable cells. *Biochimica et Biophysica Acta (BBA) - Molecular Cell Research*, 1813(5), pp.992–1002. doi:https://doi.org/10.1016/j.bbamcr.2010.09.007.

Lawrence, J.M., Schardien, K., Wigdahl, B. and Nonnemacher, M.R. (2023). Roles of neuropathology-associated reactive astrocytes: a systematic review. *Acta Neuropathologica Communications*, 11(1). doi:https://doi.org/10.1186/s40478-023-01526-9.

Lenhossék MV (1895). Der feinere Bau des Nervensystems im Lichte neuester Forschung. *2nd edn, Fischer's Medicinische Buchhandlung H. Kornfield, Berlin*.

Levison, S.W., Jiang, F.-J., Stoltzfus, O.K. and Ducceschi, M.H. (2000). IL-6-type cytokines enhance epidermal growth factor-stimulated astrocyte proliferation. *Glia*, 32(3), pp.328–337. doi:https://doi.org/10.1002/1098-1136(200012)32:3%3C328::aid-glia110%3E3.0.co;2-7.

Lezmy, J. (2023). How astrocytic ATP shapes neuronal activity and brain circuits. *Current Opinion in Neurobiology*, 79, p.102685. doi:https://doi.org/10.1016/j.conb.2023.102685.

Lia, A., Sansevero, G., Chiavegato, A., Sbrissa, M., Pendin, D., Mariotti, L., Pozzan, T., Berardi, N., Carmignoto, G., Fasolato, C. and Zonta, M. (2023). Rescue of astrocyte activity by the calcium sensor STIM1 restores long-term synaptic plasticity in female mice

modelling Alzheimer's disease. *Nature Communications*, [online] 14(1), p.1590. doi:https://doi.org/10.1038/s41467-023-37240-2.

Liddelow, S.A., Guttenplan, K.A., Clarke, L.E., Bennett, F.C., Bohlen, C.J., Schirmer, L., Bennett, M.L., Münch, A.E., Chung, W.-S., Peterson, T.C., Wilton, D.K., Frouin, A., Napier, B.A., Panicker, N., Kumar, M., Buckwalter, M.S., Rowitch, D.H., Dawson, V.L., Dawson, T.M. and Stevens, B. (2017). Neurotoxic reactive astrocytes are induced by activated microglia. *Nature*, [online] 541(7638), pp.481–487. doi:https://doi.org/10.1038/nature21029.

Lin, C.-W., Chen, L.-J., Lee, P.-L., Lee, C.-I., Lin, J.-C. and Chiu, J.-J. (2006). The inhibition of TNF-α-induced E-selectin expression in endothelial cells via the JNK/NF-κB pathways by highly N-acetylated chitooligosaccharides. *Biomaterials*, [online] 28(7), pp.1355–1366. doi:https://doi.org/10.1016/j.biomaterials.2006.11.006.

Lin, N., Yang, A., Chang, C. and Perng, M. (2021). Elevated GFAP isoform expression promotes protein aggregation and compromises astrocyte function. *The FASEB Journal*, 35(5). doi:https://doi.org/10.1096/fj.202100087r.

Liu, C. and Hermann, T. (1978). Characterization of ionomycin as a calcium ionophore. *Journal of Biological Chemistry*, 253(17), pp.5892–5894. doi:https://doi.org/10.1016/s0021-9258(17)34550-7.

Liu, L., Liu, J., Bao, J., Bai, Q. and Wang, G. (2020). Interaction of Microglia and Astrocytes in the Neurovascular Unit. *Frontiers in Immunology*, 11. doi:https://doi.org/10.3389/fimmu.2020.01024.

Liva, S.M. and de Vellis, J. (2001). IL-5 Induces Proliferation and Activation of Microglia via an Unknown Receptor. *Neurochemical Research*, 26(6), pp.629–637. doi:https://doi.org/10.1023/a:1010983119125.

Lomiguen, C., Vidal, L., Kozlowski, P., Prancan, A. and Stern, R. (2018). Possible Role of Chitin-Like Proteins in the Etiology of Alzheimer's Disease. *Journal of Alzheimer's Disease*, 66(2), pp.439–444. doi:https://doi.org/10.3233/jad-180326.

Lye-Barthel, M., Sun, D. and Jakobs, T.C. (2013). Morphology of Astrocytes in a Glaucomatous Optic Nerve. *Investigative Ophthalmology & Visual Science*, 54(2), pp.909–909. doi:https://doi.org/10.1167/iovs.12-10109.

Maisonpierre, P.C., Suri, C., Jones, P.F., Bartunkova, S., Wiegand, S.J., Radziejewski, C., Compton, D., McClain, J., Aldrich, T.H., Papadopoulos, N., Daly, T.J., Davis, S., Sato, T.N. and Yancopoulos, G.D. (1997). Angiopoietin-2, a Natural Antagonist for Tie2 That Disrupts in vivo Angiogenesis. *Science*, 277(5322), pp.55–60. doi:https://doi.org/10.1126/science.277.5322.55.

Man, S., Ubogu, E.E., Williams, K.A., Tucky, B., Callahan, M.K. and Ransohoff, R.M. (2008). Human Brain Microvascular Endothelial Cells and Umbilical Vein Endothelial Cells Differentially Facilitate Leukocyte Recruitment and Utilize Chemokines for T Cell Migration. *Clinical & Developmental Immunology*, 2008, pp.1–8. doi:https://doi.org/10.1155/2008/384982.

Markel Olabarria, Putilina, M., Riemer, E.C. and Goldman, J.E. (2015). Astrocyte pathology in Alexander disease causes a marked inflammatory environment. *Acta Neuropathologica*, 130(4), pp.469–486. doi:https://doi.org/10.1007/s00401-015-1469-1.

Marsland, B.J., Bättig, P., Bauer, M., Ruedl, C., Lässing, U., Beerli, R.R., Dietmeier, K., Ivanova, L., Pfister, T., Vogt, L., Nakano, H., Nembrini, C., Saudan, P., Kopf, M. and Bachmann, M.F. (2005). CCL19 and CCL21 Induce a Potent Proinflammatory Differentiation Program in Licensed Dendritic Cells. *Immunity*, 22(4), pp.493–505. doi:https://doi.org/10.1016/j.immuni.2005.02.010.

Messing, A. and Brenner, M. (2020). GFAP at 50. *Asn Neuro*, 12, p.175909142094968-175909142094968. doi:https://doi.org/10.1177/1759091420949680.

Mogha, P., Iyer, S. and Majumder, A. (2023). Extracellular matrix protein gelatin provides higher expansion, reduces size heterogeneity, and maintains cell stiffness in a long-term culture of mesenchymal stem cells. *Tissue and Cell*, 80, p.101969. doi:https://doi.org/10.1016/j.tice.2022.101969.

Murakami, S. and Yoshihisa Kurachi (2015). Mechanisms of astrocytic K+ clearance and swelling under high extracellular K+ concentrations. *Journal of Physiological Sciences*, 66(2), pp.127–142. doi:https://doi.org/10.1007/s12576-015-0404-5.

Muthusamy, K., Ajith Sivadasan, Dixon, L., Sudhakar, S., Thomas, M., Danda, S., Wszołek, Z.K., Wierenga, K.J., Radhika Dhamija and Gavrilova, R.H. (2023). Adult-onset leukodystrophies: a practical guide, recent treatment updates, and future directions. *Frontiers in Neurology*, 14. doi:https://doi.org/10.3389/fneur.2023.1219324.

Nag, S., Tripti Papneja, Roopa Venugopalan and Stewart, D.J. (2005). Increased angiopoietin2 expression is associated with endothelial apoptosis and blood–brain barrier breakdown. *Laboratory Investigation*, [online] 85(10), pp.1189–1198. doi:https://doi.org/10.1038/labinvest.3700325.

Navarrete, M., Perea, G., de Sevilla, D.F., Gómez-Gonzalo, M., Núñez, A., Martín, E.D. and Araque, A. (2012). Astrocytes Mediate In Vivo Cholinergic-Induced Synaptic Plasticity. *PLoS Biology*, 10(2), p.e1001259. doi:https://doi.org/10.1371/journal.pbio.1001259.

Ogrodzinski, L., Platt, S., Goulding, J., Alexander, C., Farr, T.D., Woolard, J., Hill, S.J. and Kilpatrick, L.E. (2023). Probing expression of E-selectin using CRISPR-Cas9-mediated tagging with HiBiT in human endothelial cells. *iScience*, [online] 26(7), p.107232. doi:https://doi.org/10.1016/j.isci.2023.107232.

Ou, X., O'Leary, H.A. and Broxmeyer, H.E. (2013). Implications of DPP4 modification of proteins that regulate stem/progenitor and more mature cell types. *Blood*, 122(2), pp.161–169. doi:https://doi.org/10.1182/blood-2013-02-487470.

Perdan-Pirkmajer, K., Pirkmajer, S., Černe, K. and Kržan, M. (2012). Molecular and kinetic characterization of histamine transport into adult rat cultured astrocytes. *Neurochemistry International*, [online] 61(3), pp.415–422. doi:https://doi.org/10.1016/j.neuint.2012.05.002.

Perea, G., Gómez, R., Mederos, S., Covelo, A., Ballesteros, J.J., Schlosser, L., Hernández-Vivanco, A., Martín-Fernández, M., Quintana, R., Rayan, A., Díez, A., Fuenzalida, M., Agarwal, A., Bergles, D.E., Bettler, B., Manahan-Vaughan, D., Martín, E.D., Kirchhoff, F. and Araque, A. (2016). Activity-dependent switch of GABAergic inhibition into glutamatergic excitation in astrocyte-neuron networks. *eLife*, [online] 5. doi:https://doi.org/10.7554/elife.20362.

Perng, M.D., Su, M., Wen, S.F., Li, R., Gibbon, T., Prescott, A.R., Brenner, M. and Quinlan, R.A. (2006). The Alexander Disease–Causing Glial Fibrillary Acidic Protein Mutant, R416W, Accumulates into Rosenthal Fibers by a Pathway That Involves Filament Aggregation and the Association of αB-Crystallin and HSP27. *The American Journal of Human Genetics*, 79(2), pp.197–213. doi:https://doi.org/10.1086/504411.

Robinson, C., Apgar, C. and Shapiro, L.A. (2016). Astrocyte Hypertrophy Contributes to Aberrant Neurogenesis after Traumatic Brain Injury. *Neural Plasticity*, 2016, pp.1–10. doi:https://doi.org/10.1155/2016/1347987.

Roelofs, R.F., Fischer, D.F., Houtman, S.H., Sluijs, J.A., Haren, W.V., Van, F.W. and Hol, E.M. (2005). Adult human subventricular, subgranular, and subpial zones contain astrocytes with a specialized intermediate filament cytoskeleton. *Glia*, 52(4), pp.289–300. doi:https://doi.org/10.1002/glia.20243.

Saito, K., Eiji Shigetomi, Yasuda, R., Sato, R., Nakano, M., Tashiro, K., Tanaka, K.F., Kazuhiro Ikenaka, Katsuhiko Mikoshiba, Mizuta, I., Yoshida, T., Nakagawa, M., Mizuno, T. and Koizumi, S. (2018). Aberrant astrocyte Ca^{2+} signals 'AxCa signals' exacerbate pathological alterations in an Alexander disease model. *Glia*, 66(5), pp.1053–1067. doi:https://doi.org/10.1002/glia.23300.

Saraste, M., Bezukladova, S., Matilainen, M., Sucksdorff, M., Kuhle, J., Leppert, D. and Airas, L. (2021). Increased serum glial fibrillary acidic protein associates with microstructural white matter damage in multiple sclerosis. *Multiple Sclerosis and Related Disorders*, 50, p.102810. doi:https://doi.org/10.1016/j.msard.2021.102810.

Sawada, M., Suzumura, A., Itoh, Y. and Marunouchi, T. (1993). Production of interleukin-5 by mouse astrocytes and microglia in culture. *Neuroscience letters*, [online] 155(2), pp.175–8. doi:https://doi.org/10.1016/0304-3940(93)90701-l.

Sea, K., Sohn, S.H., Durazo, A., Sheng, Y., Shaw, B.F., Cao, X., Taylor, A.B., Whitson, L.J., Holloway, S.P., Hart, P.J., Cabelli, D.E., Gralla, E.B. and Valentine, J.S. (2015). Insights into the Role of the Unusual Disulfide Bond in Copper-Zinc Superoxide Dismutase. *The Journal of Biological Chemistry*, [online] 290(4), pp.2405–2418. doi:https://doi.org/10.1074/jbc.M114.588798.

Semple, B.D., Frugier, T. and Morganti-Kossmann, M.C. (2010). CCL2 modulates cytokine production in cultured mouse astrocytes. *Journal of Neuroinflammation*, 7(1), p.67. doi:https://doi.org/10.1186/1742-2094-7-67.

Seo, Y., Pak, J., Han, J., Bae, J. and Hwang, S.S. (2026). Viral transduction for T cell engineering in immunotherapy. *Molecules and Cells*, [online] 49(2), p.100311. doi:https://doi.org/10.1016/j.mocell.2026.100311.

Shah, D., Himmelreich, U., Jérôme Wahis, Emma Susanne Luckett, Tarik Jamoulle, Vermaercke, B., Pranav Preman, Daan Moechars, Hendrickx, V., Jaspers, T., Katleen Craessaerts, Katrien Horré, Wolfs, L., Fiers, M., Holt, M.T., Dietmar Rudolf Thal, Zsuzsanna Callaerts-Vegh, Rudi D'Hooge, Vandenberghe, R. and Himmelreich, U. (2022). Astrocyte calcium dysfunction causes early network hyperactivity in Alzheimer's disease. *Cell Reports*, 40(8), pp.111280–111280. doi:https://doi.org/10.1016/j.celrep.2022.111280.

Sheng, W.S., Hu, S., Feng, A. and Rock, R.B. (2013). Reactive Oxygen Species from Human Astrocytes Induced Functional Impairment and Oxidative Damage. *Neurochemical Research*, 38(10), pp.2148–2159. doi:https://doi.org/10.1007/s11064-013-1123-z.

Shi, A. and Mansour, S.G. (2023). The Role of Vascular Biomarkers in Outcomes of Patients with Kidney Disease. *Nephron*, 147(12), pp.778–781. doi:https://doi.org/10.1159/000533415.

Shigetomi, E., Saito, K., Sano, F. and Koizumi, S. (2019). Aberrant Calcium Signals in Reactive Astrocytes: A Key Process in Neurological Disorders. *International Journal of Molecular Sciences*, [online] 20(4), p.996. doi:https://doi.org/10.3390/ijms20040996.

Siddharthan, V., Kim, Y.V., Liu, S. and Kim, K.S. (2007). Human astrocytes/astrocyte-conditioned medium and shear stress enhance the barrier properties of human brain microvascular endothelial cells. *Brain Research*, 1147, pp.39–50. doi:https://doi.org/10.1016/j.brainres.2007.02.029.

Sie, M., Wagemakers, M., Molema, G., Mooij, J.J.A., de Bont, E.S.J.M. and den Dunnen, W.F.A. (2009). The angiopoietin 1/angiopoietin 2 balance as a prognostic marker in primary glioblastoma multiforme. *Journal of neurosurgery*, [online] 110(1), pp.147–55. doi:https://doi.org/10.3171/2008.6.17612.

Sim, A.Y., Choi, D.H., Kim, J.Y., Kim, E.R., Goh, A-Ra., Lee, Y.-H. and Lee, J.E. (2023). SGLT2 and DPP4 inhibitors improve Alzheimer's disease-like pathology and cognitive function through distinct mechanisms in a T2D-AD mouse model. *Biomedicine & pharmacotherapy = Biomedecine & pharmacotherapie*, [online] 168, p.115755. doi:https://doi.org/10.1016/j.biopha.2023.115755.

Simpson, J.E., Ince, P.G., Lace, G., Forster, G., Shaw, P.J., Matthews, F., Savva, G., Brayne, C. and Wharton, S.B. (2010). Astrocyte phenotype in relation to Alzheimer-type pathology in the ageing brain. *Neurobiology of Aging*, 31(4), pp.578–590. doi:https://doi.org/10.1016/j.neurobiolaging.2008.05.015.

Sofroniew, M.V. and Vinters, H.V. (2009). Astrocytes: biology and pathology. *Acta Neuropathologica*, [online] 119(1), pp.7–35. doi:https://doi.org/10.1007/s00401-009-0619-8.

Srivastava, S. and Naidu, S. (2015). *Alexander Disease*. [online] Nih.gov. Available at: https://www.ncbi.nlm.nih.gov/books/NBK1172/.

Sun, L., Li, Y., Jia, X., Wang, Q., Li, Y., Hu, M., Tian, L., Yang, J., Xing, W., Zhang, W., Wang, J., Xu, H., Wang, L., Zhang, D. and Ren, H. (2017). Neuroprotection by IFN-γ *via* astrocyte-secreted IL-6 in acute neuroinflammation. *Oncotarget*, [online] 8(25). doi:https://doi.org/10.18632/oncotarget.16990.

Tang, G., Perng, M.D., Wilk, S., Quinlan, R. and Goldman, J.E. (2010). Oligomers of Mutant Glial Fibrillary Acidic Protein (GFAP) Inhibit the Proteasome System in Alexander Disease Astrocytes, and the Small Heat Shock Protein αB-Crystallin Reverses the Inhibition. *Journal of Biological Chemistry*, 285(14), pp.10527–10537. doi:https://doi.org/10.1074/jbc.m109.067975.

Tarassishin, L., Suh, H.-S. and Lee, S.C. (2014). LPS and IL-1 differentially activate mouse and human astrocytes: Role of CD14. *Glia*, 62(6), pp.999–1013. doi:https://doi.org/10.1002/glia.22657.

Tournier, B.B., Farha Bouteldja, Amossé, Q., Nicolaides, A., Azevedo, M.D., Tenenbaum, L., Garibotto, V., Ceyzériat, K. and Millet, P. (2023). 18 kDa Translocator Protein TSPO Is a Mediator of Astrocyte Reactivity. *ACS Omega*, 8(34), pp.31225–31236. doi:https://doi.org/10.1021/acsomega.3c03368.

University of Wisconsin-Madison, W.C., University of Wisconsin-Madison (n.d.). *Alexander Disease Lab*. [online] Alexander Disease Lab. Available at: https://alexander-disease.waisman.wisc.edu/.

van Kralingen, C., Kho, D.T., Costa, J., Angel, C.E. and Graham, E.S. (2013). Exposure to Inflammatory Cytokines IL-1β and TNFα Induces Compromise and Death of Astrocytes; Implications for Chronic Neuroinflammation. *PLoS ONE*, 8(12), p.e84269. doi:https://doi.org/10.1371/journal.pone.0084269.

van and Roberts, L.Jackson. (1999). Contrasting roles for nitric oxide and peroxynitrite in the peroxidation of myelin lipids. *Journal of Neuroimmunology*, 95(1-2), pp.1–7. doi:https://doi.org/10.1016/s0165-5728(98)00239-2.

Vanderver, A., Prust, M., Tonduti, D., Mochel, F., Hussey, H.M., Helman, G., Garbern, J., Eichler, F., Labauge, P., Aubourg, P., Rodriguez, D., Patterson, M.C., Van Hove, J.L.K., Schmidt, J., Wolf, N.I., Boespflug-Tanguy, O., Schiffmann, R., van der Knaap, M.S. and GLIA Consortium (2015). Case definition and classification of leukodystrophies and leukoencephalopathies. *Molecular Genetics and Metabolism*, [online] 114(4), pp.494–500. doi:https://doi.org/10.1016/j.ymgme.2015.01.006.

Wang, L., Hagemann, T.L., Kalwa, H., Michel, T., Messing, A. and Feany, M.B. (2015). Nitric oxide mediates glial-induced neurodegeneration in Alexander disease. *Nature Communications*, 6(1). doi:https://doi.org/10.1038/ncomms9966.

Wen, J.-H., He, X.-H., Feng, Z.-S., Li, D.-Y., Tang, J.-X. and Liu, H.-F. (2023). Cellular Protein Aggregates: Formation, Biological Effects, and Ways of Elimination. *International Journal of Molecular Sciences*, [online] 24(10), p.8593. doi:https://doi.org/10.3390/ijms24108593.

Wenta, T., Nastaly, P., Lipinska, B. and Manninen, A. (2024). Remodeling of the extracellular matrix by serine proteases as a prerequisite for cancer initiation and progression. *Matrix Biology*. doi:https://doi.org/10.1016/j.matbio.2024.10.007.

White, K.E., Bailey, H.L., Shaw, B.S., Geiszler, P.C., Mesquita-Ribeiro, R., Scott, D., Layfield, R. and Serres, S. (2024). A convenient model of serum-induced reactivity of human astrocytes to investigate astrocyte-derived extracellular vesicles. *Frontiers in cellular neuroscience*, 18. doi:https://doi.org/10.3389/fncel.2024.1414142.

Williamson, M.R., Fuertes, C.J.A., Dunn, A.K., Drew, M.R. and Jones, T.A. (2021). Reactive astrocytes facilitate vascular repair and remodeling after stroke. *Cell Reports*, [online] 35(4), p.109048. doi:https://doi.org/10.1016/j.celrep.2021.109048.

Wippold, F., Perry, A. and Lennerz, J. (2025). *Rosenthal Fibers Neuropathology for the Neuroradiologist*.

Wunderlich, M.T., Wallesch, C.W. and Goertler, M. (2006). Release of glial fibrillary acidic protein is related to the neurovascular status in acute ischemic stroke. *European journal of neurology*, [online] 13(10), pp.1118–23. doi:https://doi.org/10.1111/j.1468-1331.2006.01435.x.

Wylot, B., Mieczkowski, J., Niedziolka, S., Kaminska, B. and Zawadzka, M. (2019). Csf1 Deficiency Dysregulates Glial Responses to Demyelination and Disturbs CNS White Matter Remyelination. *Cells*, 9(1), p.99. doi:https://doi.org/10.3390/cells9010099.

Xu, J., Zhang, X., Qian, Q., Wang, Y., Dong, H., Li, N., Qian, Y. and Jin, W. (2018). Histamine upregulates the expression of histamine receptors and increases the neuroprotective effect of astrocytes. *Journal of Neuroinflammation*, 15(1). doi:https://doi.org/10.1186/s12974-018-1068-x.

Yang, Z. and Wang, K.K.W. (2015). Glial Fibrillary acidic protein: From intermediate filament assembly and gliosis to neurobiomarker. *Trends in neurosciences*, 38(6), pp.364–374. doi:https://doi.org/10.1016/j.tins.2015.04.003.

Yasuda, R., Nakano, M., Yoshida, T., Sato, R., Adachi, H., Tokuda, Y., Mizuta, I., Saito, K., Matsuura, J., Nakagawa, M., Tashiro, K. and Mizuno, T. (2019). Towards genomic database of Alexander disease to identify variations modifying disease phenotype. *Scientific Reports*, 9(1). doi:https://doi.org/10.1038/s41598-019-51390-8.

Yoshida, T., Sasaki, M., Yoshida, M., Namekawa, M., Okamoto, Y., Tsujino, S., Sasayama, H., Mizuta, I., Nakagawa, M. and Alexander Disease Study Group in Japan (2011). Nationwide survey of Alexander disease in Japan and proposed new guidelines for diagnosis. *Journal of Neurology*, [online] 258(11), pp.1998–2008. doi:https://doi.org/10.1007/s00415-011-6056-3.

Yu, P., Wang, H., Katagiri, Y. and Geller, H.M. (2011). An In Vitro Model of Reactive Astrogliosis and Its Effect on Neuronal Growth. *Methods in molecular biology*, [online] pp.327–340. doi:https://doi.org/10.1007/978-1-61779-452-0_21.

Zhou, Z., Lin, T., Liu, Z., Ding, Q., Ma, Z., Li, W., Xie, F., Lan, Y. and Feng, Y. (2022). IL-17A Mediates Demyelination by Activating A1 Astrocytes via SOCS3 During Angiostrongylus cantonensis Infection. *Frontiers in Immunology*, 13. doi:https://doi.org/10.3389/fimmu.2022.845011.

Zou, L.-H., Shi, Y.-J., He, H., Jiang, S.-M., Huo, F.-F., Wang, X.-M., Wu, F. and Ma, L. (2019). Effects of FGF2/FGFR1 Pathway on Expression of A1 Astrocytes After Infrasound Exposure. *Frontiers in Neuroscience*, 13. doi:https://doi.org/10.3389/fnins.2019.00429.